

**DIELECTRIC RESONATOR ANTENNA REFLECTARRAY ELEMENTS
WITH UNDER-LOADING SLOTS**

LEE SHIN ROU

**A project report submitted in partial fulfilment of the
requirements for the award of Bachelor of Engineering
(Hons.) Electronic and Communications Engineering**

**Faculty of Engineering and Science
Universiti Tunku Abdul Rahman**

April 2014

DECLARATION

I hereby declare that this project report is based on my original work except for citations and quotations which have been duly acknowledged. I also declare that it has not been previously and concurrently submitted for any other degree or award at UTAR or other institutions.

Signature : _____

Name : LEE SHIN ROU

ID No. : 10UEB01518

Date : 14 APRIL 2014

APPROVAL FOR SUBMISSION

I certify that this project report entitled **“DIELECTRIC RESONATOR ANTENNA REFLECTARRAY ELEMENTS WITH UNDER-LOADING SLOTS”** was prepared by **LEE SHIN ROU** has met the required standard for submission in partial fulfilment of the requirements for the award of Bachelor of Engineering (Hons.) Electronic and Communications Engineering at Universiti Tunku Abdul Rahman.

Approved by,

Signature : _____

Supervisor : **DR. LIM ENG HOCK**

Date : **14 APRIL 2014**

The copyright of this report belongs to the author under the terms of the copyright Act 1987 as qualified by Intellectual Property Policy of Universiti Tunku Abdul Rahman. Due acknowledgement shall always be made of the use of any material contained in, or derived from, this report.

© 2014, Lee Shin Rou. All right reserved.

Specially dedicated to
my beloved parents and friends

ACKNOWLEDGEMENTS

First of all, I would like to hand in millions of thanks to my supervisor, Dr. Lim Eng Hock for helping and assisting me throughout my final year project. The encouragement and support given have contributed to the successful completion of this project.

Besides that, I would like to express my gratitude to my seniors for their invaluable advice and guidance which had contributed to the success of this project. Their enormous patience in leading me to the completion of this project was appreciated.

In addition, I would also like to thank my loving parents and friends who have given me encouragement all the way which have helped in driving me to the success point at the end of this project.

DIELECTRIC RESONATOR ANTENNA REFLECTARRAY ELEMENTS WITH UNDER-LOADING SLOTS

ABSTRACT

First project presents three dielectric resonator (DR) unit elements loaded with one, two, and three narrow slots underneath for designing reflectarrays. The slots are aligned in parallel and the lengths are varied to function as phase shifter for changing reflection phase. It is found that the dominant TE mode of the square DR element can be easily excited by placing multiple parallel slots beneath a DR element. Study shows that the number and width of the slots can be used as additional design parameters for tuning the reflection loss and phase range of the reflectarray. Rectangular waveguide method has been deployed, showing reasonable agreement between simulation and measurement. It is found that a reasonable reflection phase range of 313° with slow slope is obtainable when the DRA is loaded with two slots beneath, which can be used for designing a small-size reflectarray. The reflection characteristics of the unit elements are studied, along with a complete parametric analysis.

Second project explores a dielectric resonator antenna (DRA) reflectarray unit element with multiple loading circular slots underneath in concentric form. The radii of the three slots are varied simultaneously to function as phase-shifting elements. For the case of three under-loading slots, it is very interesting to find out that the slot and DRA resonances can be pulled together to provide a very broad phase range of 916° . Study shows that the gradient and phase range of the S curve can be easily tuned by manipulating the dimensions of the under-loading slots. Waveguide method has been used to establish the simulation and measurement models. The reflection properties of the DRA unit elements loaded with different ring-shaped slots are compared, along with a complete parametric analysis. The

proposed reflectarray unit element is very compact as its phase shifter can be entirely hidden beneath the DRA.

TABLE OF CONTENTS

DECLARATION	ii
APPROVAL FOR SUBMISSION	iii
ACKNOWLEDGEMENTS	vi
ABSTRACT	vii
TABLE OF CONTENTS	ix
LIST OF FIGURES	xii

CHAPTER

1	INTRODUCTION	1
	1.1 Background	1
	1.2 Reflectarray Working Principle	2
	1.3 Unit Element Key Performance Parameters	4
	1.3.1 Reflection Loss	4
	1.3.2 Reflection Phase	4
	1.4 Reflectarray Key Performance Parameters	5
	1.4.1 Antenna Gain	5
	1.4.2 Gain Bandwidth	6
	1.5 Aims and Objectives	6
	1.6 Thesis Overview	7
2	LITERATURE REVIEW AND DESIGN METHODOLOGY	8
	2.1 Review on Reflectarray Antennas	8
	2.2 Design Method Review	9
	2.3 Simulation of Unit Element	11

2.3.1	Waveguide Method	11
2.3.2	Floquet Method	12
2.4	Configuration of Reflectarray	13
2.5	Calculation of Path Length	14
2.6	Calculation of Path Difference	15
2.7	Extraction of Radiating Element Dimension	16
2.8	Simulation of Reflectarray	16
3	DRA REFLECTARRAY UNIT ELEMENTS WITH THIN UNDER-LOADING PARALLEL SLOTS	17
3.1	Introduction	17
3.2	Reflectarray Unit Cell Configuration	19
3.3	Unit Cell Simulation and Measurement	22
3.4	Field Distribution in Reflectarray Unit Element	25
3.5	Parametric Analysis	27
3.5.1	Gap Separation between Slots	27
3.5.2	Slot Width	29
3.5.3	Slot Length	33
3.5.4	Multiple Under-Loading Slots	35
3.5.5	Oblique Incidence	38
3.5.6	DRA Alignment	39
3.5.7	Substrate Thickness	42
3.5.8	Substrate Dielectric Constant	43
3.5.9	Substrate Loss Tangent	45
3.6	Conclusion	46
4	BROADRANGE REFLECTARRAY ELEMENT WITH COMBINED SLOT AND DIELECTRIC RESONATOR RESONANCES	47
4.1	Introduction	47
4.2	Reflectarray Unit Cell Configuration	49
4.3	Unit Cell Simulation and Measurement	52
4.4	Field Distribution in Reflectarray Unit Element	55

4.5	Parametric Analysis	57
4.5.1	Gap Separation between Slots	58
4.5.2	Slot Widths	62
4.5.3	Multiple Slots underneath a DRA	67
4.5.4	DRA Alignment	75
4.6	Conclusion	78
5	CONCLUSION AND RECOMMENDATIONS	79
	REFERENCES	80

LIST OF FIGURES

FIGURE	TITLE	PAGE
1.1	Wave Beams Reflected by a Planar Metal Plate.	2
1.2	Typical Configuration of Reflectarray with Wave Beams Reflected to achieve the Same Wave Front.	3
2.1	Step of Designing a Reflectarray Antenna using Phase Only Optimization Technique.	10
2.2	Oblique Incidence in the Waveguide Model with the Boundary Conditions given.	12
2.3	Oblique Incidence in the Floquet Model with the Boundary Conditions given.	13
2.4	Side View of a General Reflectarray.	14
2.5	Path Lengths from the Feeder to the Radiating Elements.	15
3.1	Square DRA Unit Element Loaded with 2 Slots Underneath. (a) Perspective View. (b) Top-Down View. (c) Photograph of the Fabricated Prototype.	21
3.2	(a) Simulation model for the DRA unit cell. (b) Experimental setup for the waveguide method.	22
3.3	Simulated and Measured (a) Reflection Loss, (b) Reflection Phase of the DRA Reflectarray Unit Element with Two Under-Loading Slots ($L_1 = L_2 = 5.5$ mm, $W_1 = W_2 = 0.15$ mm, $G = 0.5$ mm).	23
3.4	Simulated and Measured (a) Reflection Loss, (b) Reflection Phase at 7.5 GHz of DRA Unit Element with Two Under-Loading Slots.	25

3.5	Electric Field Distribution of the DRA Reflectarray Unit Element at 7.5 GHz. (a) Top-down view. (b) Side view.	26
3.6	Effect of Gap Separation Between the Two Slots on (a) Reflection Loss, (b) Reflection Phase.	28
3.7	Effect of Varying the Widths of the Two Slots on the (a) Reflection Loss, (b) Reflection Phase.	30
3.8	Effect of Changing the Slot Width W_2 on the (a) Reflection Loss, (b) Reflection Phase.	31
3.9	Effect of Changing the Slot Width W_1 on the (a) Reflection Loss, (b) Reflection Phase.	32
3.10	Effect of the Slot Length L_1 on the (a) Reflection Loss, (b) Reflection Phase.	34
3.11	Effect of the Slot Length L_2 on the (a) Reflection Loss, (b) Reflection Phase.	35
3.12	(a) Square DRA Unit Element Loaded with (a) 1 Slot and (b) 3 Slots Underneath.	36
3.13	Comparison of the (a) Reflection Loss, (b) Reflection Phase of the DRA Reflectarray Unit Element with Different Under-Loading Slots.	37
3.14	Comparison of the (a) Reflection Loss, (b) Reflection Phase of the DRA Reflectarray Unit Element at Different Oblique Incident Angles.	39
3.15	Effect of the DRA Misaligned (x-direction) on the (a) Reflection Loss, (b) S Curve.	40
3.16	Effect of the DRA Misaligned (y-direction) on the (a) Reflection Loss, (b) S Curve.	41
3.17	Effect of the Substrate Thickness on the (a) Reflection Loss, (b) S Curve.	43
3.18	Effect of the Substrate Dielectric Constant on the (a) Reflection Loss, (b) S Curve.	44
3.19	Effect of the Substrate Loss Tangent on the (a) Reflection Loss, (b) S Curve.	46
4.1	Square DRA Unit Element Loaded with 3 Concentric Circular Slots Underneath. (a)	

	Perspective view. (b) Top-down view. (b) Photograph of the Fabricated Prototype.	51
4.2	(a) DRA Unit Element Simulation Model. (b) Experimental Setup for the Waveguide Method.	52
4.3	Simulated and Measured (a) Reflection Coefficients; (b) Reflection Phases of the Proposed DRA Reflectarray Unit Element Loaded with Three Circular Slots ($G_1 = G_2 = 0.5$ mm and $W_1 = W_2 = W_3 = 0.5$ mm) Beneath.	53
4.4	Simulated and Measured (a) Reflection Losses, (b) S Curves at 7.5 GHz for the Proposed DRA Unit Element with Three Under-Loading Circular slots.	55
4.5	Electric Field Distribution of the DRA Reflectarray Unit Element for $R_1 = 1.5$ mm at 7.5 GHz. (a) Top-down View. (b) Side View.	56
4.6	Electric Field Distribution of the DRA Reflectarray Unit Element for $R_1 = 2.6$ mm at 7.5 GHz. (a) Top-down View. (b) Side View.	57
4.7	Effect of the Gap Separation on (a) Reflection Loss; (b) S Curve.	59
4.8	Effect of Changing the Gap Separation G_1 (with $G_2 = 0.2$ mm) on the (a) Reflection Loss; (b) S Curve.	60
4.9	Effect of Changing the Gap Separation G_2 (with $G_1 = 0.2$ mm) on the (a) Reflection Loss; (b) S Curve.	61
4.10	Effect of Changing Slot Widths (W_1, W_2, W_3) of the Three Circular Slots on the (a) Reflection Loss; (b) S Curve.	63
4.11	Effect of Changing the Circular Slot Width W_1 on the (a) Reflection Loss; (b) S Curve.	64
4.12	Effect of Changing the Circular Slot Width W_3 on the (a) Reflection Loss; (b) S Curve.	65
4.13	Effect of Changing the Inner and Outer Slots (W_1 and W_3) on the (a) Reflection Loss; (b) S Curve.	67
4.14	(a) Square DRA Reflectarray Unit Element Loaded with (a) One Circular Slot and (b) Two Circular Slots Underneath.	68

4.15	Comparison of the (a) Reflection Loss, (b) S Curve of the DRA Reflectarray Unit Elements with One, Two, and Three Under-Loading Slots.	69
4.16	Effect of Changing Slot Width (W_1) on the (a) Reflection Loss, (b) S Curve.	71
4.17	Effect of Gap Separation G_1 between Two Slots on the (a) Reflection Loss, (b) S Curve.	72
4.18	Effect of Changing Slots Widths (W_1 and W_2) of the Two Slots on the (a) Reflection Loss, (b) S Curve.	74
4.19	Effect of Changing Slot Width W_2 on the (a) Reflection Loss, (b) S Curve.	75
4.20	Effect of DRA Misalignment (x-direction) on the (a) Reflection Loss, (b) S Curve.	76
4.21	Effect of DRA Misalignment (y-direction) on the (a) Reflection Loss, (b) S Curve.	77

CHAPTER 1

INTRODUCTION

1.1 Background

Parabolic reflectors and phased arrays are the two most popular antennas that are broadly used by various wireless applications because they are able to provide high gain. Reflector antenna can effectively focus microwave signals into a certain direction through its parabolic dish. However, it can be very challenging and expensive to fabricate the curved surface of the reflector (Zhou, et al., 2013). Also, parabolic dish is typically made of metallic materials which makes it very bulky (Huang, 1995). This, however, may not be desired by certain applications such as space-related missions. Different angles of signal transmission and reception can be easily achieved by incorporating a mechanical rotator with the parabolic reflector so that the direction of its radiation aperture can be changed. Such structure, however, may not be fast-responding because of the involvement of slow-moving mechanical components. Phased array antenna seems to be a possible solution as it is able to provide beam scanning by combining several antennas into array arrangement, with a certain input phase supplied to each of them. Yet, it can be very complicated and expensive as a multiple power dividers are required to provide different input phases. Also, additional components can introduce losses.

Later, in 1963, a new type antenna, called reflectarray, was introduced by Berry *et al.* (Berry, et al., 1963). Such antenna has combined the good features of both the parabolic reflector and phased array antennas (Mener, et al., 2013). Attention has since shifted from dishes to reflectarrays. This is because reflectarray

has a planar reflecting surface, making it easier to fabricate than the curved surface of the parabolic dish (Huang, 1996). Besides that, it has lower profile and lighter weight, requiring less supporting fixtures. All of these attractive features have made reflectarrays popular in the space-related applications. Unlike the phased array, all of the radiating elements of a reflectarray are spatially excited by a feed antenna and they do not require any power dividing networks to feed its individual element (Pan, et al., 2012).

1.2 Reflectarray Working Principle

If electromagnetic wave beams are illuminated to the flat metal plate shown in Fig. 1.1, they will get reflected following Snell's law. The wave fronts of the beams are different as they reach the surface at different time instances, resulting in incoherence in the broadside direction. Reflectarray is fed in the similar fashion. But now the reflecting surface is replaced by arrays of planar resonators so that the wave fronts can be made coherent in the broadside.

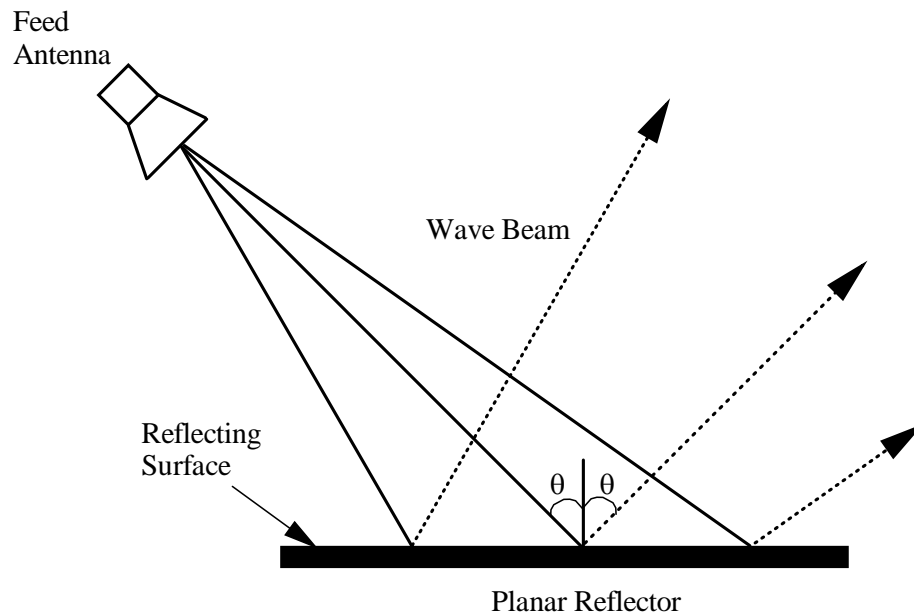


Figure 1.1: Wave Beams Reflected by a Planar Metal Plate.

A typical reflectarray consists of multiple radiating elements placed on top of a grounded substrate. Side-feeding scheme is usually more preferred as it does not block the radiation beams. These radiating elements are designed in the manner such that each of them is adding the incoming wave with a certain phase shift so that all the reflected wave beams have the same wave front along the line $P - P'$ (Zhang, et al., 2007), as shown in Figure 1.2. This will make all of the beams to be forced into a particular direction (Boccia, et al., 2002). In other words, the incoming spherical wave can be transformed into a planar wave with the use of the reflectarray elements (Bialkowski & Sayidmarie, 2008). This can be done by introducing different phase shifts to all of the radiating elements (Venneri, et al., 2013). One common approach to introduce phase shifts to the radiating elements is by varying one of its geometrical design parameters. Such change will be converted into a reflection phase variation (Nayeri, et al., 2012).

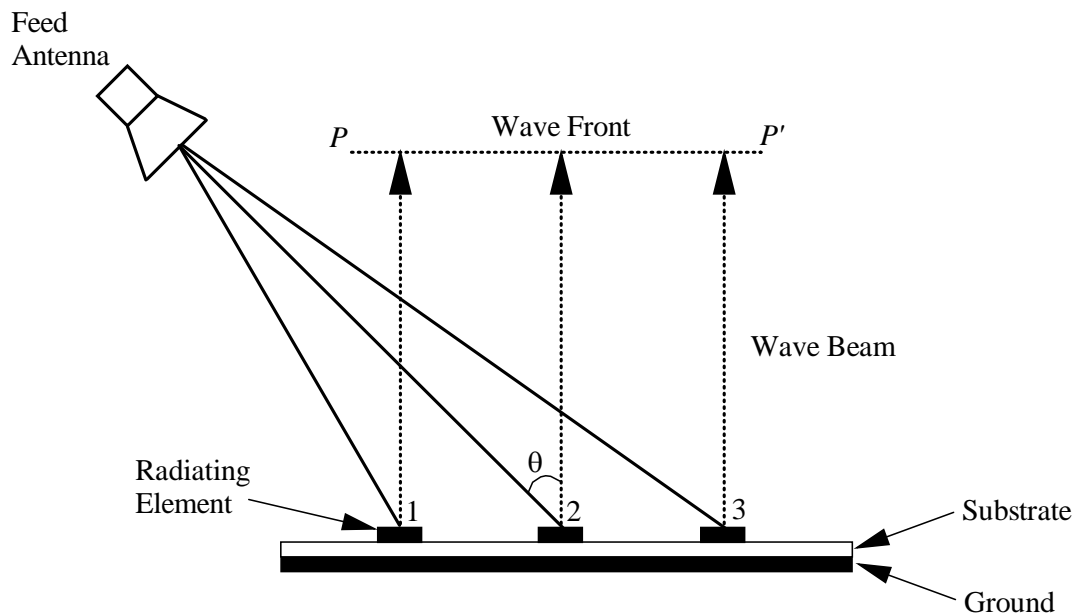


Figure 1.2: Typical Configuration of Reflectarray with Wave Beams Reflected to achieve the Same Wave Front.

1.3 Unit Element Key Performance Parameters

As mentioned in the previous sections, reflectarray is a combination of multiple radiating elements which are placed on the top surface of a grounded substrate. The terminology “unit element” refers to only one radiating element. In order to design a good reflectarray, a reflectarray unit element must be able to provide a minimum reflection phase range of 360° as well as low reflection loss. In this section, two reflection parameters are discussed - reflection loss and reflection phase.

1.3.1 Reflection Loss

When electromagnetic wave beams are reflected from the reflectarray elements, some losses will be introduced by the elements themselves. The losses can be classified into two types - metallic loss and dielectric loss (Bozzi, et al., 2004). Metallic loss refers to the loss incurred on the metallic resonators whereas dielectric loss is the loss introduced by the substrate. The loss amount can also be affected by the geometrical shape of the radiating element (Bozzi, et al., 2004). Loss tangent and thickness of the substrate will affect the reflection characteristics (Rajagopalan & Rahmat-Samii, 2010) as well. In unit cell simulation, reflection loss of a particular radiating element can be obtained from the magnitude of the reflection coefficient. It is good to have minimum loss factor when designing a reflectarray.

1.3.2 Reflection Phase

Reflection phase is another important parameter that can be obtained from the unit cell simulation. Reflection phase, which is also known as S-Curve, describes the relationship between the reflection phase and the phase-shifting design parameter (Niaz, et al., 2010). By knowing the phase shift required by each element, the S-curve can be used to calculate all the dimensions of the radiating elements. There are two crucial things that are needed to be taken into consideration when analysing an

S-Curve. Firstly, the changing rate (gradient) of the reflection phase slope must be as slow as possible. The rate tells how sensitive the reflection phase is to variation of the phase-shifting design parameter. The slower the gradient is, the more distinguishable the dimensions of the radiating elements are. It was shown that the gradient can be reduced (Hasani, et al., 2010) with the use of thicker substrate (Karnati, et al., 2011), stacked patches (Encinar, 1999; Encinar, 2001), and phase delay line (Carrasco, et al., 2008). It is also very desirable to achieve a minimum phase range of 360° in the S curve so that it can be used to design a large-size reflectarray.

1.4 Reflectarray Key Performance Parameters

As mentioned earlier, reflectarray is a combination of multiple radiating elements in array form. The elements are used to convert the spherical wave emitted by a feed horn into a planar wave. Since all of the radiating elements are located at different distances from the feed horn (Makdissy, et al., 2012; Mussetta, et al., 2012; Robinson, et al., 1999), the incoming waves will travel through different path distances before impinging on the radiating elements, which are designed to compensate all the wave beams so that they are reflected coherently to form a directive radiation beam. Two important parameters that affect the reflectarray performance are antenna gain and gain bandwidth.

1.4.1 Antenna Gain

Antenna gain refers to the potentiality of an antenna in directing wave beams to a particular direction. It mainly depends on the aperture size of the reflectarray (Huang & Encinar, 2007). A larger aperture size can provide a higher antenna gain. It needs more radiating elements to be placed on the grounded substrate. The reflectarray antenna gain can also be affected by the spill-over losses, which occur when the elements are placed far away from the feed horn. To mitigate spill-over, the feed

horn must be placed at a distance where its radiation lobe is just enough to cover the reflectarray aperture and the elements must be at its far field. Feeding scheme is another factor that affects the reflectarray antenna gain. Side-fed ($\theta > 0^\circ$) is usually preferred to prevent blockage of the radiation beams (Abd-Elhady, et al., 2012; Han, et al., 2006).

1.4.2 Gain Bandwidth

Gain bandwidth is another crucial parameter that affects the reflectarray performance. It refers to the frequency range where the antenna gain drops by 1 dB. The bandwidth of the reflectarray is always limited by the bandwidth of the single element (Huang & Encinar, 2007). For example, microstrip reflectarray has narrow bandwidth performance, being limited by the high-Q factor of the microstrip resonator.

1.5 Aims and Objectives

The original aim of this project is to apply novel ideas to design the DRA reflectarrays. However, due to time limitation, the aim has been changed to focus on the exploration of the DRA reflectarray unit elements. The CST microwave studio software is used to design and simulate the proposed new DRA elements. Later, waveguide method is employed to verify the performances. The details of the proposed unit elements will be provided in the following paragraphs.

In Chapter 3, it is the first time to place multiple parallel slots underneath a square DRA. The slots are used as phase shifters and their lengths are varied to provide phase change. It is found that the DRA with two under-loading slots is able to achieve a phase range of 313° at the operating frequency of 7.5 GHz. Experiment is conducted to substantiate the simulated results. The effects of other design parameters are also studied.

In Chapter 4, three concentric circular slots are placed beneath a square DRA. In this design, the radii of the slots are varied to obtain changeable phase shift. It is found that a phase range of 916° is attainable at the operating frequency of 7.5 GHz. Experiment has been conducted to verify the simulated results. The effects of placing one and two slots underneath the DRA are also studied.

1.6 Thesis Overview

In Chapter 1, review on the background of the parabolic reflectors and the phased arrays has been carried out. Here, the working principle of the reflectarray will be presented and explained, along with a complete study on the key performance parameters of the reflectarray unit element. Finally, it comes to the objectives and motivations of my project.

In Chapter 2, some of the issues of the reflectarrays are reviewed and discussed. Various design methods have been covered and explained in detail. Also, the step-by-step design procedure will be briefly described for a general reflectarray.

Chapter 3 presents the design process of a DRA reflectarray unit element loaded with multiple parallel slots underneath. Details of the design and configuration are included, along with the measurement and simulation results. Finally, parametric analysis on various design parameters has been performed.

Chapter 4 presents the design procedure of a DRA reflectarray unit element with multiple under-loading concentric circular ring slots. The unit cell will be analysed. Simulation and measurement results will be shown. Parametric analysis on the unit element design parameters has also been performed.

Chapter 5 concludes the works done in this project and some other important findings are included. Recommendation is made for future work.

CHAPTER 2

LITERATURE REVIEW AND DESIGN METHODOLOGY

2.1 Review on Reflectarray Antennas

Berry, Malech, and Kennedy first introduced the concept of reflectarray antenna in 1963 (Berry, et al., 1963). They had designed a waveguide reflectarray using the short-ended waveguide elements with varied lengths to achieve coherent re-radiated wave beams. Since then, many types of reflectarrays have been developed. In (Phelan, 1977), a spiraphase reflectarray was designed by incorporating switching diodes with a spiral antenna to achieve wide-angle beam scanning.

In 1978, use of microstrip elements for designing reflectarray was demonstrated by Malagisi (Malagisi, 1978). Some simple microstrip reflectarrays have started to appear since the late 80s. One way to generate phase shift is to load identical-size patch elements with variable phase delay lines (Javor, et al., 1994). Other designs such as dipole elements with variable lengths (Kelkar, 1991) and microstrip patches with tuneable sizes (Pozar & Metzler, 1993) were also proposed.

In the early 20s, the idea of designing the reflectarray antenna using the dielectric resonator antenna (DRA) was also introduced. In (Keller, et al., 2000), a dielectric resonator antenna (DRA) with variable length was used to design a reflectarray antenna. Other configurations such as the DRA with a top-loading strip (Jamaluddin, et al., 2009) and the DRA with an under-loading alphabet-shaped slot (Dzulkipli, et al., 2012) were also proposed. The recent developments of the DRA reflectarrays will be reviewed in Chapter 3 and 4.

2.2 Design Method Review

There are two popular methods for designing a reflectarray - direct optimization technique (DOT) and phase only optimization technique (POT). DOT is mainly used for designing a reflectarray with elements of randomly-shaped. In this case, the positions and orientations of the reflectarray elements are usually placed in random. However, the DOT is not a low-cost technique as it requires the use of intensive computation resources. A good example was demonstrated by (Zhou, et al., 2013). In contrast, the POT is a simple and cheap design method. It has fewer requirements on the processor speed and computer memory. To use the POT method, the number of radiating elements must first be determined. The reflection phases for all the radiating elements are then compared with a referencing element to determine their compensating phase shifts (Zhou, et al., 2013). The reference is usually selected to be the one which has the shortest path length from the feed horn. Many types of reflectarrays have been demonstrated using this technique (Encinar & Zornoza, 2004; Carrasco, et al., 2008; Capozzoli, et al., 2009; Arrebola, et al., 2009; Capozzoli, et al., 2010).

The POT technique is adopted in this thesis. A flowchart that describes the design steps of a general reflectarray is shown in Figure 2.1. First of all, simulation is done by applying an oblique incident wave on the proposed unit element to obtain its reflection phase. After identified the particular design parameter that contributes to phase shift, the variation of reflection phase is then generated by changing this parameter to generate a curve, which is also called S curve. It shows the reflection phases of the elements at all dimensions. Phase compensation for each radiating element in the reflectarray can be obtained from the S curve. The second step is to define the configuration of the desired reflectarray. After deciding the locations of the elements, the path distances travelled by the EM wave beams can then be calculated between the feed horn and the radiating elements. With the working frequency given, the propagation phase for each path can be calculated. By referencing to the element which has the shortest path from the horn, the phase differences between this element and others can then be determined. The difference is exactly the phase shift required by that particular radiating element. By knowing the phase differences, the dimensions of all of the radiating elements can be directly

extracted from the S curve to construct the reflectarray model, which can be simulated using the CST Microwave Studio software. The performances of the reflectarray will then be verified by experiments. Every design step shown in Figure 2.1 will be further explained in the subsequent sections.

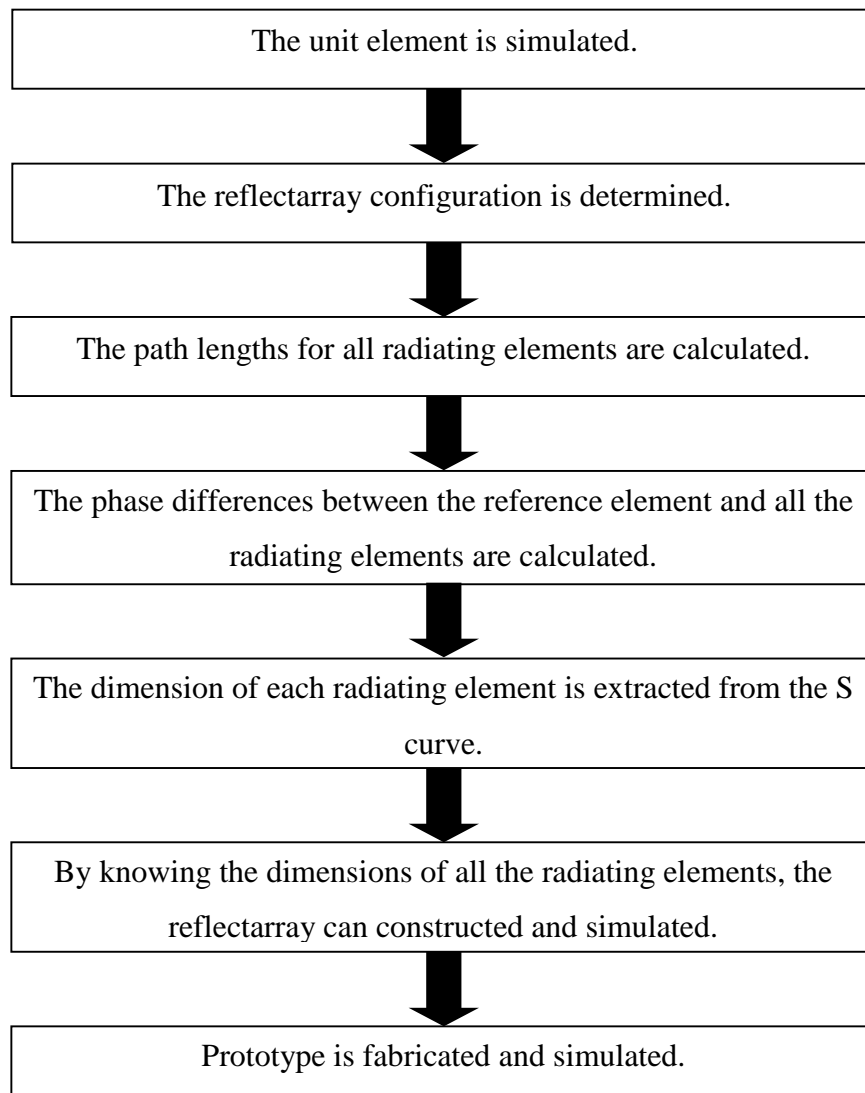


Figure 2.1: Steps for Designing a General Reflectarray Antenna using Phase Only Optimization Technique.

2.3 Simulation of Unit Element

The objective of simulating the unit element of a reflectarray is to understand the characteristics of its reflection loss and phase. It can be done by varying the design parameter that contributes to phase shift. Therefore, it is important to find a design parameter that is able to give sufficient changeable phase range when it is varied. Two popular simulation methods that have been used for designing and simulating the reflectarray unit element are Floquet method and Waveguide method.

2.3.1 Waveguide Method

When the waveguide method is applied for unit element simulation, all of the boundaries of the waveguide walls are defined to be perfect electric conductors (PEC). With reference to Figure 2.2, the unit element is placed at one end of the waveguide whereas the port excitation is at the other end of the waveguide. The incident angle (θ) of the incident wave at the waveguide port can be calculated using (2.1) at a certain operating frequency. In this method, it is not possible to simulate a square unit element as the cell dimension has to follow the aperture size of the waveguide ($a \times b$).

$$\theta = 90^\circ - \cos^{-1} \sqrt{1 - \left(\frac{f_c}{f}\right)^2} \quad (2.1)$$

where

f_c = waveguide cutoff frequency, Hz

f = operating frequency, Hz

θ = incident angle of the incident wave at the waveguide port ($^\circ$)

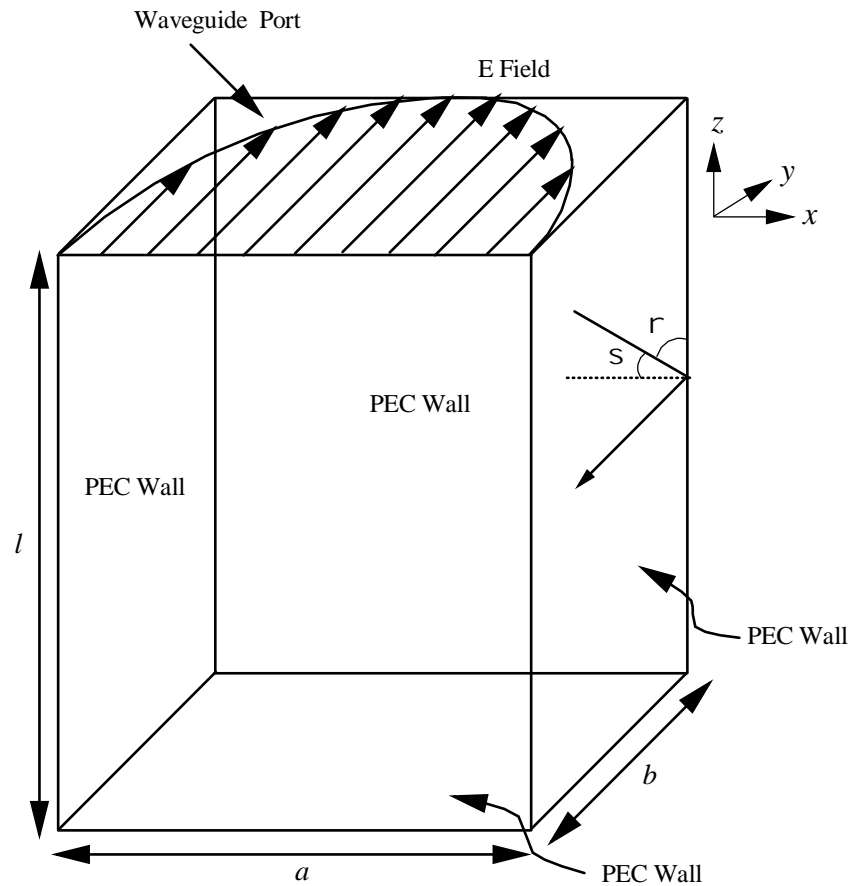


Figure 2.2: Oblique Incidence in the Waveguide Model with the Boundary Conditions given.

2.3.2 Floquet Method

When applying the Floquet method, the boundary conditions must be defined to be perfect magnetic conductors (PMC) for the two lateral walls and perfect electric conductor (PEC) for other two, as shown in Figure 2.3. This method can provide more precise simulation results as it has considered mutual coupling between the radiating elements (Dzulkipli, et al., 2012). It has provided more degrees of design freedom as the incident angle, θ , at the Floquet port is not a function of operating frequency. Therefore, the incident angle and the working frequency can be freely chosen. However, the performances of a unit element cannot be verified as Floquet method cannot be implemented in practice.

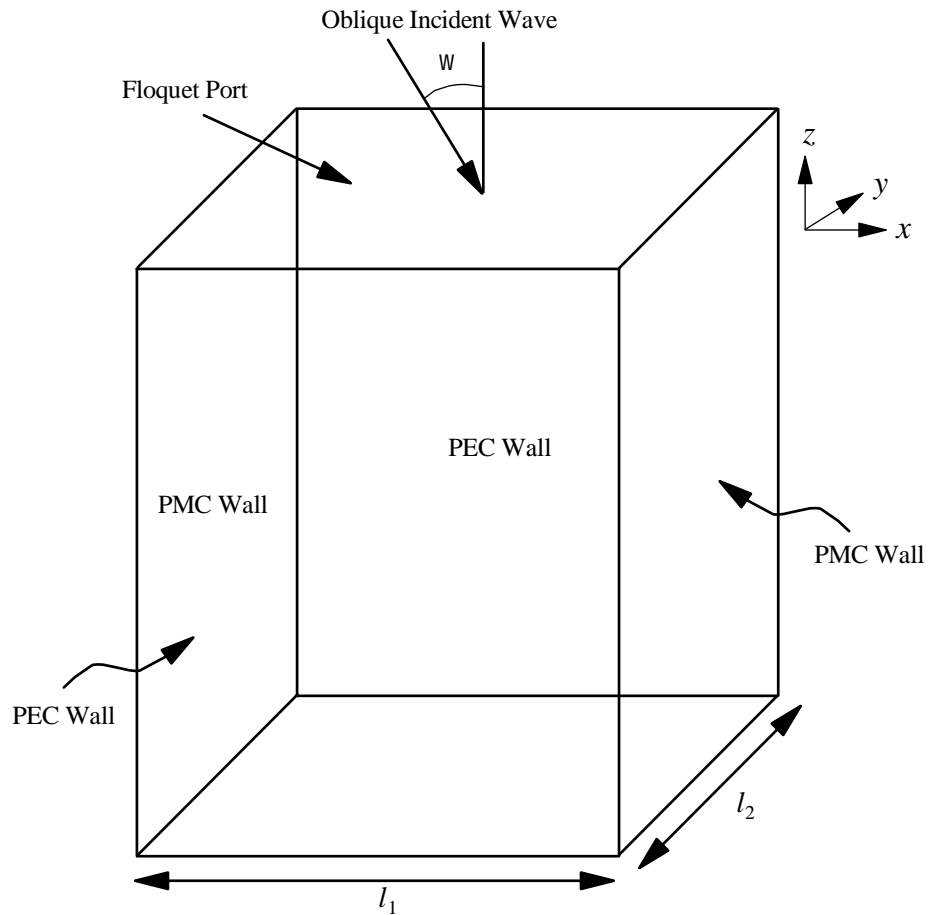


Figure 2.3: Oblique Incidence in the Floquet Model with the Boundary Conditions given.

2.4 Configuration of Reflectarray

Before designing a reflectarray, the position of the feeder and the array size must be first determined. The antenna gain is much dependent on the number of radiating elements in the reflectarray. Normally, a larger antenna gain can be achieved if more radiating elements are used to design the reflectarray. The side view of a general reflectarray is displayed in Figure 2.4. As can be seen from the figure, the feeder is commonly placed at a focal distance (f) from the middle point of the reflectarray radiation aperture. The positions of all the radiating elements must be located in the far-field region of the feeder. Figure 2.4 shows the side-fed ($>0^\circ$) configuration, which is usually more favourable as the feeder does not block the radiation beam. The focal distance (f) and the dimension (D) of the reflectarray aperture are linked

together and they are usually expressed as a ratio f/D , which is typically around $f/D = 1$ (Zhao, et al., 2013).

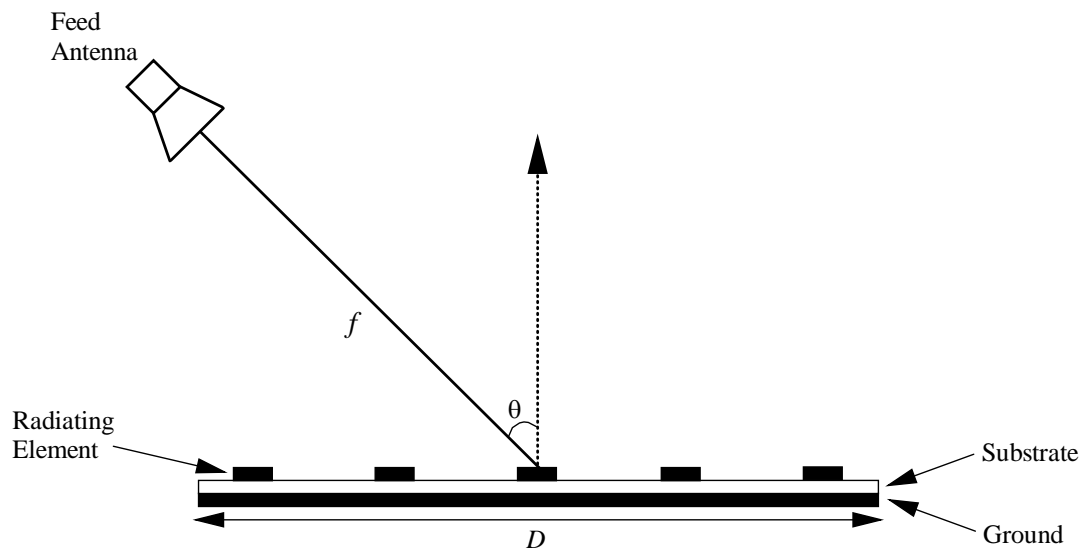


Figure 2.4: Side View of a General Reflectarray.

2.5 Calculation of Path Length

The propagation paths of the EM wave beams from the feeder to all of the radiating elements are labelled as $L_1, L_2, L_3, L_4, \dots, L_n$, which are shown in Figure 2.5. After determining the feeder position and the location of a particular radiating element, the path length that is travelled by the wave beam from the feed horn to this specific element can then be calculated. This path length is equal to the propagation phase of the wave beam at a constant frequency. Since all of the radiating elements are placed at different distances from the feed horn, the respective propagating wave beams will experience different path lengths ($L_1, L_2, L_3, L_4, \dots, L_n$).

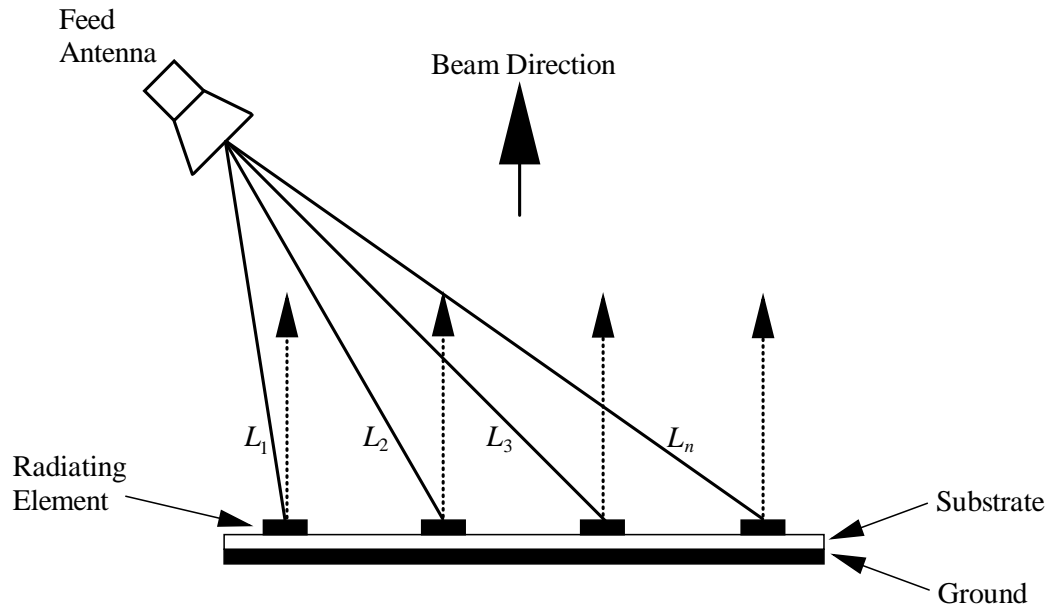


Figure 2.5: Path Lengths from the Feeder to the Radiating Elements.

2.6 Calculation of Path Difference

By referencing to the shortest-path element, the phase difference between the reference and a particular element can be calculated using (2.2). It can be seen that this is actually done by comparing the path lengths of the two.

$$\phi_{1-n} = \frac{2f(P_n - P_1)}{\lambda_0} \quad (2.2)$$

where

P_n = path length from feeder to n -element, m

P_1 = path length from feeder to reference element, m

λ_0 = wavelength at the operating frequency of reflectarray, m

ϕ_{1-n} = phase difference between the reference element and the n -th element, rad

The calculated phase difference is the extra phase shift that is required by the n -th element so that it can have equal propagation phase with the reference element. By introducing additional phase shifts to all radiating element, a planar wave front can

then be formed right before the reflectarray radiation aperture, forming a coherent wave beam.

2.7 Extraction of Radiating Element Dimension

The dimensions of all of the radiating elements can be extracted from the S-curve, provided the phase difference between each element and the reference is known.

2.8 Simulation of Reflectarray

The reflectarray model is then constructed based on the extracted dimensions from the S curve. CST Microwave Studio software is used to simulate the model. In the simulation, a feed horn is used as the microwave source and its actual dimension is known. Once completing the construction of the reflectarray model and the feed horn, simulation can be started. Radiation properties of the reflectarray can be easily visualized from the simulated results.

CHAPTER 3

DRA REFLECTARRAY UNIT ELEMENTS WITH THIN UNDER-LOADING PARALLEL SLOTS

3.1 Introduction

Reflectarray antenna was first introduced by Berry *et al.* (Berry, et al., 1963) in 1963. However, the structure was constructed using matrices of open-ended apertures made of bulky truncated waveguides. This serious drawback had limited the applications of the reflectarrays in many places. Not until the late 1980s, has the introduction of printed microstrip reflectarrays (Huang & Encinar, 2007; Pozar, et al., 1997) shed light on the possibility of making such reflector structure planar and light. Since then, a myriad of planar reflectarrays have been proposed because they can provide the good features of both of the reflector antenna and phased array. Reflectarray is also well received by space-related applications because of its light weight, low profile, and low cost. However, the antenna bandwidth of a microstrip reflectarray is somehow tied up with its resonator bandwidth, which is usually narrow. Over the past decades, much effort has been dedicated to broadening the bandwidth of microstrip reflectarrays. Among those suggested, multilayer structures (Encinar, 2001) and multiple resonators (Bialkowski & Sayidmarie, 2008) are the popular ways that have been used for extending bandwidth.

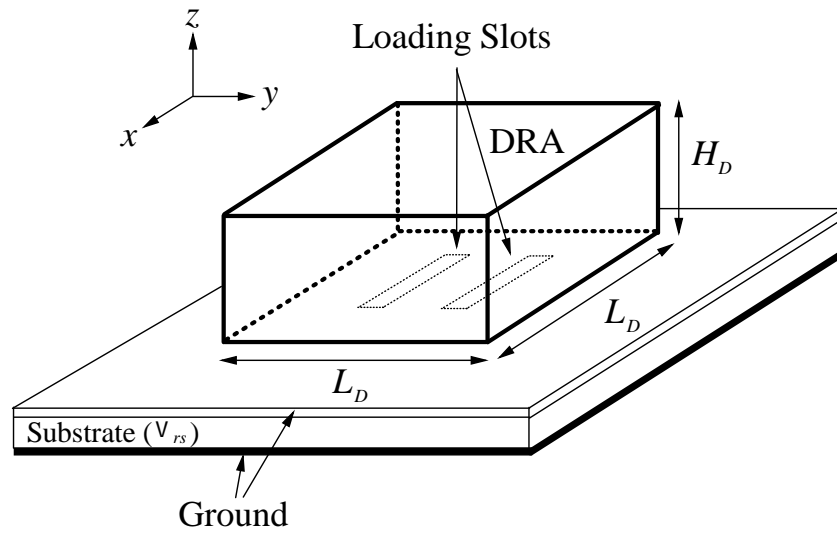
Microstrip elements can introduce significant conductive loss at high frequencies. And it can be translated into reflection loss for a reflectarray. As a result, dielectric resonator antenna (DRA) has attracted much attention because it is made of dielectric material (Long, et al., 1983). DRA can appear in different shapes such as

cylindrical, rectangular, square, conical, and triangular (Petosa & Ittipiboon, 2010). Due to having low loss and the ability to generate efficient radiation, DRA has been explored for designing various reflectarray antennas to achieve large reflection phase range, slow gradient of reflection phase slope, as well as low reflection loss. In (Abd-Elhady, et al., 2012; Zainud-Deen, et al., 2011), the length of the DRA element is varied so that a reflection phase range of 360° is obtainable. However, this can cause many problems in the manufacturing process as different sizes of DRAs are needed. Cutting the super-hard dielectric resonators into different sizes is always very tough. Etching slots onto the ground surface beneath a DRA unit element was also demonstrated to be a possible way to introduce reflection phase shift to an incoming wave (Zainud-Deen, et al., 2010; Abd-Elhady, et al., 2010). However for both cases, very little design freedom is available as slot width is the only parameter to tune. Later, in (Abd-Elhady, et al., 2010), the under-loading slot is combined with a metal stub tuner in a multilayer structure where the stub length is varied for changing reflection phase. The involvement of multilayer structure, unfortunately, has made the implementation extremely tedious.

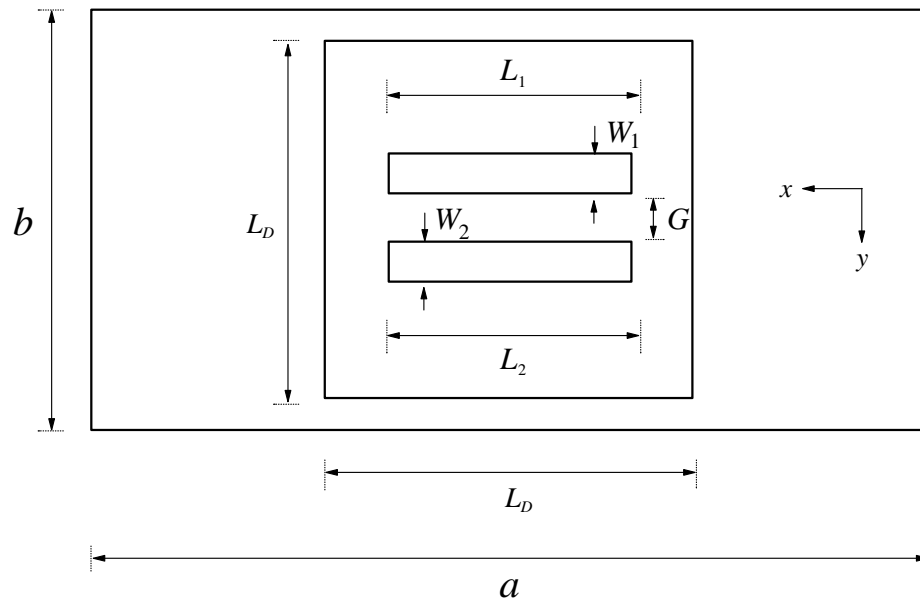
In this chapter, three DRA reflectarray elements loaded with multiple under-loading slots on a single layer are studied. It is found that the case loaded with two slots on the ground plane can offer a reflection phase range of larger than 300° . Slots with different dimensions will be studied. Simulation was done using the CST Microwave Studio software, with measurement carried out on a Vector Network Analyzer (VNA) for substantiation. Good agreement is found between the simulation and measurement results.

3.2 Reflectarray Unit Cell Configuration

Figure 3.1 (a) shows the perspective view of the proposed reflectarray unit element loaded with two rectangular slots underneath the DRA. Duroid RO4003C (thickness of $h = 1.524$ mm and dielectric constant of $\nu_r = 3.38$) is used as the substrate. With reference to Figure 3.1 (b), the dimensions of the slots are given by: $W_1 = W_2 = 0.15$ mm and $G = 0.5$ mm. In this case, the slot lengths L_1 and L_2 are functioning as phase-shifting parameters. As can be seen from the figure, two rectangular slots are etched on the top metallic surface of the substrate, with its bottom laminated by another layer of metal. A square DRA ($L_D = 14$ mm, $H_D = 6$ mm, and dielectric constant of $\nu_r = 7$) is then stacked on top of the slots. As can be seen in Figure 3.1 (b), the slots are symmetrically aligned to the center point of the bottom surface of the DRA. Figure 3.1 (c) is the photograph of the fabricated prototype. Waveguide method is used to model the reflectarray element. Figure 3.2 (a) illustrates the simulation model of the DRA reflectarray element. CST Microwave Studio is used for all of the simulations. The slots are aligned orthogonal to the direction of electric fields in a section of C-band (5.8 GHz – 8.2 GHz) waveguide ($a = 34.85$ mm \times $b = 15.8$ mm) with a length of 154 mm. With reference to Figure 3.2 (a), a y -polarized wave is generated at the wave port and it propagates to the DRA element, which is placed on another end of the waveguide section. All of the lateral walls are defined to be perfect electric conductors (PEC). Figure 3.2 (b) shows the measurement setup which composes of a waveguide section which is connected to a coaxial-to-waveguide adaptor. In measurements, with the use of a flat shorting plate, the reference plane is de-embedded flush to the adaptor flange. The substrate is carefully trimmed so that it can fit into the waveguide aperture. A rectangular trench with depth of ~ 1.5 mm is cut on the metal plate to accommodate the substrate, as can be seen in Figure 3.2 (b).



(a)

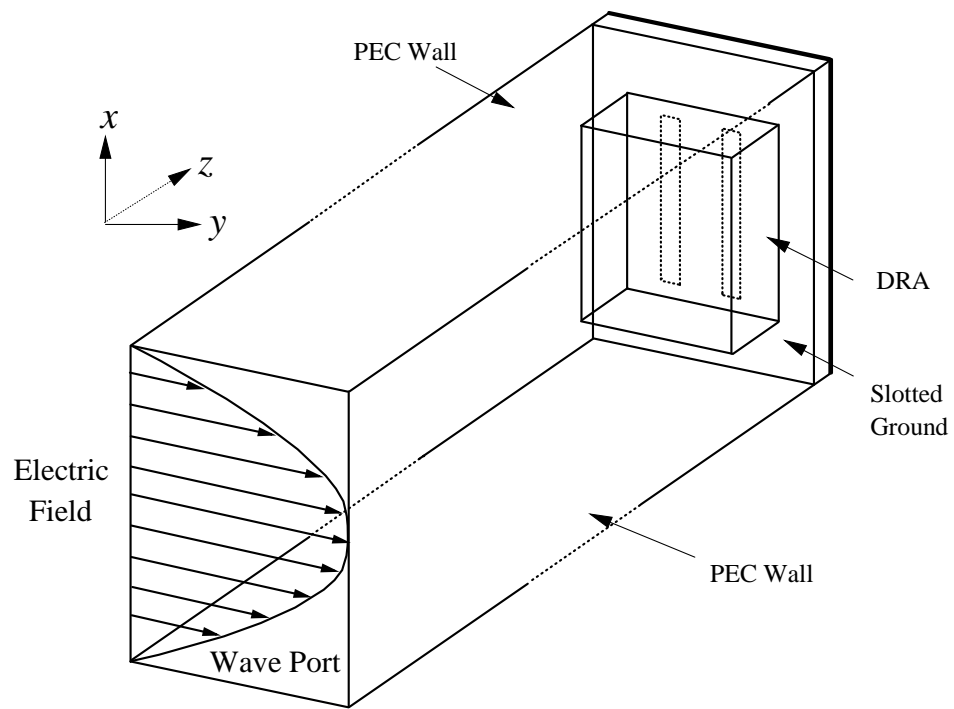


(b)



(c)

Figure 3.1: Square DRA Unit Element Loaded with 2 Slots Underneath. (a) Perspective View. (b) Top-Down View. (c) Photograph of the Fabricated Prototype.



(a)



(b)

Figure 3.2: (a) Simulation model for the DRA unit cell. (b) Experimental setup for the waveguide method.

3.3 Unit Cell Simulation and Measurement

The field characteristics of the DRA unit element are first studied for $L_1 = L_2 = 5.5$ mm. Figure 3.3 depicts the simulated and measured reflection loss and reflection phase. Reasonable agreement with low reflection loss (> -0.65 dB) is found across the frequency bandwidth of 7.3 – 7.7 GHz. Low reflection loss is achievable due to the absence of conductive loss in the dielectric resonator.

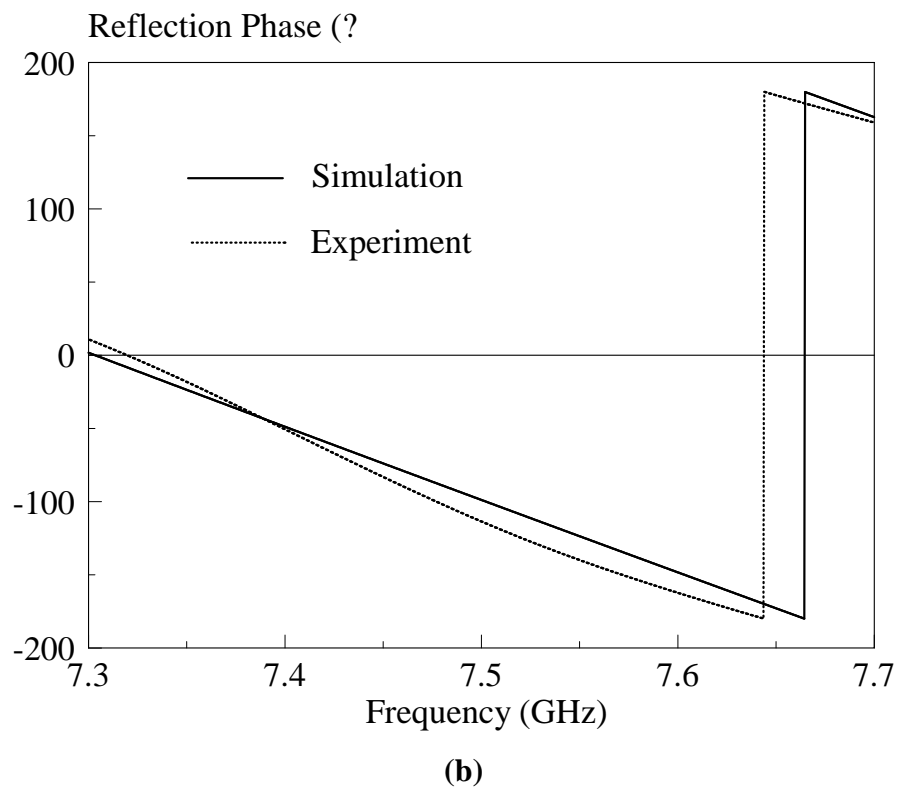
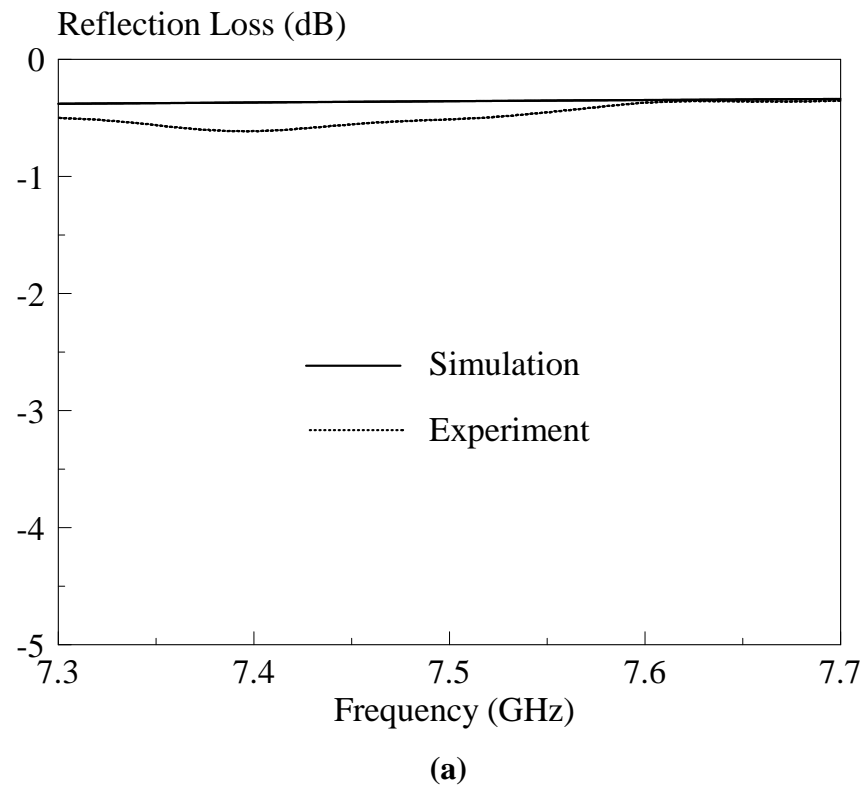
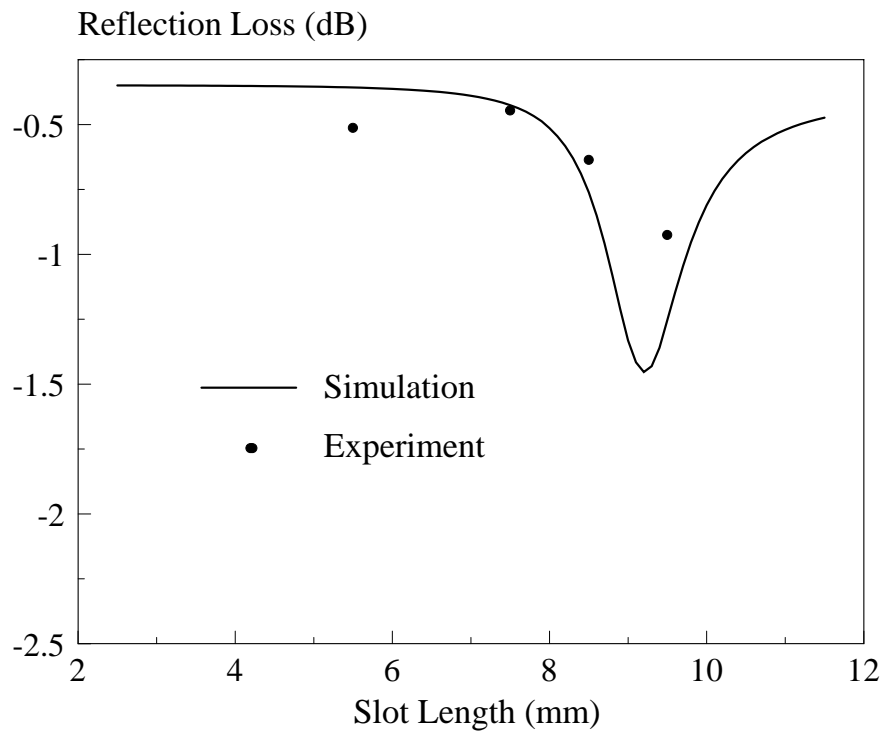


Figure 3.3: Simulated and Measured (a) Reflection Loss, (b) Reflection Phase of the DRA Reflectarray Unit Element with Two Under-Loading Slots ($L_1 = L_2 = 5.5$ mm, $W_1 = W_2 = 0.15$ mm, $G = 0.5$ mm).

Next, the phase-shifting effect of the unit element is studied by varying the slot lengths L_1 and L_2 , both of which are made equal in this case. Figure 3.4 shows the simulated and measured reflection loss and phase range of the proposed unit element with two under-loading slots beneath. Reasonable agreement has been observed. With reference to Figure 3.4 (a), the measured reflection loss maximizes at -0.9 dB (simulation: -1.4 dB) at the slot length of 9.5 mm. This can be caused by the energy loss at resonance which is around 7.5 GHz when the slot length is 9.5 mm. Figure 3.4 (b) depicts the measured and simulated reflection phases, which are more commonly known as S Curves, where good agreement is observed. By varying slot length, as can be seen from the figure, the reflection phase range is 313° , which is sufficient for designing the small-size reflectarrays.



(a)

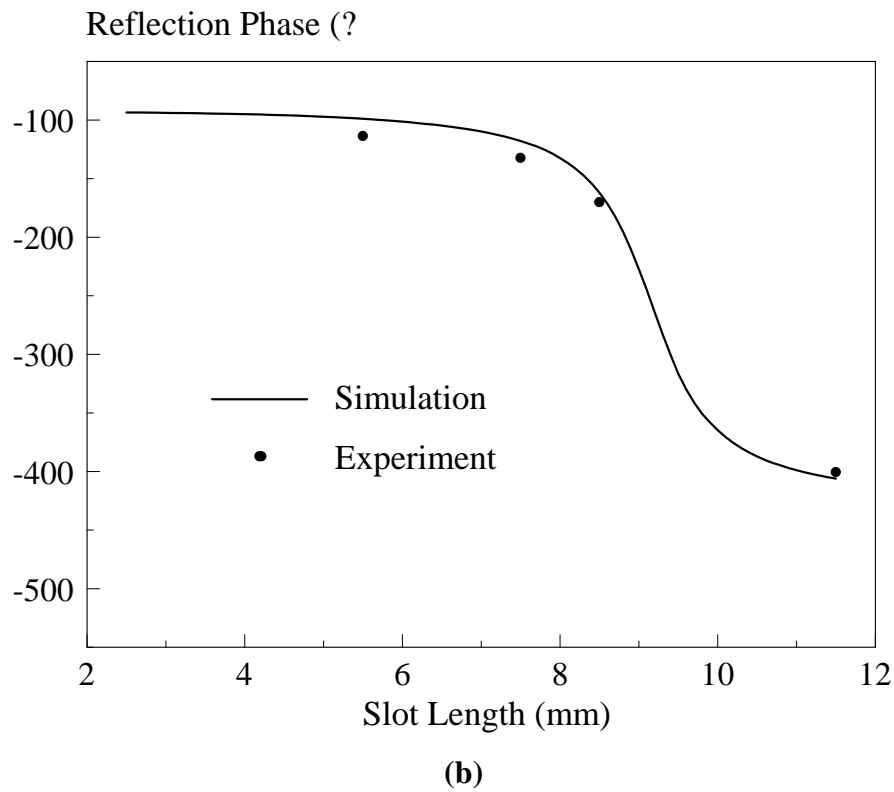
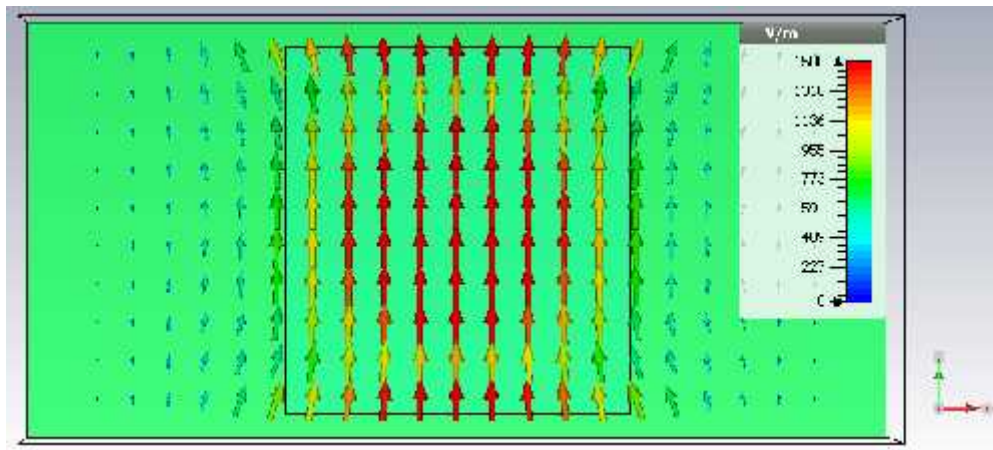


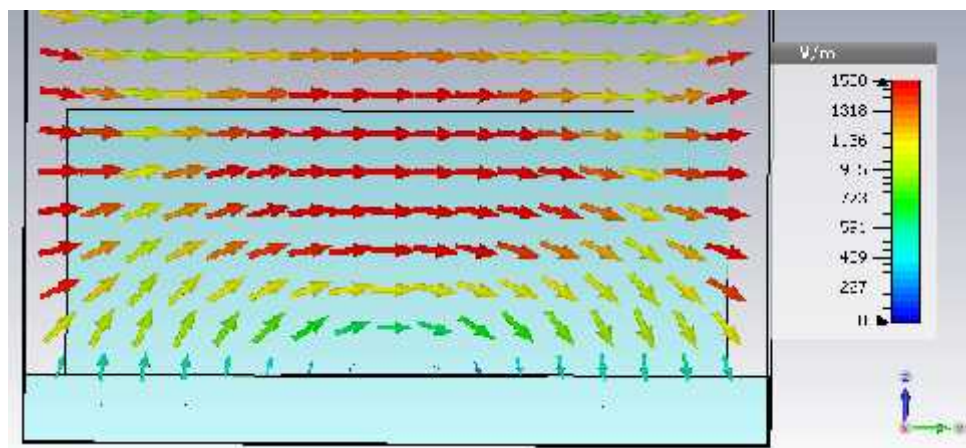
Figure 3.4: Simulated and Measured (a) Reflection Loss, (b) Reflection Phase at 7.5 GHz of DRA Unit Element with Two Under-Loading Slots.

3.4 Field Distribution in Reflectarray Unit Element

Figure 3.5 shows the electric field vectors in the DRA at the operating frequency of 7.5 GHz. It can be justified from the field distribution that this is the TE_{111}^x mode of the square DRA (Petosa, 2007).



(a)



(b)

Figure 3.5: Electric Field Distribution of the DRA Reflectarray Unit Element at 7.5 GHz. (a) Top-down view. (b) Side view.

The resonant frequency for the TE_{mnl}^x mode of the square DRA can be calculated using (3.1) (EMAG Technologies Inc., 2013; Neshati & Wu, 2000). For the square DRA with dimension of $L_D = 14\text{mm}$, $H_D = 6\text{ mm}$, and dielectric constant of $\nu_r = 7$, the resonant frequency is calculated to be $f_{111} = 7.42\text{ GHz}$ which is very close to the simulated resonant frequency of 7.5 GHz.

$$f_{r(mnl)} = \frac{c}{2f \sqrt{\epsilon_r}} \sqrt{\left(\frac{mf}{L_D}\right)^2 + \left(\frac{nf}{L_D}\right)^2 + \left(\frac{lf}{2H_D}\right)^2} \quad (3.1)$$

where

m, n and l are positive integers

$c = 3 \times 10^8$, m/s

ϵ_r = dielectric constant of DRA

L_D = length and width of DRA, m

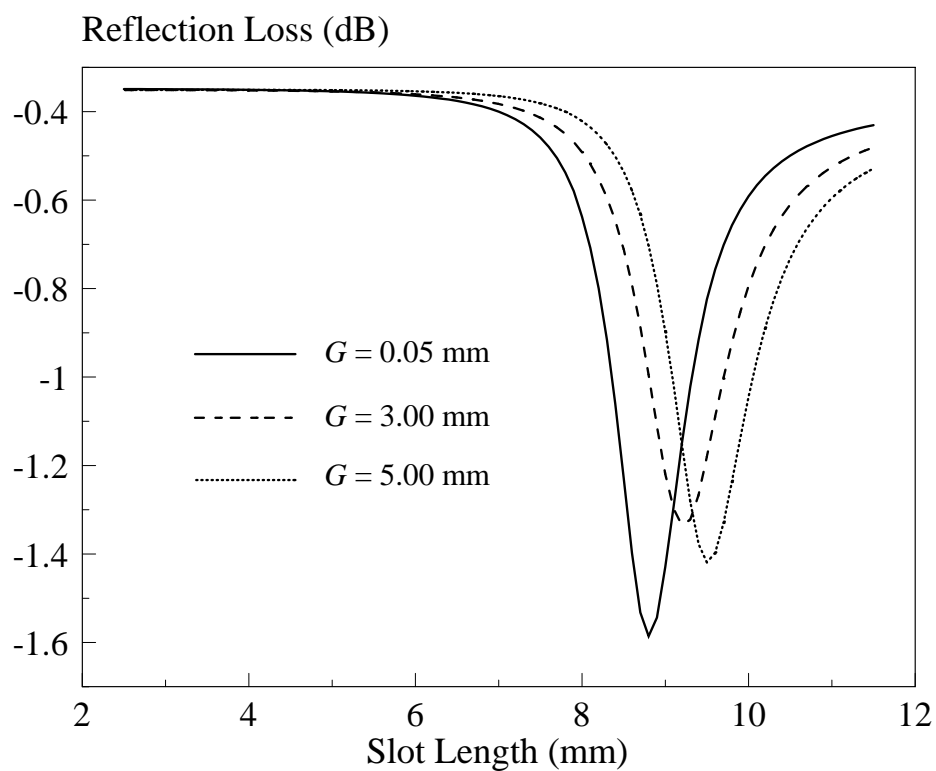
H_D = height of DRA, m

3.5 Parametric Analysis

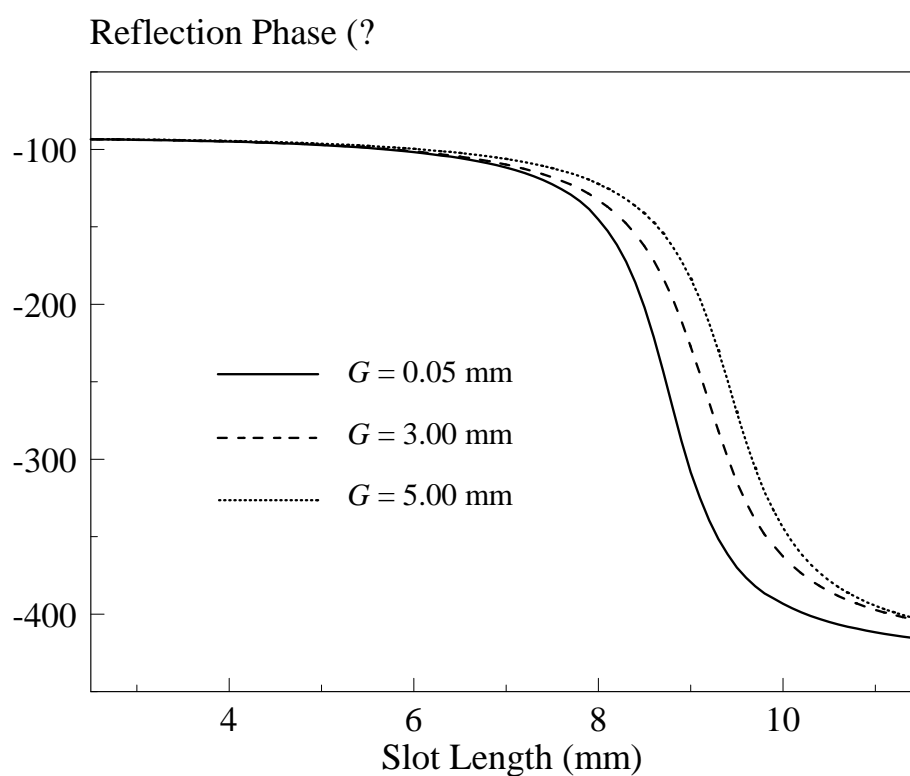
In this section, parametric analysis has been performed to study the effects of the under-loading slots on the reflection loss and S curve. First of all, the effects of slots separation and slot widths on the reflection loss and reflection phase are studied. Also, studies have been conducted to investigate multiple under-loading slots, DRA misalignment, dielectric constant, and thickness of the substrate. Detailed explanation is provided in each parametric analysis.

3.5.1 Gap Separation between Slots

The effect of the separation distance between the two gaps is first studied. Referring to Figure 3.6, it can be seen that reflection loss maximizes at a shorter slot length when the gap distance becomes closer, which can be caused by additional coupling between the two slots. For all cases, the phase ranges are greater than 300° .



(a)

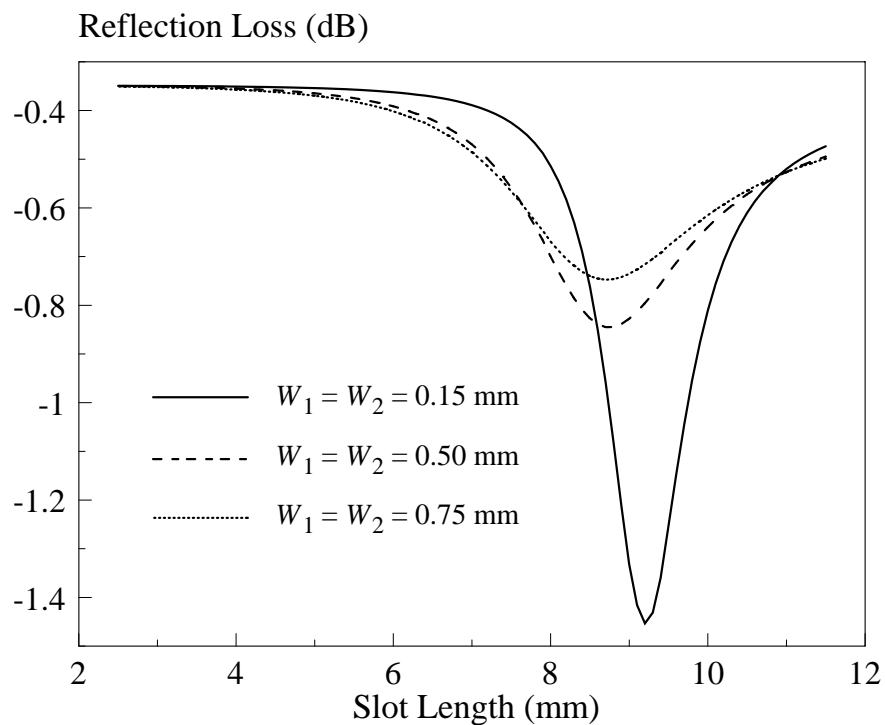


(b)

Figure 3.6: Effect of Gap Separation Between the Two Slots on (a) Reflection Loss, (b) Reflection Phase.

3.5.2 Slot Width

The effects of changing slot widths and slot lengths are studied in this section. In first study, the width (W_1 , W_2) of both of the slots are varied at the same time. With reference to Figure 3.7 (a), the maximum reflection loss reduces from -1.45 dB to -0.77 dB when both of the slots are increased from 0.15 mm to 0.75 mm. On the other hand, narrow slot is good for a larger phase range, as can be seen in Figure 3.7 (b).



(a)

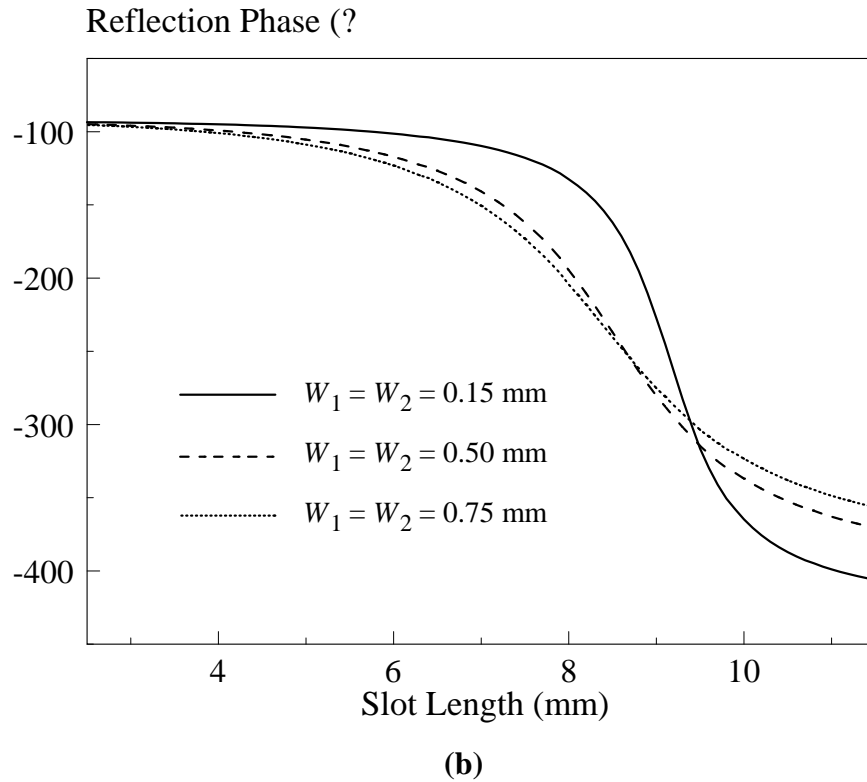


Figure 3.7: Effect of Varying the Widths of the Two Slots on the (a) Reflection Loss, (b) Reflection Phase.

In the second study, with reference to Figure 3.8 and 3.9, only one slot is varied while another is kept unchanged. Two cases are considered. In the first case, only one of the slot widths W_2 is varied while another W_1 remains unchanged ($W_1 = 0.15$ mm). In the second, only W_1 is varied while W_2 is kept a constant ($W_2 = 0.15$ mm). It can be observed that both cases have the same effects on the reflection loss and reflection phase, as depicted in Figure 3.8 and 3.9. For the cases of W_1 (or W_2) = 0.5 mm and 0.75 mm, as can be seen in Figure 3.8 (a) and Figure 3.9 (a), the reflection losses become slightly greater than those in Figure 3.7 (a) when only one of the slots is made wider. It can be seen from Figure 3.8 (b) and Figure 3.9 (b) that the phase range for each parameter is close to its counterpart in Figure 3.7 (b).

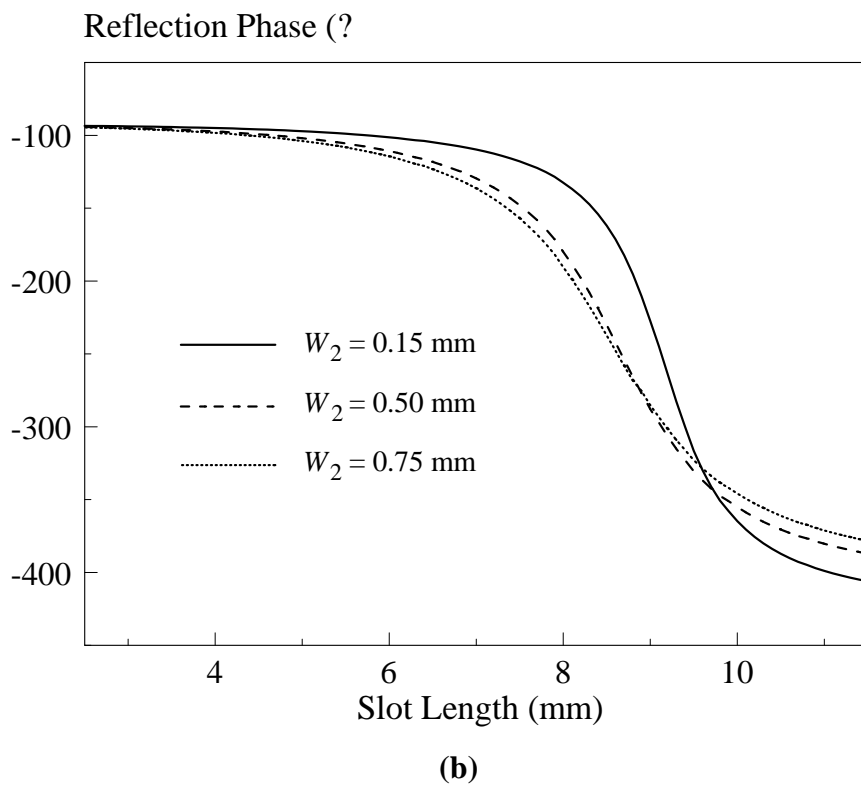
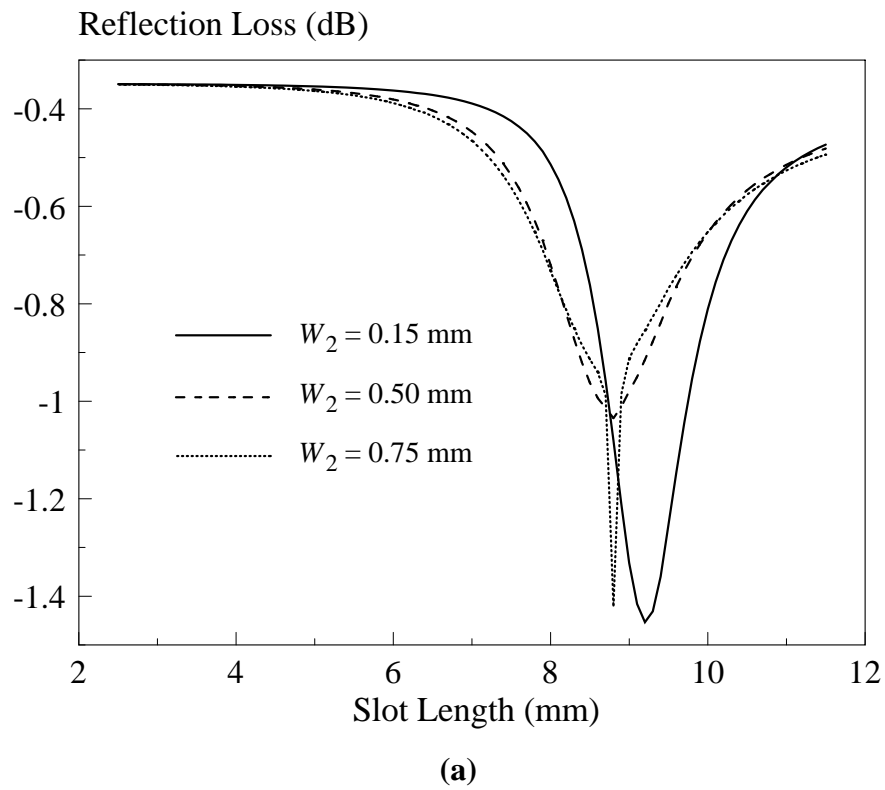


Figure 3.8: Effect of Changing the Slot Width W_2 on the (a) Reflection Loss, (b) Reflection Phase.

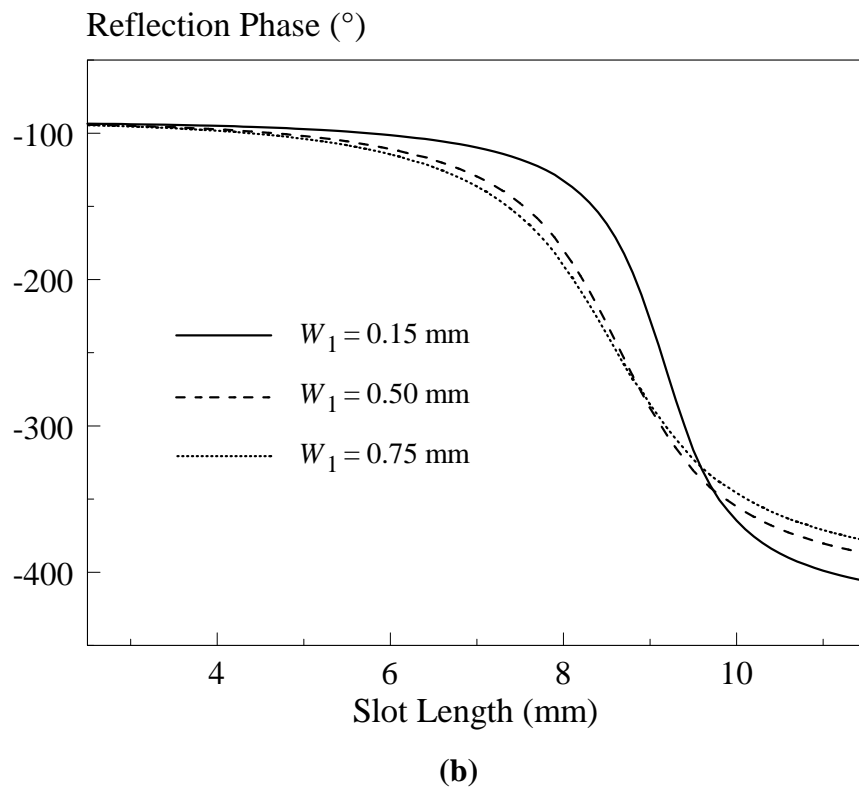
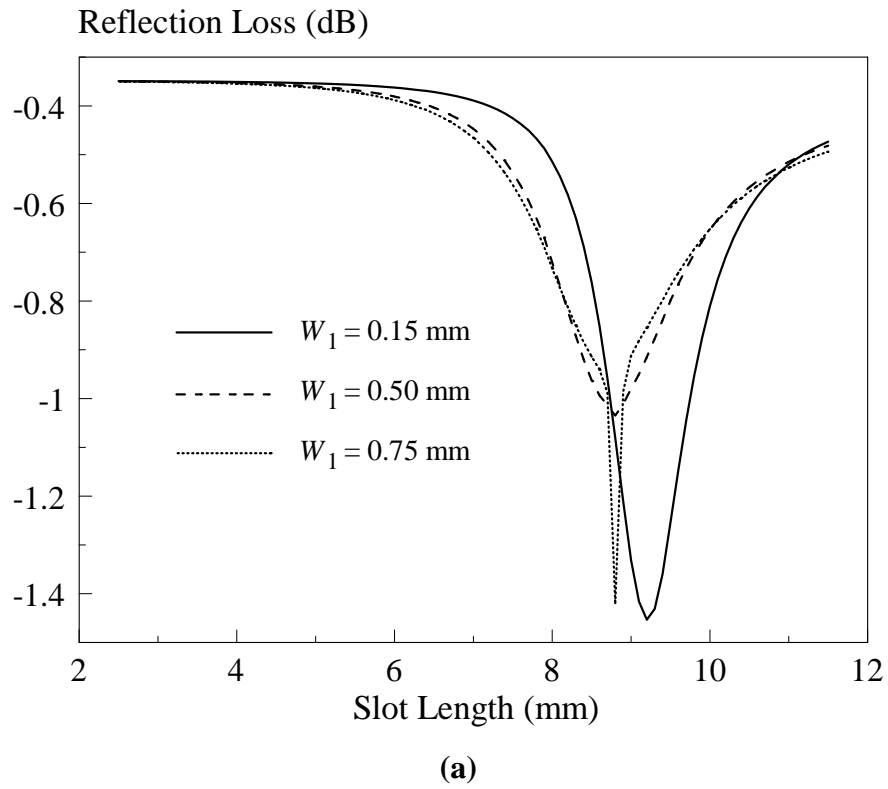
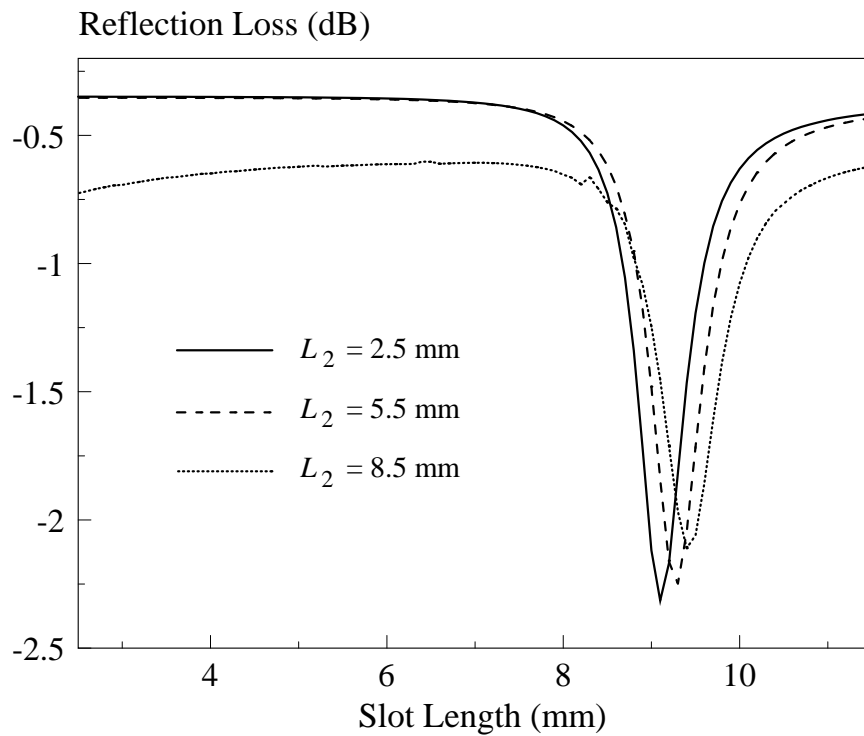


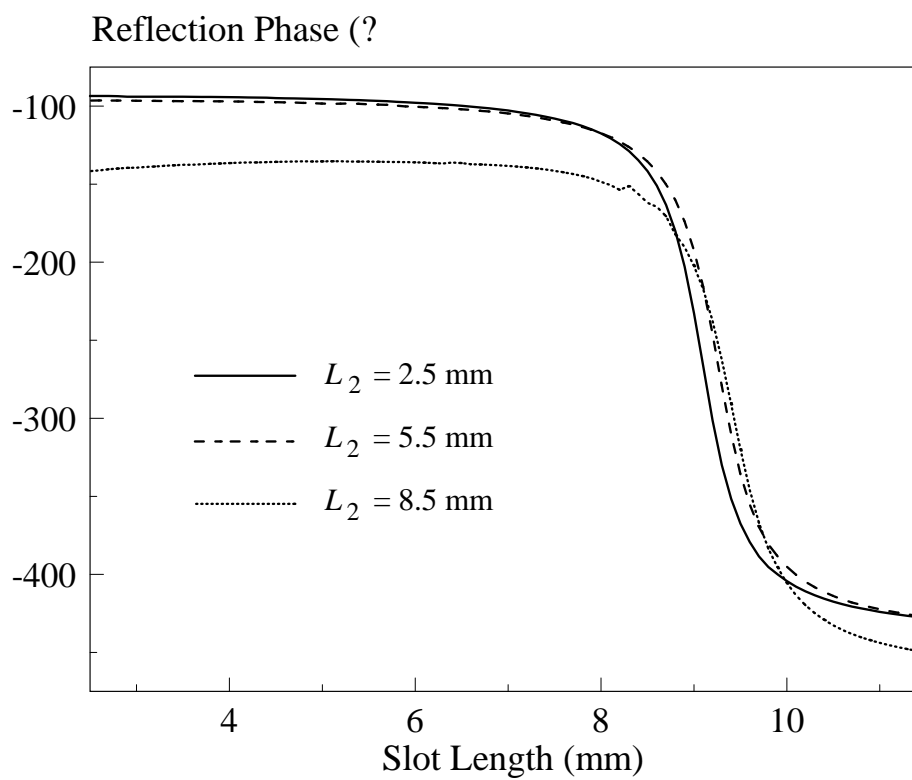
Figure 3.9: Effect of Changing the Slot Width W_1 on the (a) Reflection Loss, (b) Reflection Phase.

3.5.3 Slot Length

Next, the effects of slot lengths on the reflection loss and reflection phase are studied. Here, only one slot length is varied while another is kept unchanged. In the first case, with reference to Figure 3.10, the slot length L_1 is varied while the slot length L_2 remains unchanged. In the second case, with reference to Figure 3.11, the slot length L_2 is varied while the slot length L_1 is kept constant. It can be noticed that both of the cases have similar effects on the reflection loss and reflection phase. By fixing the slot length L_2 (shown in Figure 3.10) and the slot length L_1 (shown in Figure 3.11) at 2.5 mm, 5.5 mm, or 8.5 mm respectively, it is obvious that varying only one slot length in each case does not affect the reflection performance much.

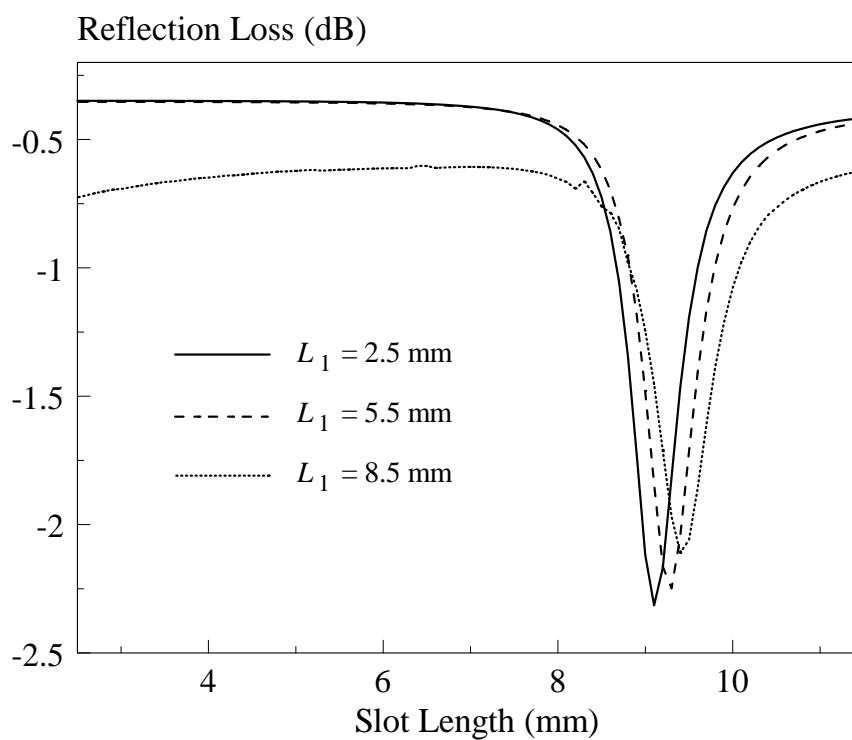


(a)



(b)

Figure 3.10: Effect of the Slot Length L_1 on the (a) Reflection Loss, (b) Reflection Phase.



(a)

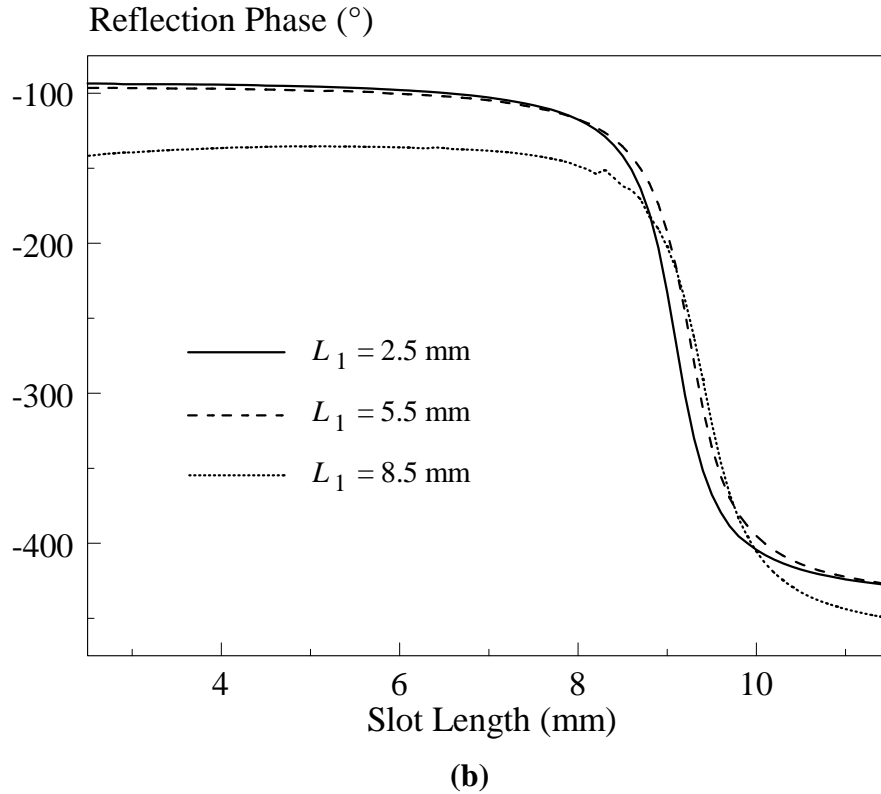
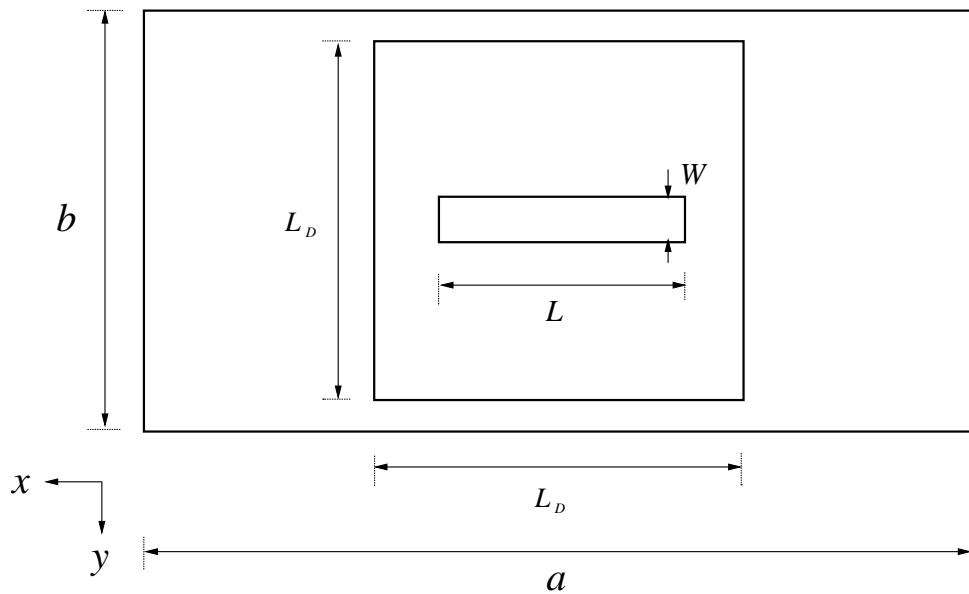


Figure 3.11: Effect of the Slot Length L_2 on the (a) Reflection Loss, (b) Reflection Phase.

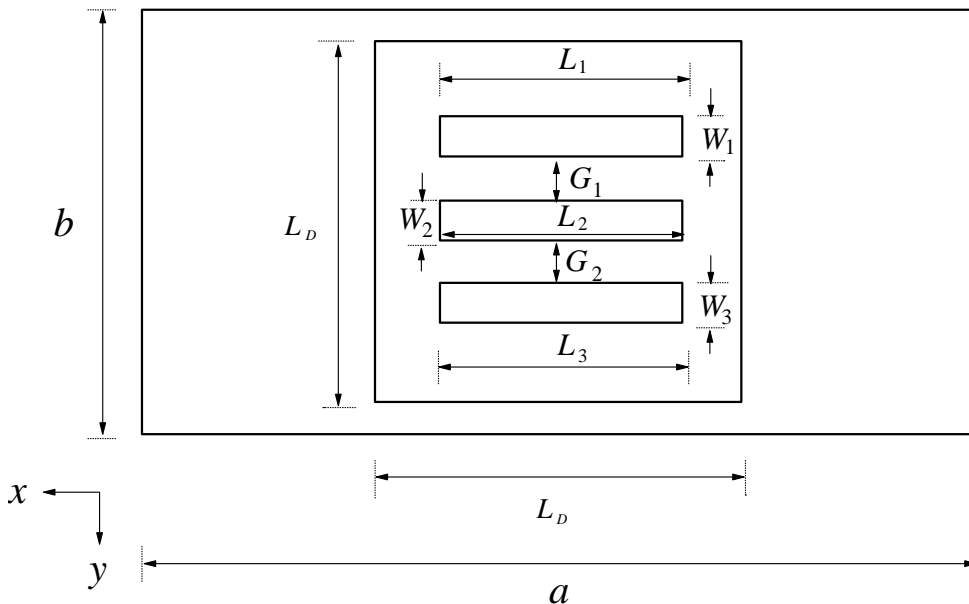
3.5.4 Multiple Under-Loading Slots

Similar DRA which is loaded with one and three slots are simulated for comparison. The configurations are given in Figure 3.12. The slot dimensions of the single slot case are given by: $W = 0.15$ mm and $L_D = 14$ mm. For the triple slots, the design parameters are $W_1 = W_2 = W_3 = 0.15$ mm, $G_1 = G_2 = 0.5$ mm. Other parameters are identical to those for the two slots case in Figure 3.1. In both cases, the lengths of all the slots are made equal and they are varied simultaneously for introducing phase change to the reflection phase. Also, their gap widths are made to be equal with that of the two-slot case (Figure 3.1) for ease of comparison. Figure 3.13 shows reflection losses and reflection phase ranges of the unit cells with one, two, and three under-loading slots. It can be seen from Figure 3.13 (a) that the reflectarray element with two slots has the lowest reflection loss (-1.45dB) at resonance. The under-loading single and triple slots have higher reflection loss of -2.4 dB and -7 dB, respectively.

Figure 3.13 (b) shows the reflection phase ranges for the three cases. The DRA reflectarray with a single under-loading slot has the broadest phase range but the steepest gradient. This may compromise the available design choices. The phase change becomes slower with increasing the number of slots, but it comes at the price of a smaller phase range.



(a)



(b)

Figure 3.12: (a) Square DRA Unit Element Loaded with (a) 1 Slot and (b) 3 Slots Underneath.

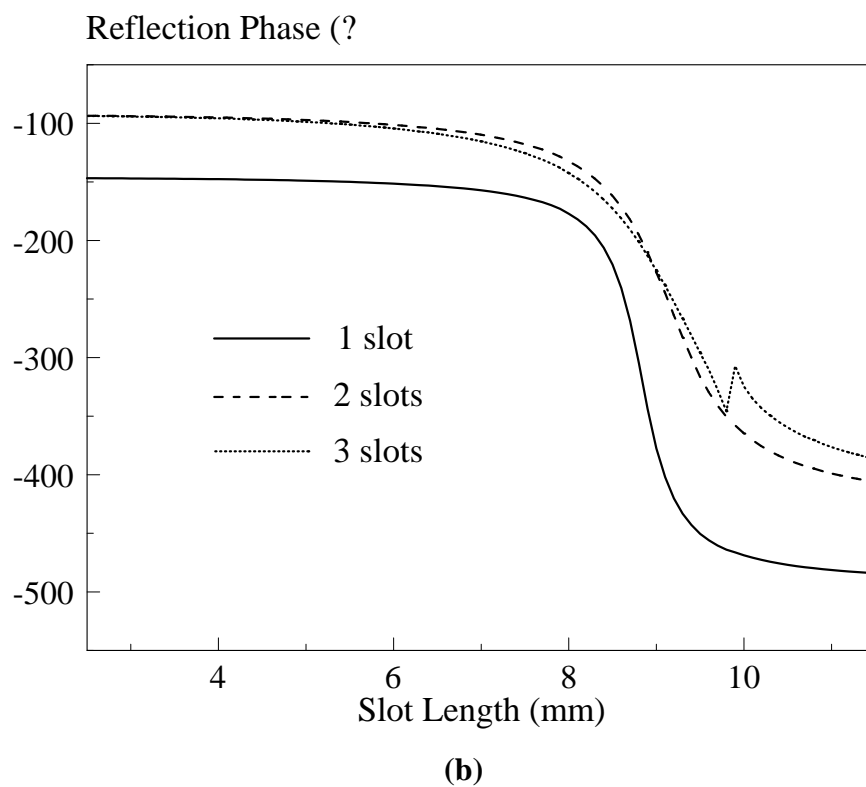
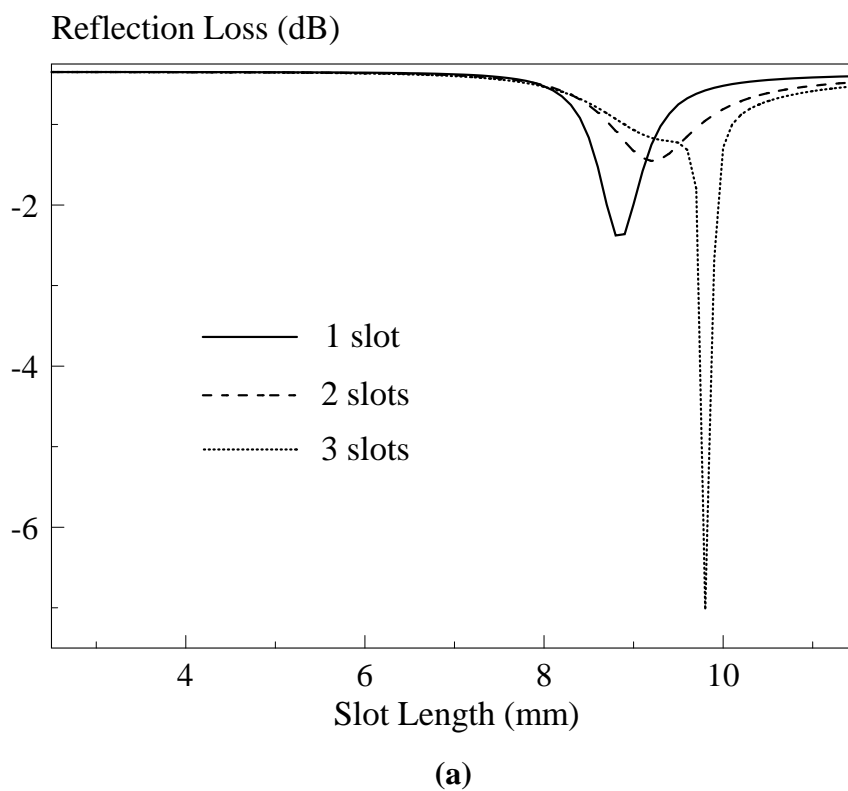
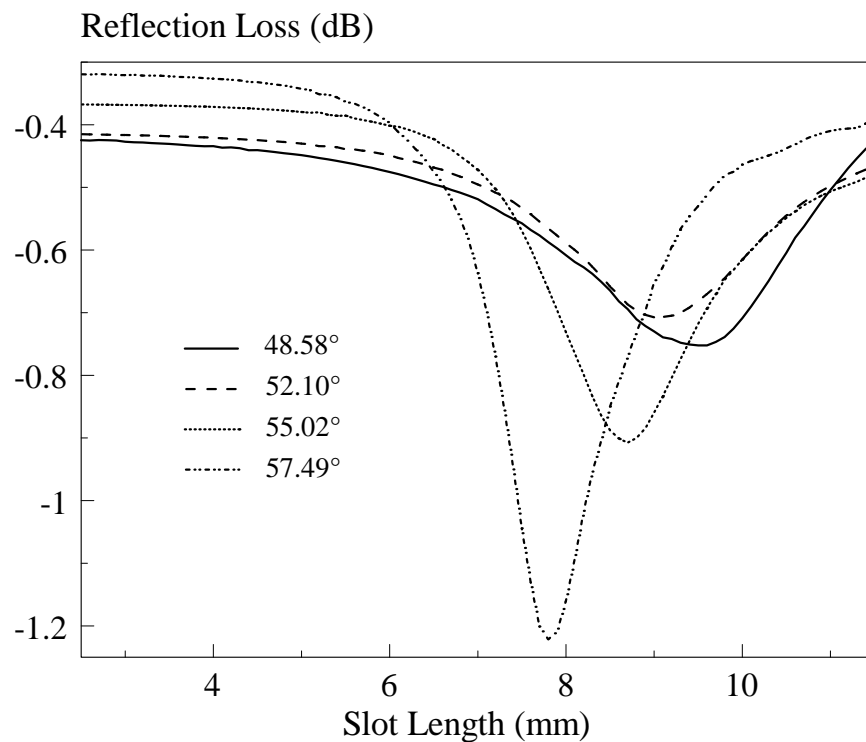


Figure 3.13: Comparison of the (a) Reflection Loss, (b) Reflection Phase of the DRA Reflectarray Unit Element with Different Under-Loading Slots.

3.5.5 Oblique Incidence

The effect of oblique incidence is now studied. In a rectangular waveguide, the incident angle (Γ) can be calculated using $\Gamma = 90^\circ - \cos^{-1} \sqrt{1 - \left(\frac{f_c}{f}\right)^2}$, where f_c (4.3 GHz) is the cutoff frequency of the waveguide and f is the operating frequency. For the C-band waveguide working in the frequency range of 5.8 GHz – 8.2 GHz, oblique incident angles of 48.58° (at 6.5 GHz), 52.1° (at 7GHz), 55.02° (at 7.5 GHz), and 57.49° (at 8 GHz) can be used to simulate the reflection losses and phase ranges shown in Figure 3.14. With reference to Figure 3.14 (a), it can be seen that reflection loss increases proportionally with the incident angle. Figure 3.14 (b) shows that the reflection phase range is not affected so much by the incident angle.



(a)

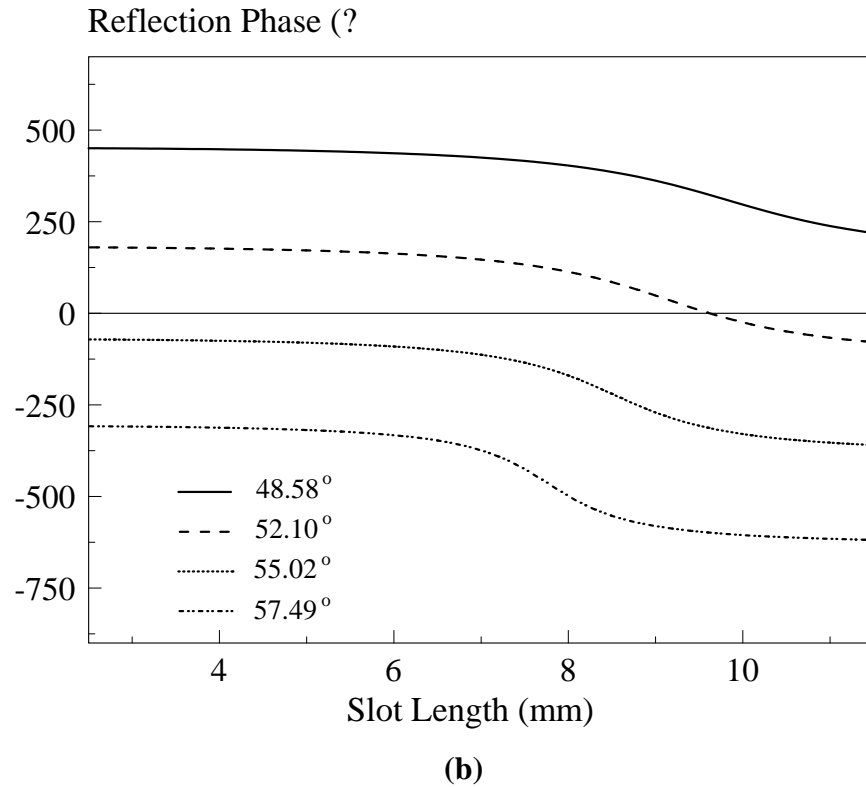


Figure 3.14: Comparison of the (a) Reflection Loss, (b) Reflection Phase of the DRA Reflectarray Unit Element at Different Oblique Incident Angles.

3.5.6 DRA Alignment

The effects of DRA alignment on the reflection loss and reflection phase are also studied. With reference to Figure 3.15 and 3.16, it was found that the reflection loss and phase range are not affected much if the slots are intentionally misaligned with a displacement of 4 mm with respect to the centre point of the DRA. This is very promising as it shows that the proposed DRA unit element has good tolerance to the DRA misplacement.

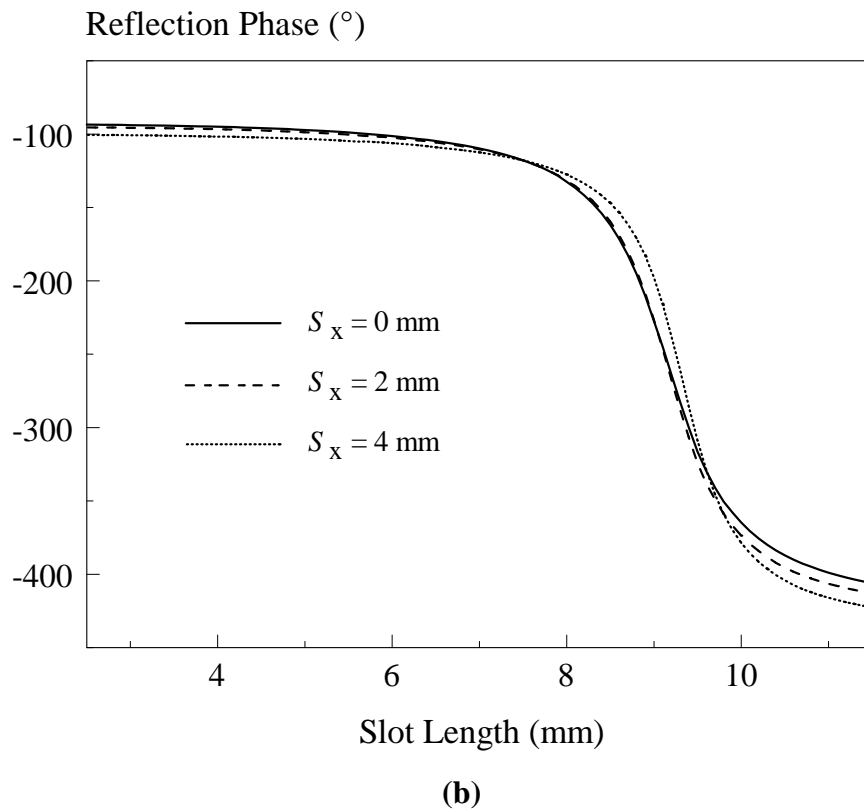
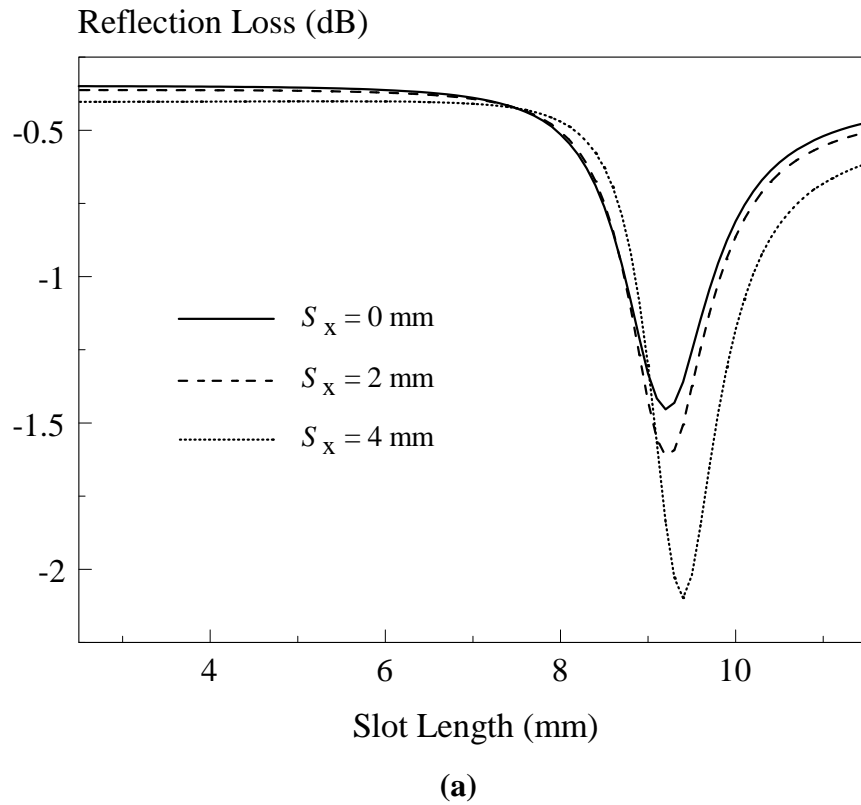
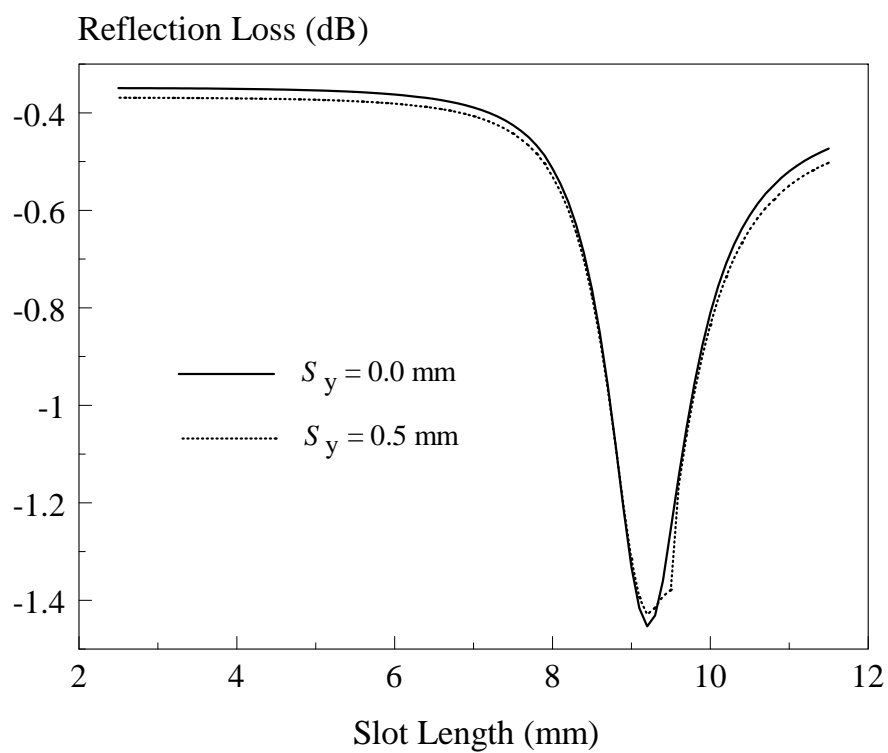
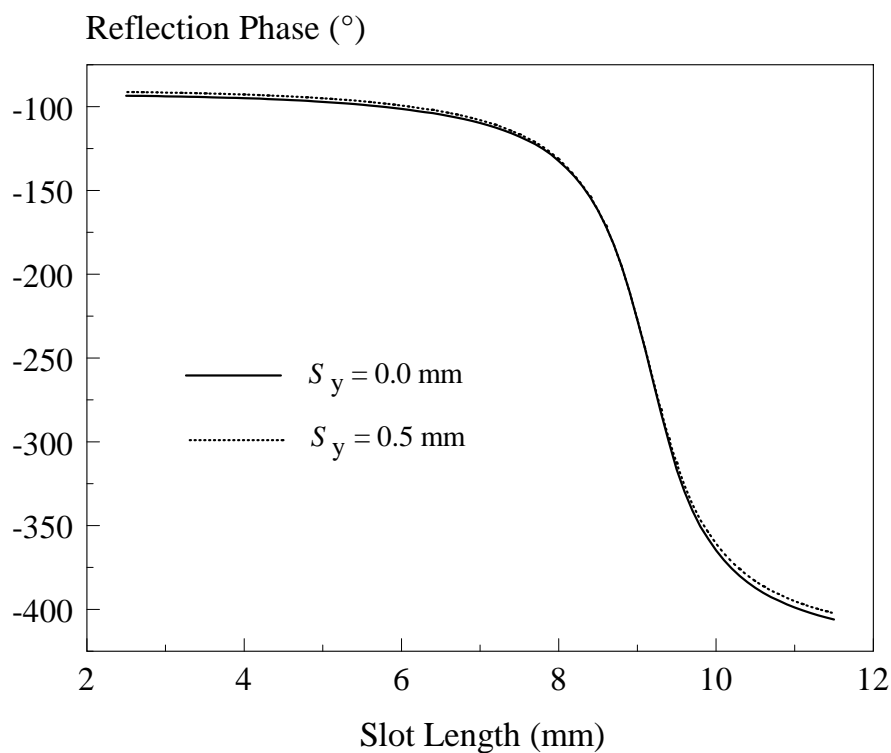


Figure 3.15: Effect of the DRA Misaligned (x -direction) on the (a) Reflection Loss, (b) S Curve.



(a)

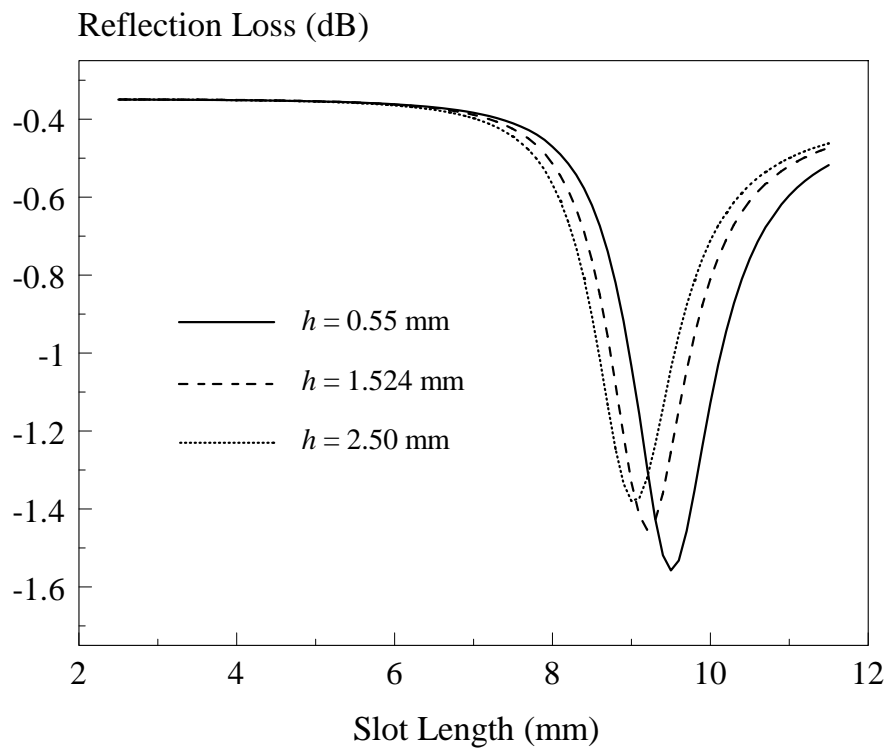


(b)

Figure 3.16: Effect of the DRA Misaligned (y-direction) on the (a) Reflection Loss, (b) S Curve.

3.5.7 Substrate Thickness

In this section, the effect of substrate thickness on the reflection loss and reflection phase is visualized. Referring to Figure 3.17, the unit element is simulated with the use of different substrate thicknesses (0.55 mm, 1.524 mm, and 2.50 mm). As can be seen from Figure 3.17 (a), the reflection loss decreases when the substrate is made thicker. However, the phase range is about the same for the substrate thicknesses of 0.55 mm, 1.524 mm, and 2.50 mm. The only change in the reflection phase is that its slope gradient becomes slower when the substrate is made thicker, as depicted in Figure 3.17 (b).



(a)

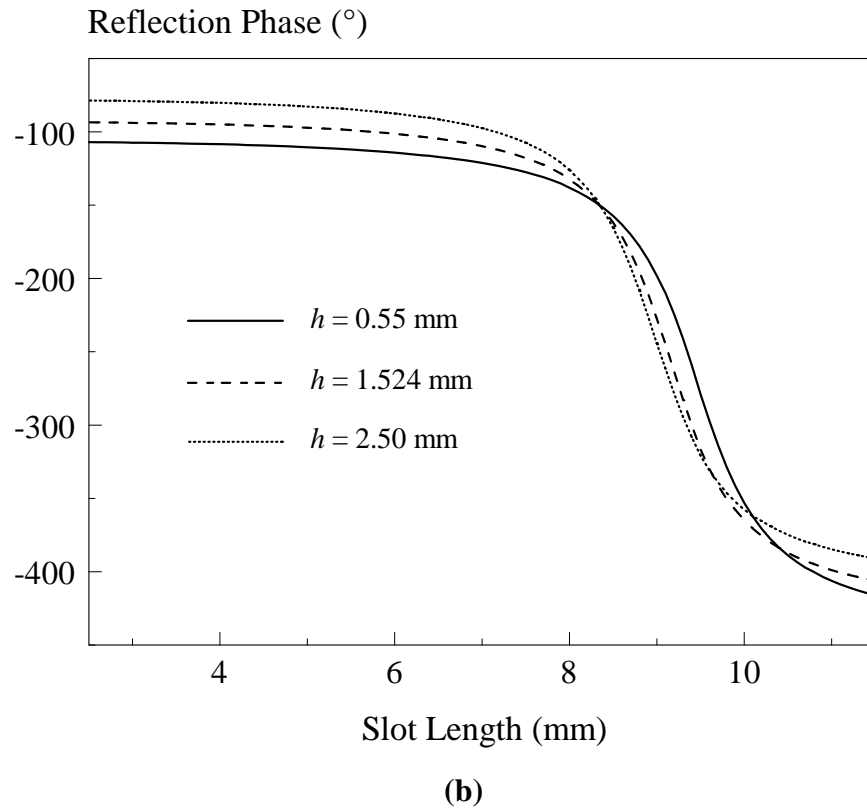
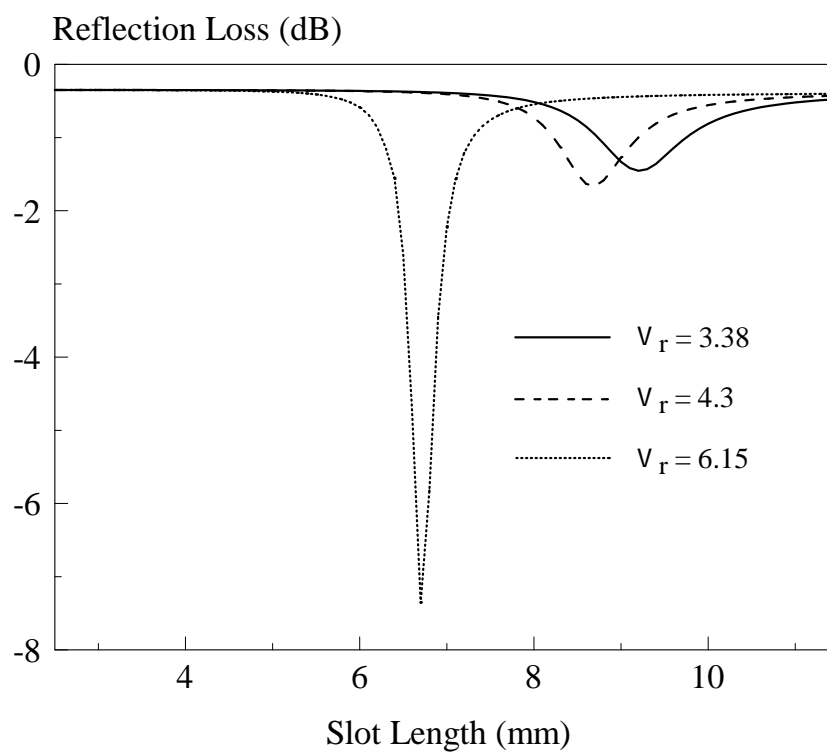


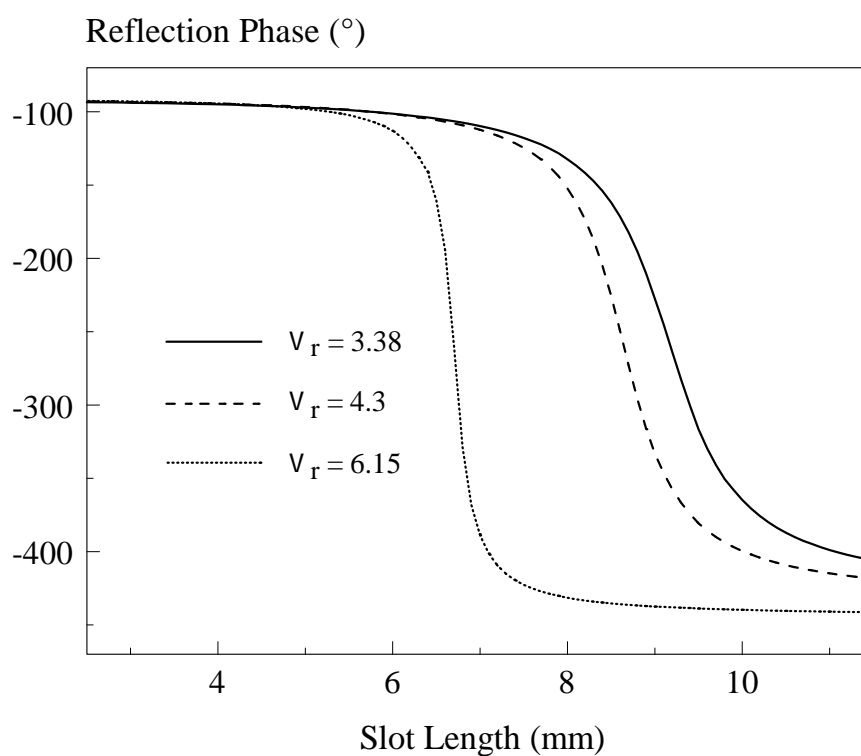
Figure 3.17: Effect of the Substrate Thickness on the (a) Reflection Loss, (b) S Curve.

3.5.8 Substrate Dielectric Constant

The effect of the substrate dielectric constant on the reflection loss and reflection phase is studied here. With reference to Figure 3.18 (a), it can be observed that the unit element resonates at different slot lengths at 7.5 GHz when the substrate is made to have dielectric constant of 3.38, 4.3 and 6.15. It is obvious that reflection loss increases with increasing of the dielectric constant of the substrate. With the use of a larger dielectric constant, steeper phase slope is obtainable, as can be seen in Figure 3.18 (b). Thus, in this case, it is good to use a substrate with dielectric constant of 3.38 as it has low loss and slower gradient of phase slope.



(a)

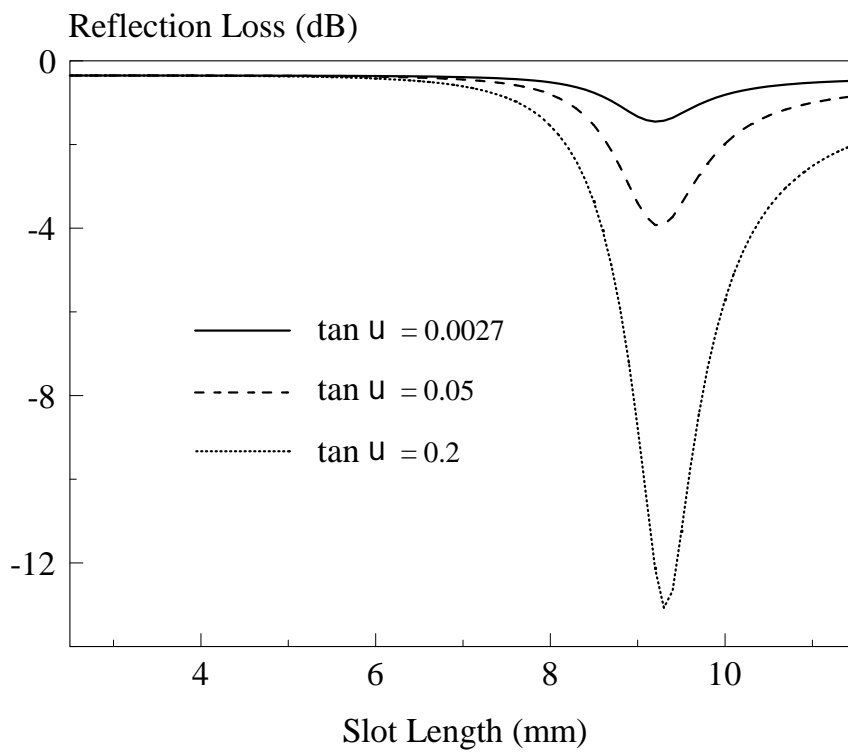


(b)

Figure 3.18: Effect of the Substrate Dielectric Constant on the (a) Reflection Loss, (b) S Curve.

3.5.9 Substrate Loss Tangent

Lastly, the effect of the substrate loss tangent on the reflection loss and reflection phase is studied. Different types of substrates can have different loss tangents. For substrates with loss tangents of 0.0027, 0.05 and 0.2, their reflection losses are peaking at ~ -1.5 dB, ~ -4 dB and ~ -13 dB, respectively, as can be seen in Figure 3.19 (a). Higher loss tangent introduces greater reflection loss, which is expected.



(a)

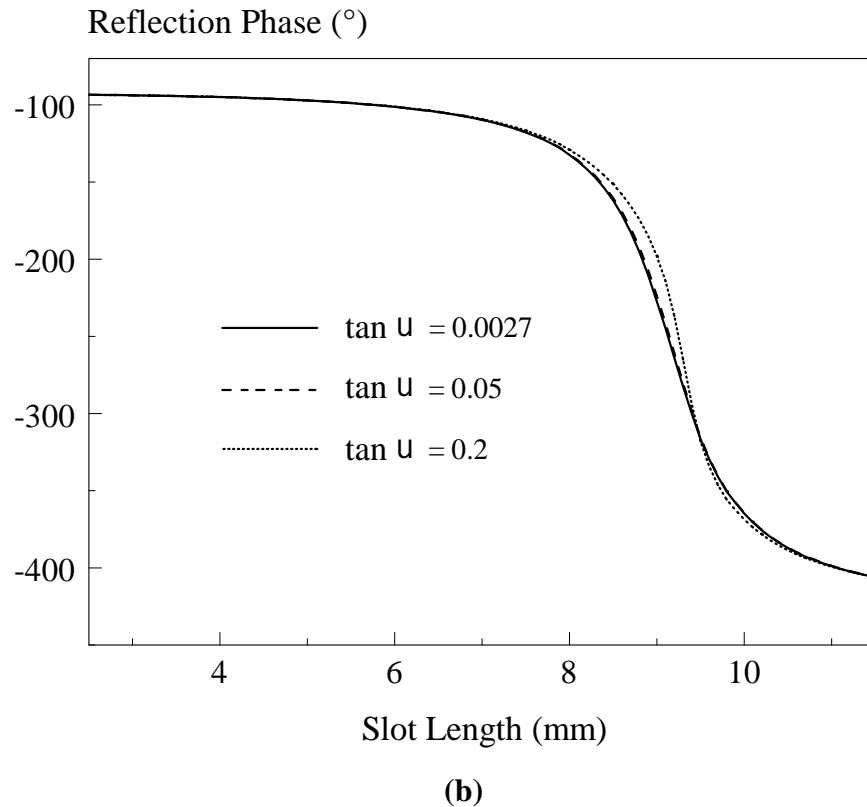


Figure 3.19: Effect of the Substrate Loss Tangent on the (a) Reflection Loss, (b) S Curve.

3.6 Conclusion

DRA unit elements loaded with one, two, and three parallel and thin slots beneath have been studied. It is found that narrowing the slot width is good for increasing the phase range of the S Curve. Also, the separation distance and width of multiple parallel thin slots can be used as additional parameters for tuning the reflectarray performance. For the proposed DRA unit element loaded with two slots underneath, a phase range of 313° is attainable for designing a small-size reflectarray. The proposed configuration is very compact as it does not require the use of any active electronic components. Good agreement has been found between the simulation and experimental data.

CHAPTER 4

BROADRANGE REFLECTARRAY ELEMENT WITH COMBINED SLOT AND DIELECTRIC RESONATOR RESONANCES

4.1 Introduction

Since its introduction in 1963 (Berry, et al., 1963), reflectarray has attracted much attention because it is able to capture the good features of both of the reflector antenna and phased array. The emergence of microstrip-based reflectarrays (Huang & Encinar, 2007; Pozar, et al., 1997) in the late 80s has made this type of planar antennas popular for space-related applications because of their light weight, simple structure, and low cost. Despite its popularity, the antenna bandwidth of a microstrip reflectarray is usually low. It is limited by the high quality factor of the microstrip patch resonator. On top of that, the conductive loss of the metal-made microstrip can also be translated to reflection loss. This is very undesirable as it causes the radiation efficiency of the reflectarray to reduce significantly. As a result, in recent years, much attention has been diverted to the dielectric resonator antenna (DRA) because it is free from conductive loss (Long, et al., 1983). DRA can appear in arbitrary shapes such as conical, triangular, rectangular, square, and cylindrical (Petosa & Ittipiboon, 2010). Various DRA reflectarrays have been explored for achieving low reflection loss, large reflection phase range, and slow changing rate in the S curve (Abd-Elhady, et al., 2012; Zainud-Deen, et al., 2011). However, most of the reported cases have a phase range of less than 360° .

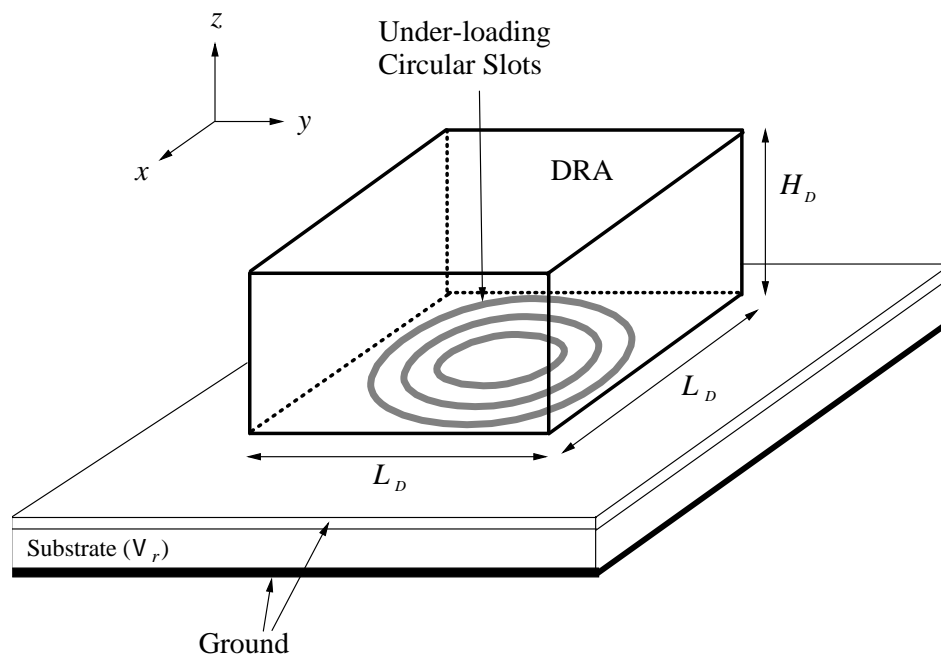
Broad reflection phase range in its S curve is one of the most important criteria in designing a large-size reflectarray. In (Li, et al., 2011), a broadrange

microstrip reflectarray that is composed of two elliptical rings has been proposed to generate a reflection phase range of 450° . In this case, phase shift is obtained by varying the minor axis of the elliptical rings. Despite its broad phase range, it has high reflection loss (-35 dB), which is very undesirable. In 2002, Misran et al. (Misran, et al., 2002) proposed a double-layered structure which is built by stacking ring elements to provide reflection phase range of greater than 500° . However, the multilayer structure has made its implementation very tedious. Later, in (Carrasco, et al., 2006), a U-shaped true time delay line was explored for designing a wideband reflectarray, where its line length is used as the phase shifter to yield a very wide phase range of 1600° . The reflection loss of this reflectarray is low, but unfortunately it requires the use of multilayer technology. A simple circular ring loaded with an open-circuited stub with variable length was also studied and it was found that it was able to give a phase range of 450° (Li, et al., 2011; Li, et al., 2011). However, it is not easy to vary the length of the stub as the impedance matching between the ring and the stub has to be done very carefully.

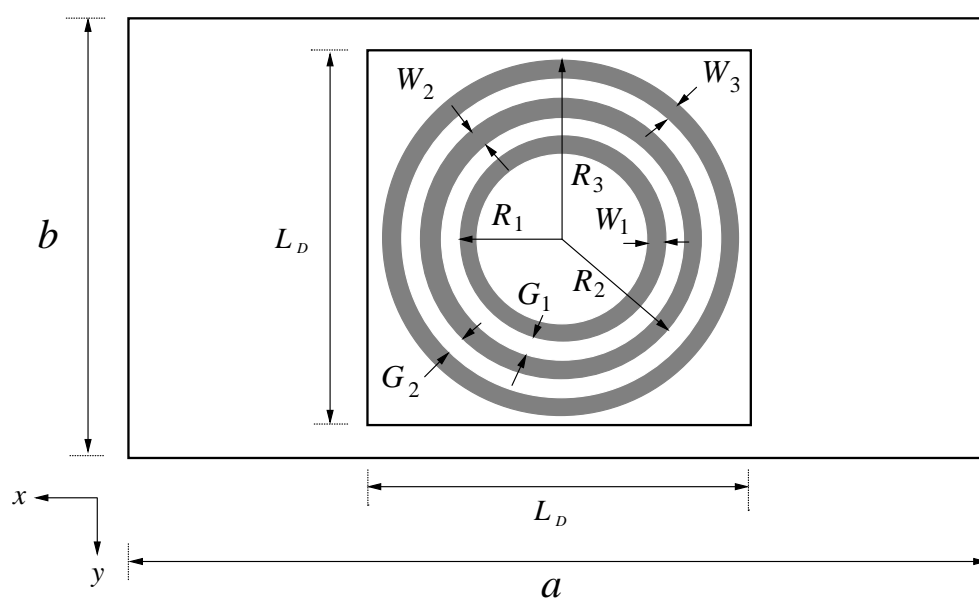
In this chapter, the square DRA reflectarray element loaded with one, two, and three circular concentric slots beneath are explored. It has been found that the resonances of the slot and the DRA can be simultaneously excited. By simply manipulating the slot dimensions, the proposed structure is able to provide a reflection phase range of more than 1000° . This is the first-ever reported DRA reflectarray unit element which is able to provide such a broad phase range, to the authors' best knowledge. The loading effects of the slots will be studied. Simulation was done using the CST Microwave Studio software and measurements were conducted on a Vector Network Analyser (VNA). Good agreement is found between the simulated and measured results.

4.2 Reflectarray Unit Cell Configuration

Figure 4.1(a) illustrates the perspective view of the proposed DRA reflectarray unit element with three under-loading circular slots, which are aligned concentrically and made to have equal slot width ($W_1 = W_2 = W_3 = 0.50$ mm). Referring to Figure 4.1(b), the three circular slots are evenly placed apart ($G_1 = G_2 = 0.5$ mm) and etched on the top copper surface of a Duroid RO4003C substrate, which has a dielectric constant of $\nu_r = 3.38$ and a thickness of $h = 1.524$ mm, with its reverse side laminated with another thin copper layer. A square DRA ($L_D = 14$ mm, $H_D = 6$ mm, and dielectric constant of $\nu_r = 7$) is then stacked right on top of the circular slots with the center point of its bottom surface coinciding with that of the ring-shaped slots. The radii of three slots function as the phase-shifting elements. The radii of the middle (R_2) and outer (R_3) ring-shaped slots are made such that $R_2 = R_1 + G_1 + W_2$ and $R_3 = R_1 + G_1 + W_2 + G_2 + W_3$. This makes the circumferences of the middle and outer slots vary with the inner one (R_1). In other words, all the ring-shaped slots can be scaled at the same time when R_1 is varied. Figure 4.1(c) shows a photograph of the fabricated prototype. The proposed reflectarray element is characterized using the waveguide method operating in C band covering the frequency range 5.85 GHz – 8.2 GHz. Figure 4.2(a) shows the simulation model. A section of waveguide ($a = 34.85$ mm \times $b = 15.8$ mm) with length of 154 mm has been deployed. With reference to Figure 4.2(a), the unit element is placed at one end of the waveguide and electromagnetic wave is generated at the wave port. The lateral walls of the waveguide are set to be perfect electric conductor (PEC) in the simulation model. During measurement, an SMA-to-waveguide adaptor is used to connect the waveguide section to a microwave source. Also, the reference plane is de-embedded to the flange of the adaptor by using a flat shorting plate. The substrate is carefully tailored and trimmed so that it is able to fit into a rectangular trench with a depth of ~ 1.5 mm, as depicted in Figure 4.2(b).

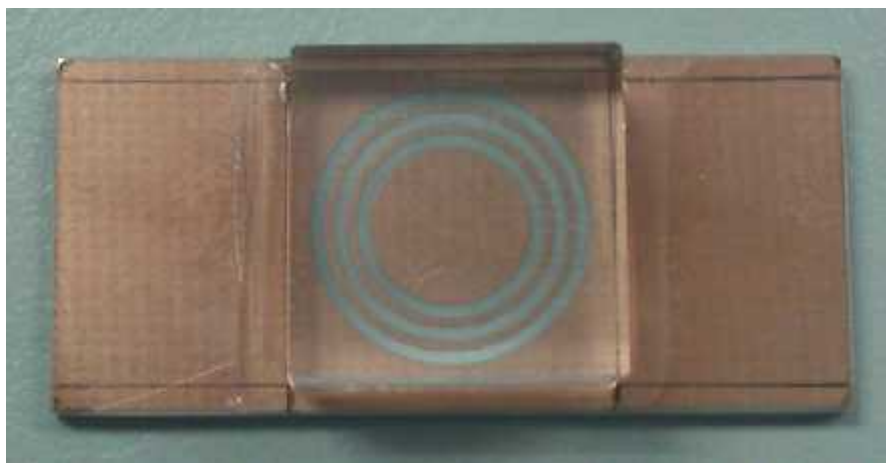


(a)



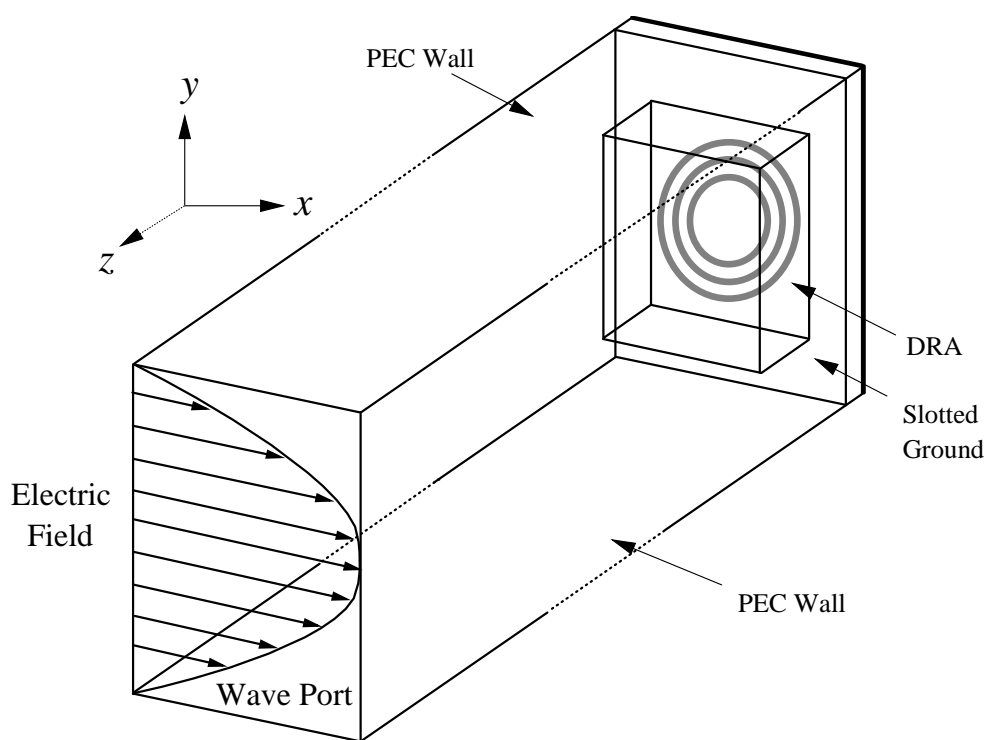
$$R_2 = R_1 + G_1 + W_2 \quad R_3 = R_1 + G_1 + W_2 + G_2 + W_3$$

(b)



(c)

Figure 4.1: Square DRA Unit Element Loaded with 3 Concentric Circular Slots Underneath. (a) Perspective view. (b) Top-down view. (b) Photograph of the Fabricated Prototype.



(a)

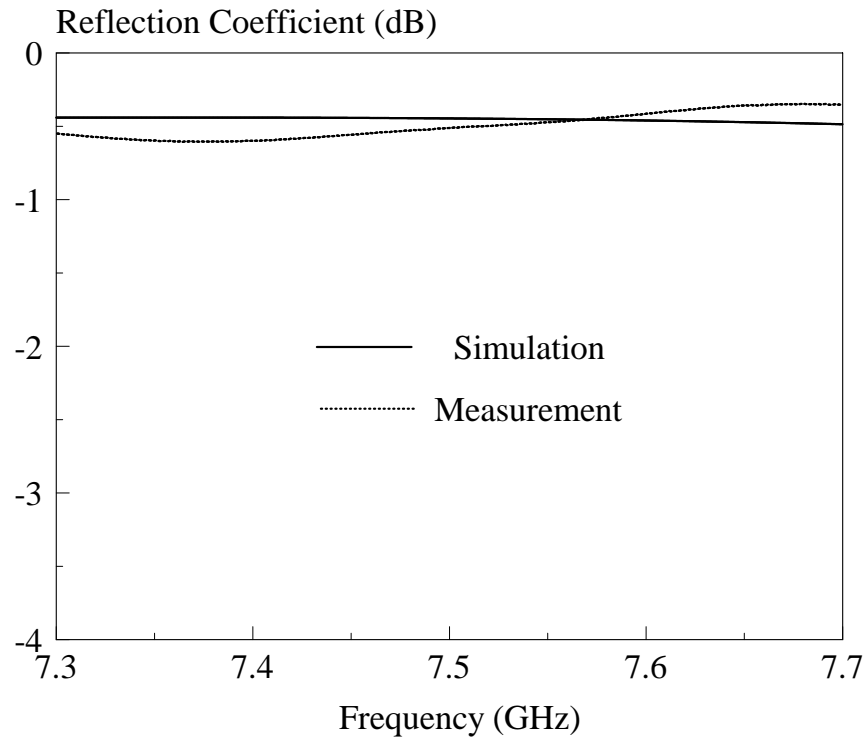


(b)

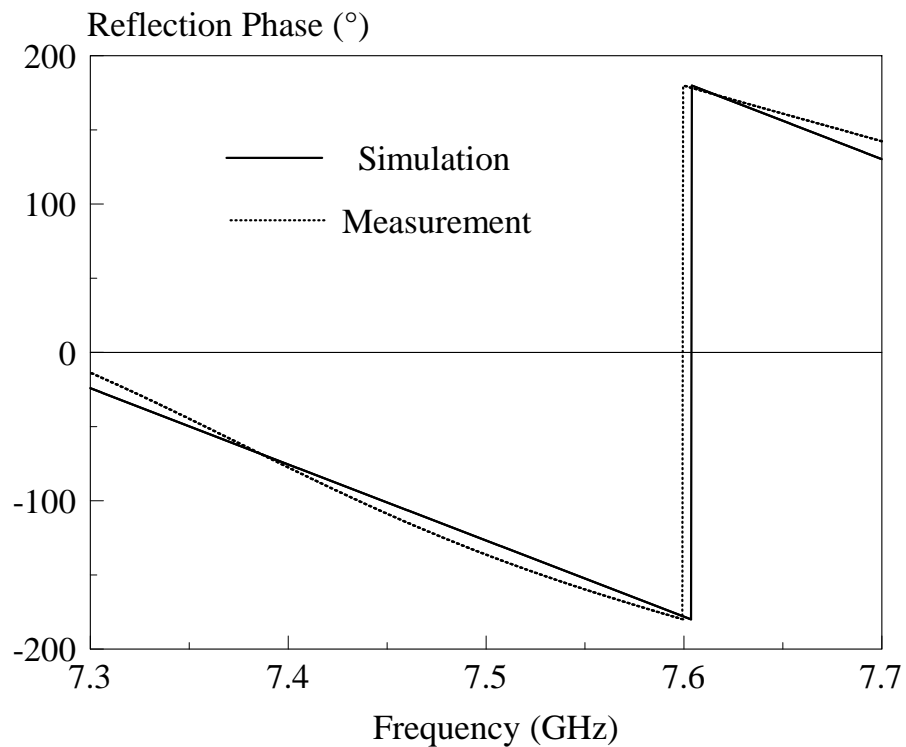
Figure 4.2: (a) DRA Unit Element Simulation Model. (b) Experimental Setup for the Waveguide Method.

4.3 Unit Cell Simulation and Measurement

First, the reflection characteristics of the square DRA with three under-loading circular slots are studied for the slot dimensions of $G_1 = G_2 = 0.5$ mm and $W_1 = W_2 = W_3 = 0.5$ mm. Figure 4.3 shows the simulated and measured reflection coefficients and reflection phases of the DRA reflectarray unit element with three under-loading slots. Referring to the figure, reasonable agreement is observed between the simulated and measured results across the frequency range of 7.3 GHz – 7.7 GHz, with a maximum discrepancy of 0.2 dB. The maximum loss reads ~ -0.7 dB at 7.36 GHz. This proves that the proposed DRA reflectarray element has only very little loss in this frequency range.



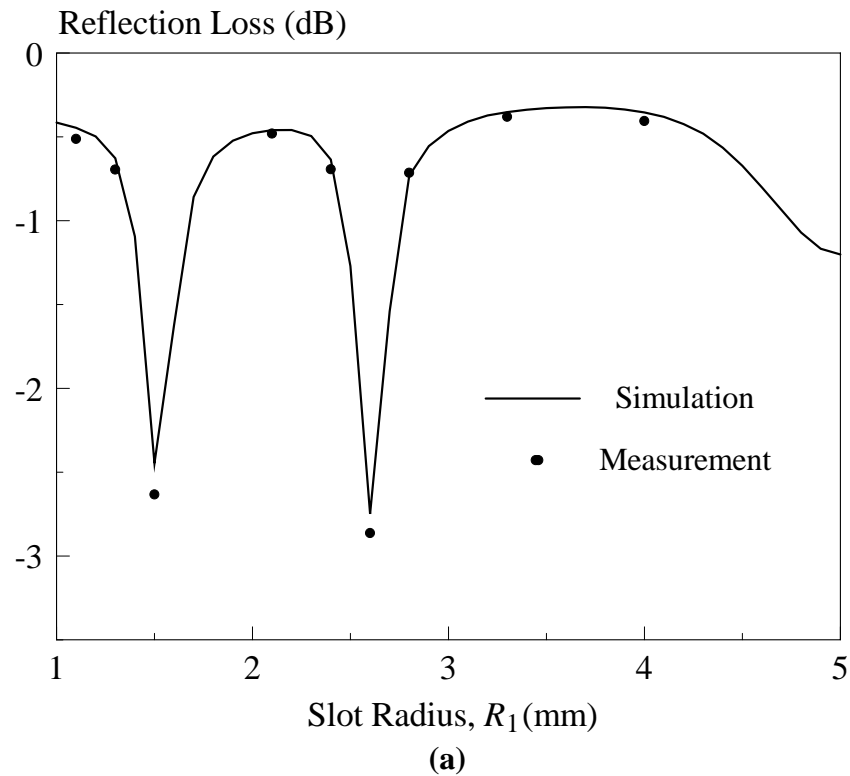
(a)



(b)

Figure 4.3: Simulated and Measured (a) Reflection Coefficients; (b) Reflection Phases of the Proposed DRA Reflectarray Unit Element Loaded with Three Circular Slots ($G_1 = G_2 = 0.5$ mm and $W_1 = W_2 = W_3 = 0.5$ mm) Beneath.

Next, the phase shifting effect of the unit element is studied by varying the radii of three circular slots R_1 , R_2 and R_3 simultaneously. As the values for R_2 and R_3 depend on R_1 , therefore it is only necessary to vary R_1 in this case. Figure 4.4 depicts the simulated and measured reflection losses and S curve of the unit element at the frequency of 7.5 GHz. Reasonable agreement is observed between simulation and measurement. With reference to Figure 4.4 (a), the reflection loss maximizes at slot radius of $R_1 = 1.5$ mm and 2.6 mm, implying that the DRA reflectarray element has resonances of close to 7.5 GHz at these two slot dimensions. The measured reflection loss at the two resonances are -2.45 dB (simulation: -2.63 dB) and -2.75 (simulation: -2.86 dB), respectively. Figure 4.4 (b) depicts the measured and simulated S curves at different R_1 . As can be seen from the figure, there is good agreement between the two, and a reflection phase range of 916° is obtainable.



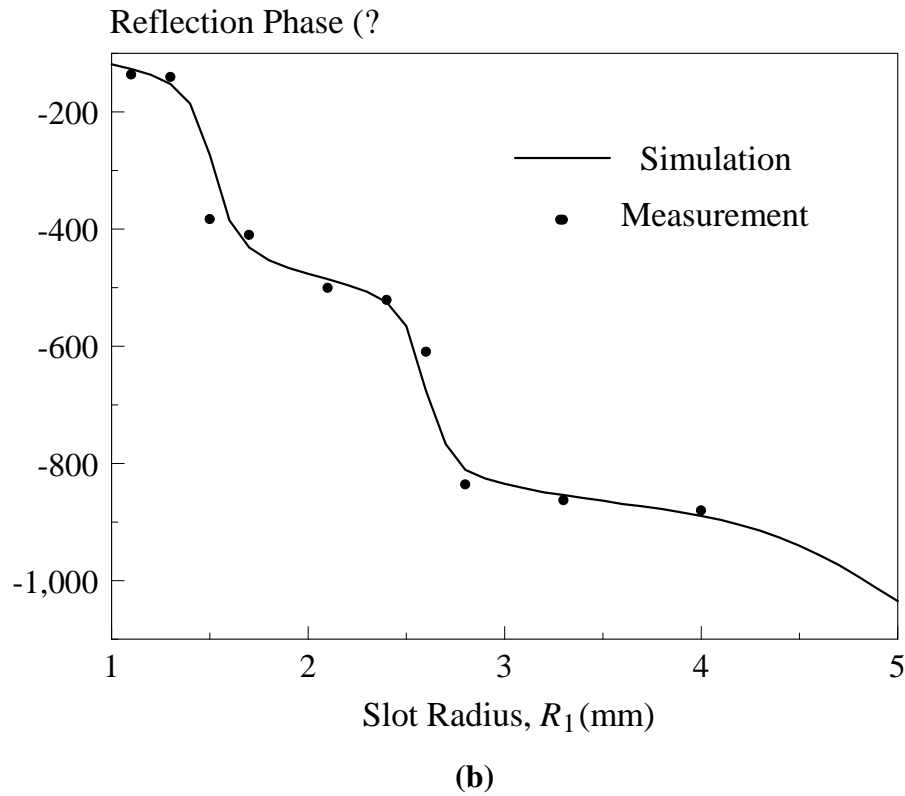
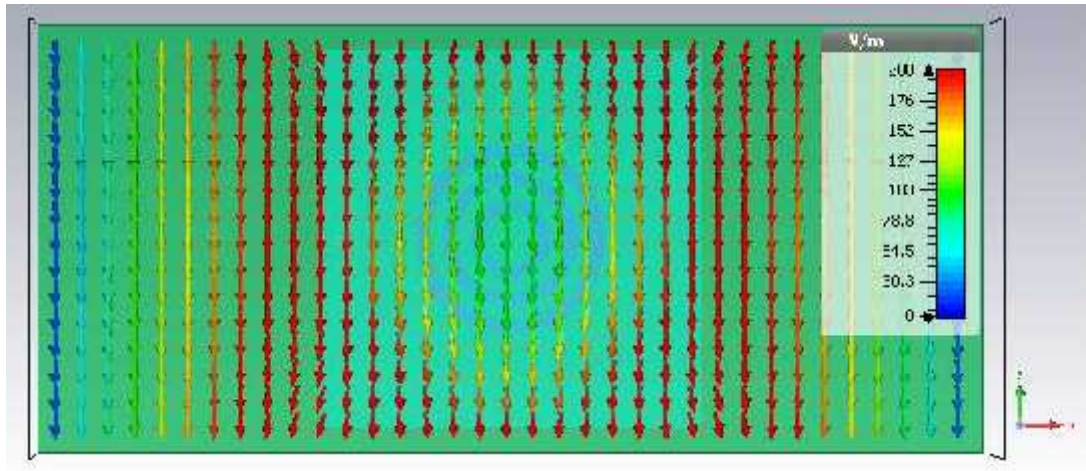


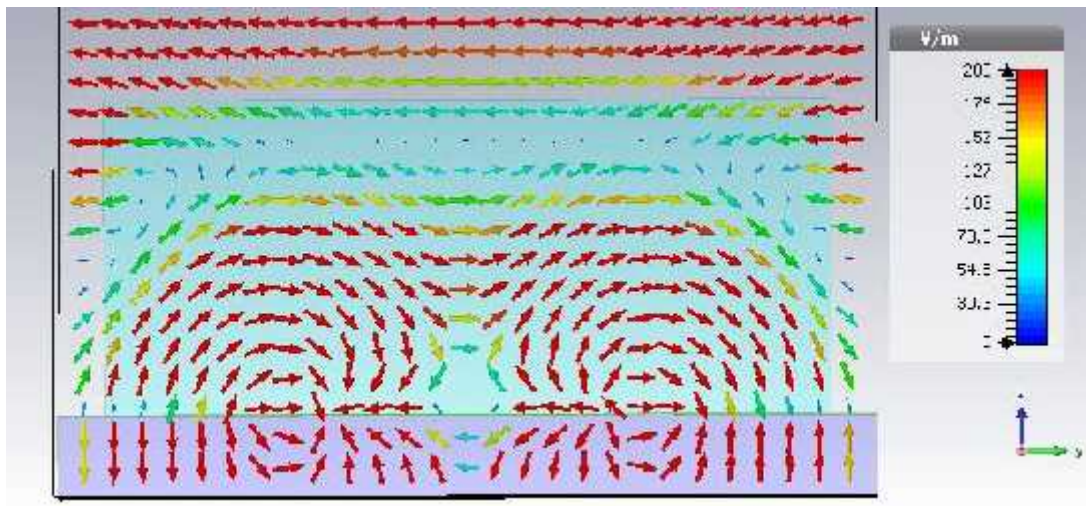
Figure 4.4: Simulated and Measured (a) Reflection Losses, (b) S Curves at 7.5 GHz for the Proposed DRA Unit Element with Three Under-Loading Circular slots.

4.4 Field Distribution in Reflectarray Unit Element

The electric field distributions for the cases $R_1 = 1.5$ mm and 2.6 mm are shown in Figure 4.5 and 4.6, respectively, at the operating frequency of 7.5 GHz. Figure 4.5 shows that the incident wave has caused the dielectric-loaded triple slots to resonate. This resonance introduces the lower phase range for the S curve. By judging from the electric field patterns in Figure 4.6, it can be concluded that this is the dominant TE_{111}^z mode of the square DRA loaded with the three ring-shaped slots underneath (Petosa, 2007). This has significantly expanded the phase range of the S curve, making it very broad.

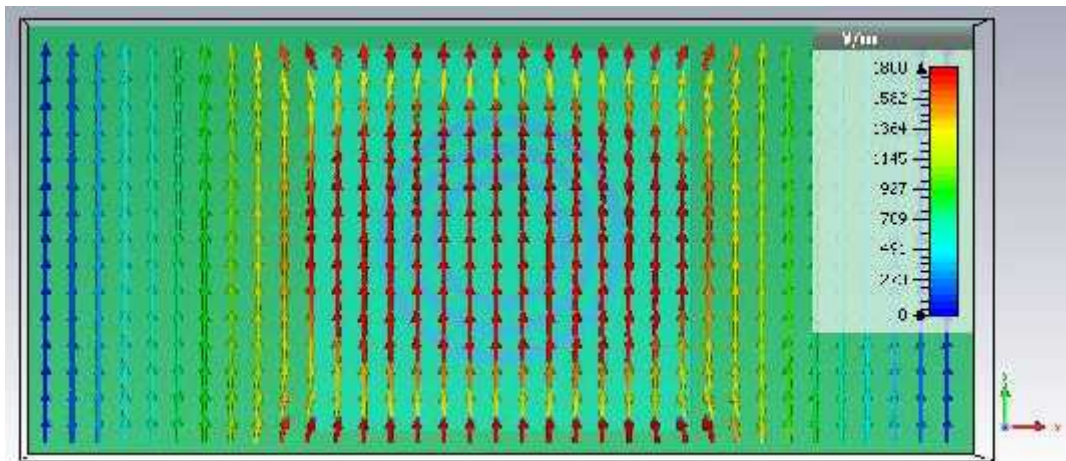


(a)

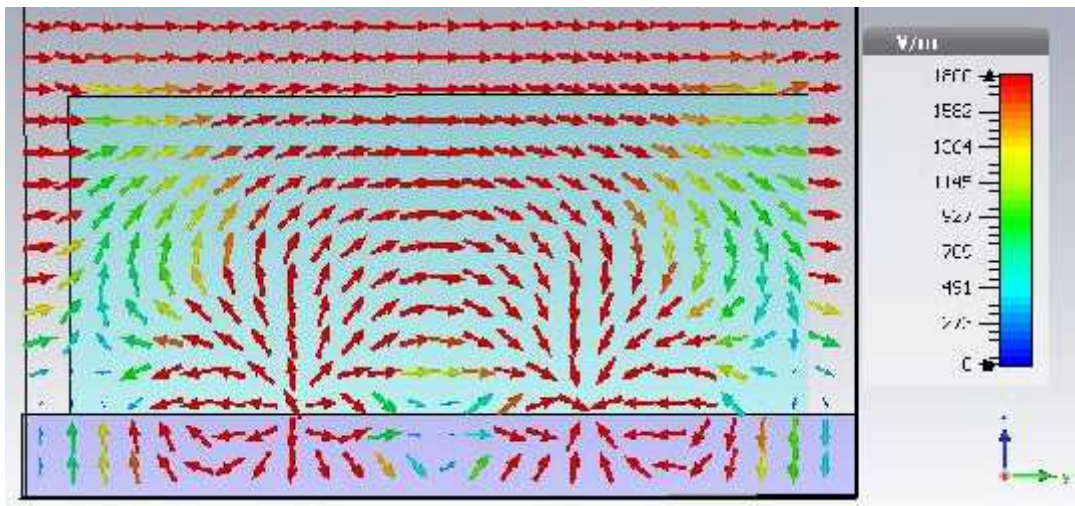


(b)

Figure 4.5: Electric Field Distribution of the DRA Reflectarray Unit Element for $R_1 = 1.5$ mm at 7.5 GHz. (a) Top-down View. (b) Side View.



(a)



(b)

Figure 4.6: Electric Field Distribution of the DRA Reflectarray Unit Element for $R_1 = 2.6$ mm at 7.5 GHz. (a) Top-down View. (b) Side View.

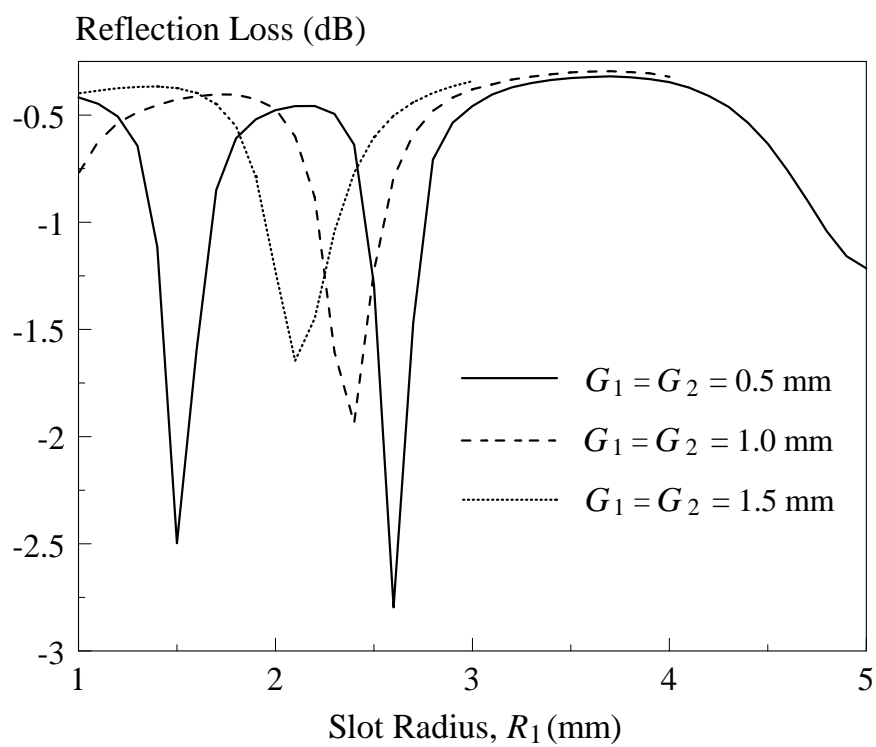
4.5 Parametric Analysis

In this section, parametric analysis has been performed to study the effects of the under-loading circular slots on the reflection loss and S curve. First of all, the effects of gap separations and slot widths are studied. Next, the DRA is designed with multiple under-loading circular slots and the relevant parametric analysis has been provided. Lastly, the effect of the DRA misalignment on the reflection loss and

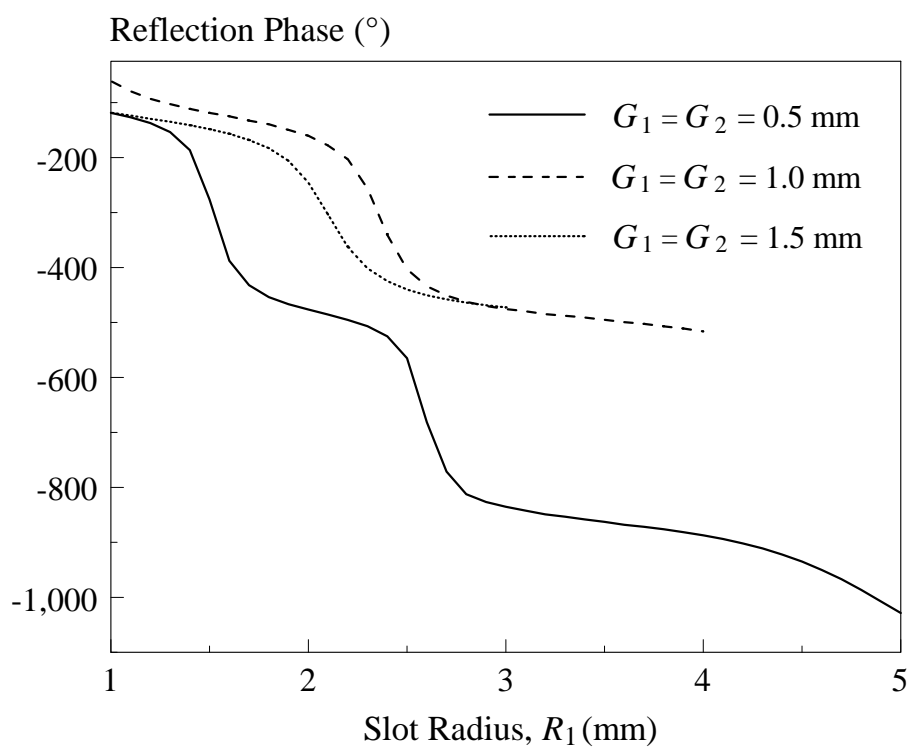
reflection phase is studied. Detailed explanation is provided in each parametric analysis.

4.5.1 Gap Separation between Slots

In the first study, separation gaps between the circular slots are all varied at the same time. With reference to Figure 4.7(a), reflection loss increases as the gaps become smaller. For the case of $G_1 = G_2 = 0.5$ mm, as can be seen in Figure 4.7(b), it is noted that the DRA unit element has two dimensions that have close resonance frequencies to the incident wave (7.5 GHz), making it able to provide very large reflection phase range. Enlarging the gap separations ($G_1, G_2 > 0.5$ mm) does not help broaden the phase range as less tuning range is available in R_1 due to the limitation posed by the top-loading DRA. In the second study, with reference to Figure 4.8, only one gap is changed while another one is kept unchanged. In the case when G_2 is fixed at 0.2 mm, it can be observed from Figure 4.8 (a) that varying gap separation (G_1) from 0.4 mm to 0.8 mm has effect on the reflection loss of the slot resonance, but less on the DRA resonance. Figure 4.8 (b) shows that the changing rate of the reflection phase differs when G_1 is varied. In the case when G_1 is fixed at 0.2 mm, with reference to Figure 4.9 (a), it is noticed that reflection loss increases when the gap separation (G_1) becomes closer. Consequently, it will result in steeper reflection phase slope with the reflection loss increased, as shown in Figure 4.9 (b). However, for both cases, the phase range maintains almost unchanged.

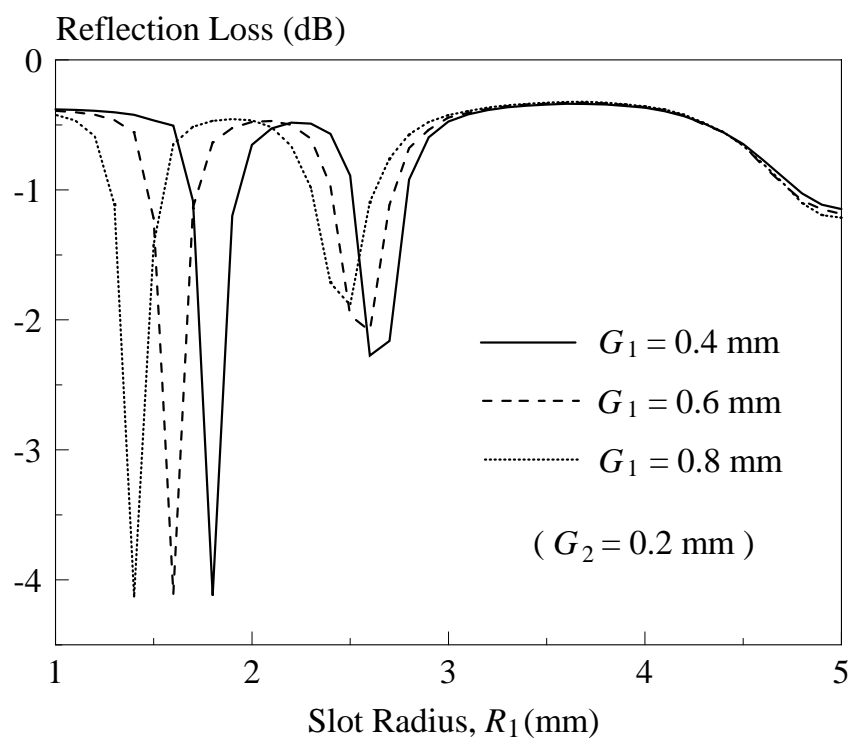


(a)

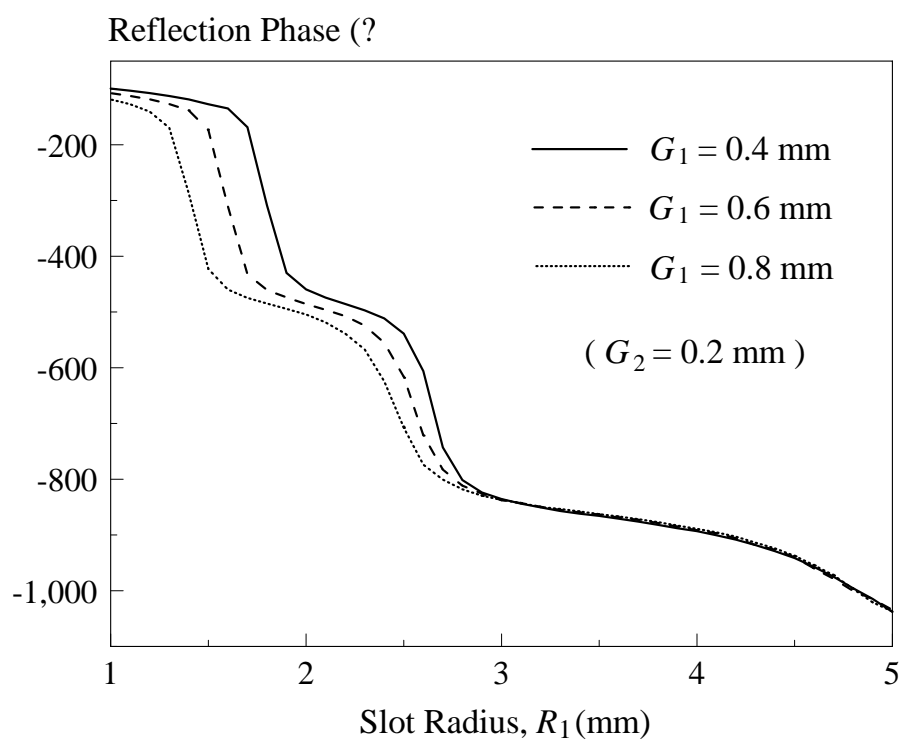


(b)

Figure 4.7: Effect of the Gap Separation on (a) Reflection Loss; (b) S Curve.

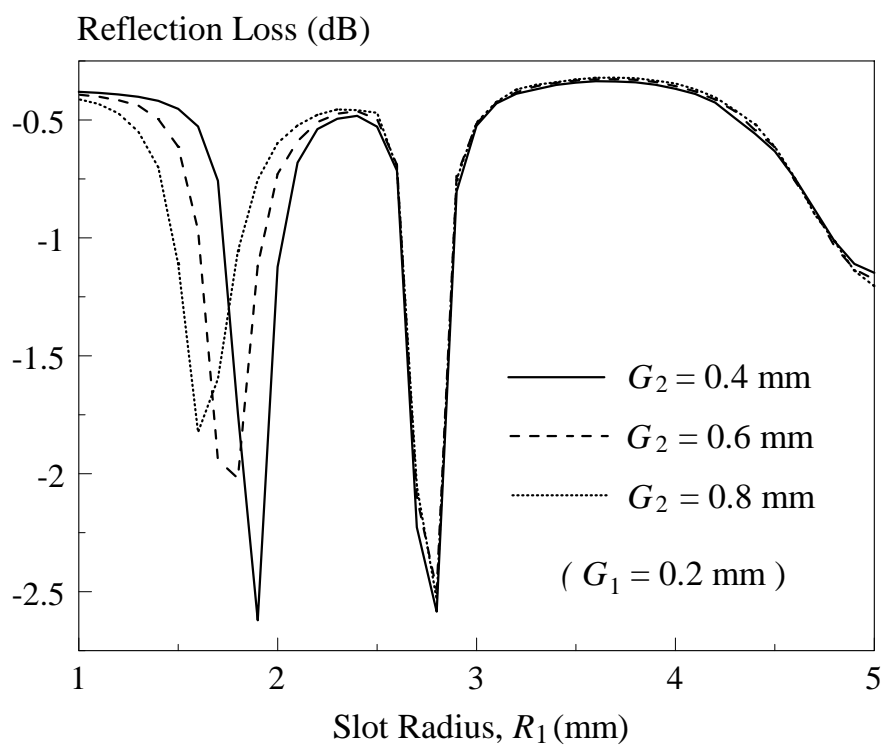


(a)

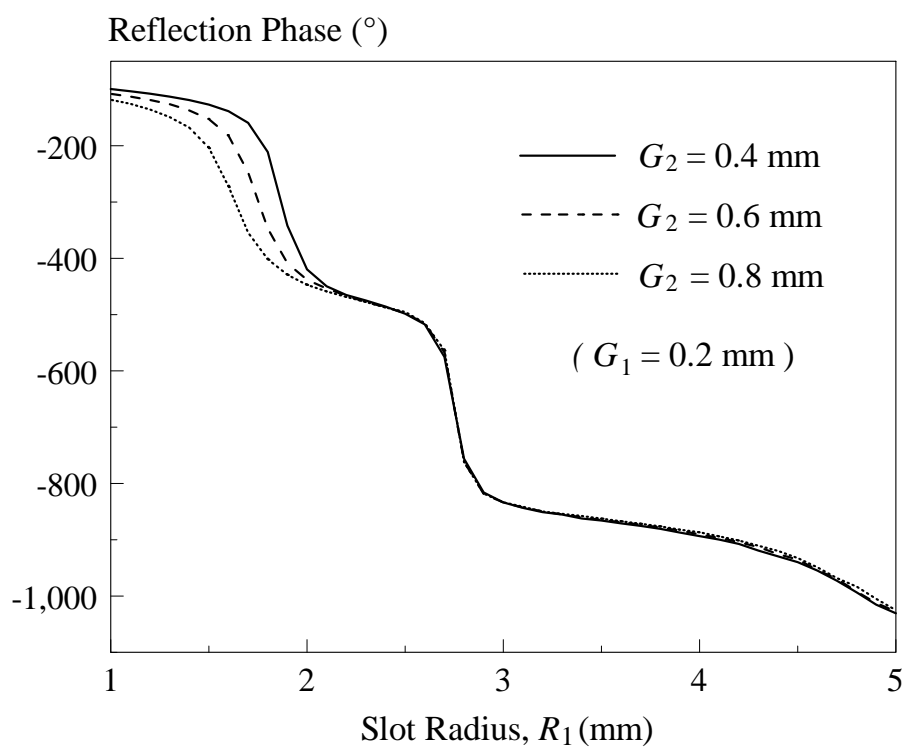


(b)

Figure 4.8: Effect of Changing the Gap Separation G_1 (with $G_2 = 0.2$ mm) on the (a) Reflection Loss; (b) S Curve.



(a)

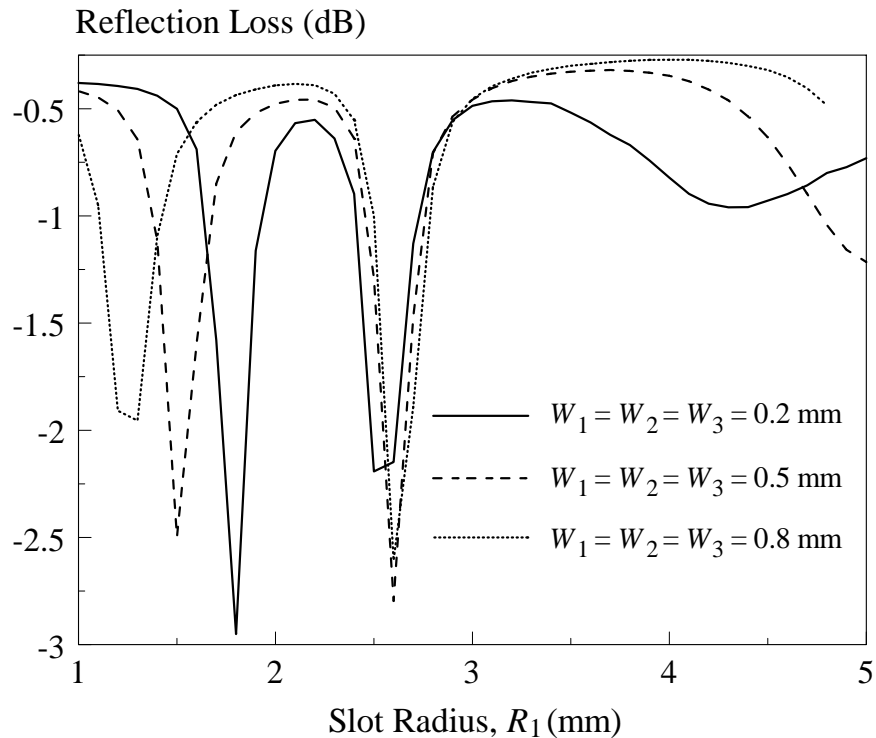


(b)

Figure 4.9: Effect of Changing the Gap Separation G_2 (with $G_1 = 0.2$ mm) on the (a) Reflection Loss; (b) S Curve.

4.5.2 Slot Widths

First, the widths of the three slots are varied simultaneously. As can be seen from Figure 4.10 (a), when the slot radius R_1 is set to be 1.8 mm, the reflection loss of the slot resonance peaks at -2.9 dB for the case $W_1 = W_2 = W_3 = 0.2$ mm. Also, the slot widths are found to affect the slot mode significantly but not too much the DRA mode. Therefore, it can be used for controlling the changing rate of the lower phase range of the S curve without affecting the higher portion (DRA mode), as can be clearly seen in Figure 4.10 (b). With reference to the same figure, it can be concluded that narrow slots are good for lowering down the gradient of the S curve which is introduced by the slot mode.



(a)

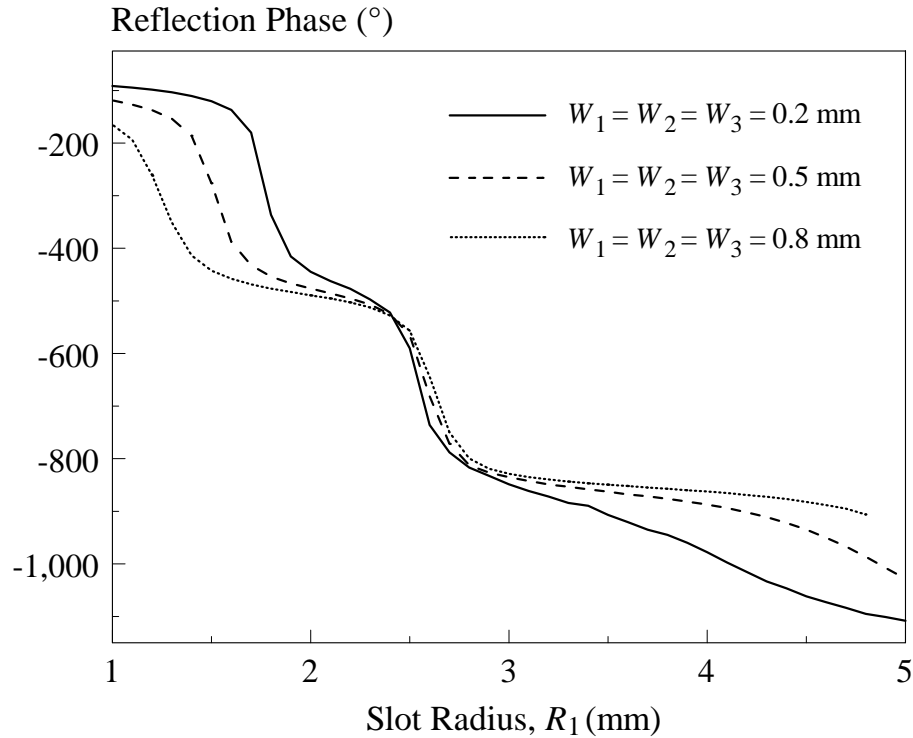
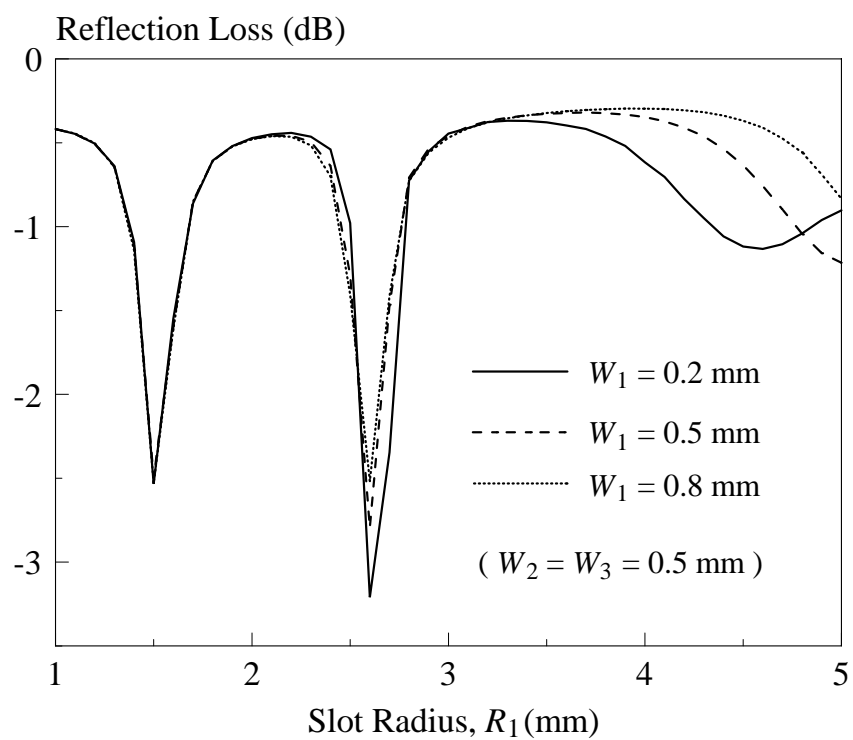
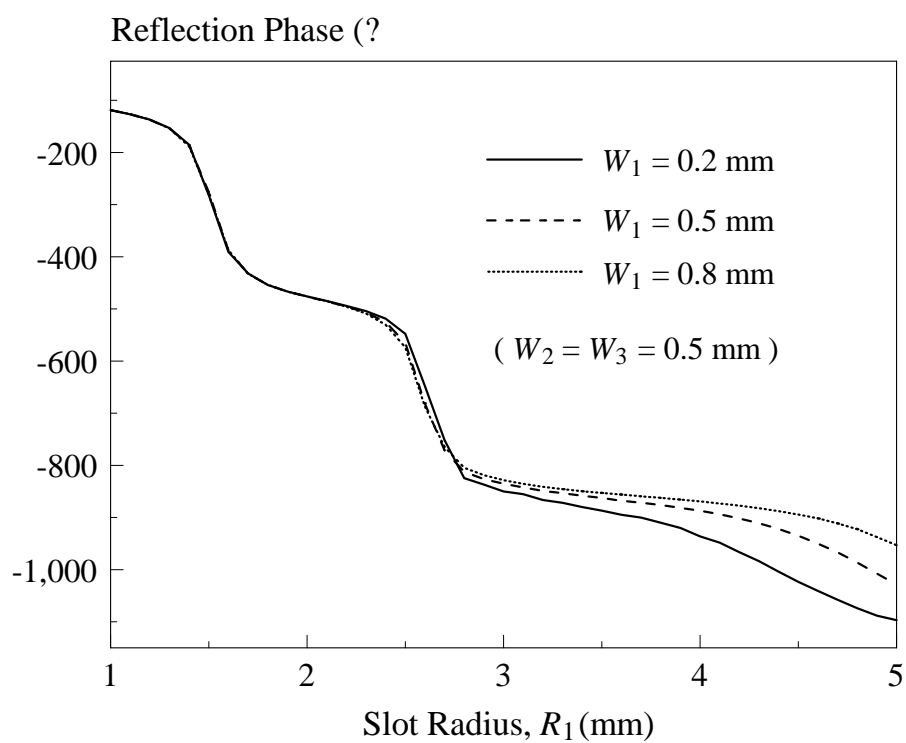


Figure 4.10: Effect of Changing Slot Widths (W_1 , W_2 , W_3) of the Three Circular Slots on the (a) Reflection Loss; (b) S Curve.

For the case of changing only one slot while keeping another two unchanged, the reflection characteristics are studied in Figure 4.11 and 4.12. Obviously, only changing slot width W_1 does not affect the reflection performance much for R_1 of less than 3.25 mm, as depicted in Figure 4.11 (a) and 4.11 (b). With reference to the Figure 4.11 (b), the phase range can be even expanded beyond $R_1 = 3.25$ mm when W_1 is made narrower. But in this case, R_1 cannot be stretched so far as this parameter is limited by the footprint of the DRA. For the case of changing only the outer slot width (W_3), with reference to Figure 4.12, unit element resonates at the frequency of 7.5 GHz. Referring to Figure 4.12 (a), the reflection loss has a peak at -2.8 dB when $R_1 = 1.4$ mm and $W_3 = 0.2$ mm. When the slot width W_3 is increased to 0.8 mm, the reflection loss increases and maximizes at -3 dB at the radius of $R_1 = 2.6$ mm. However, only minor change is observed in the reflection phase slope and reflection range.

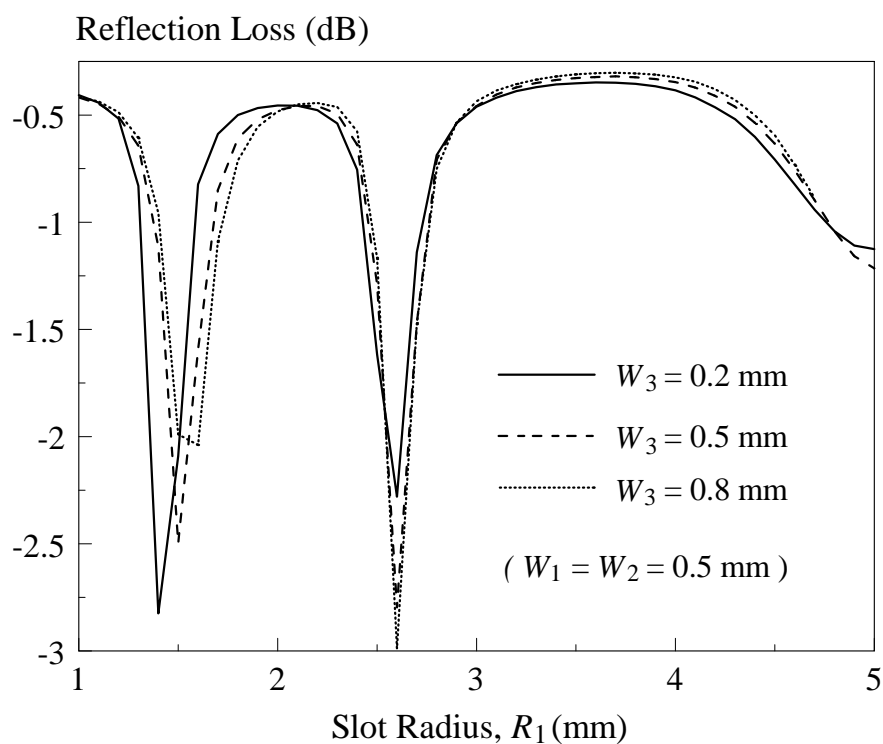


(a)

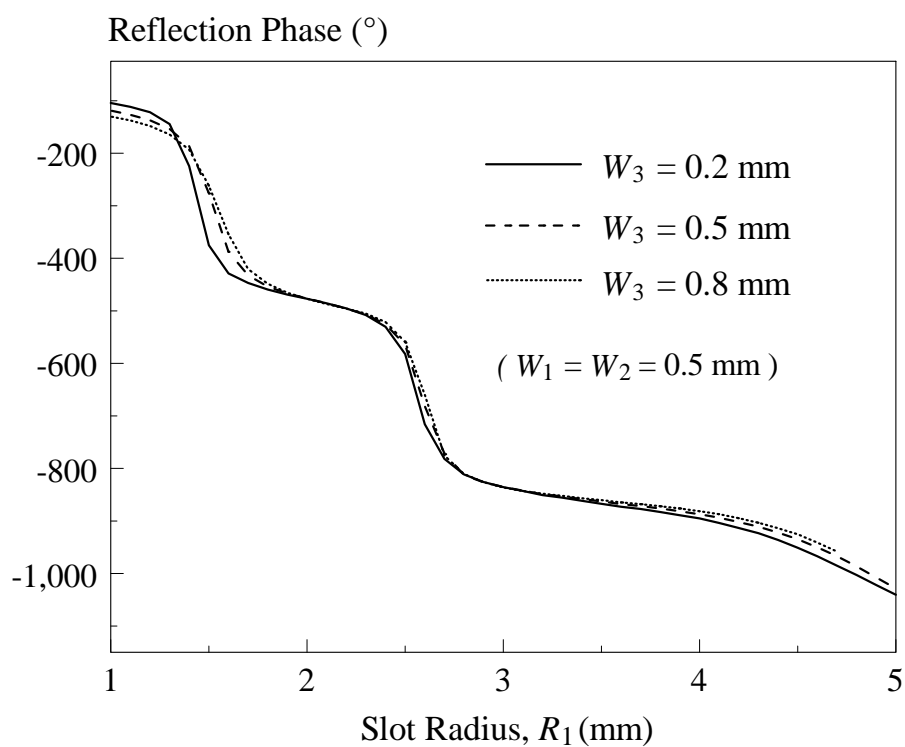


(b)

Figure 4.11: Effect of Changing the Circular Slot Width W_1 on the (a) Reflection Loss; (b) S Curve.



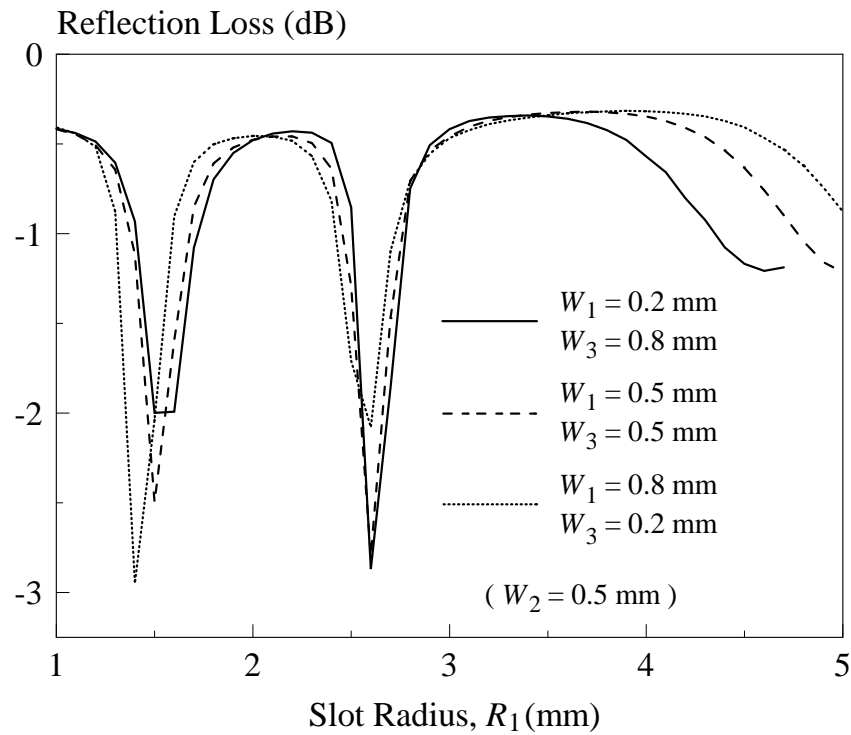
(a)



(b)

Figure 4.12: Effect of Changing the Circular Slot Width W_3 on the (a) Reflection Loss; (b) S Curve.

To further understand the slot effect, the width of the middle slot is kept a constant ($W_2 = 0.5$ mm) but the inner and outer slots (W_1 and W_3) are changed at the same time. The corresponding reflection loss and S curve are studied in Figure 4.13. As can be seen from Figure 4.13(b), it is clear that the phase range can be expanded far beyond $R_1 = 3$ mm by manipulating W_1 and W_3 . For the case ($W_1 = 0.2$ mm, $W_2 = 0.5$ mm, $W_3 = 0.8$ mm), shown in Figure 4.13(b), a nice S curve with slow gradient is obtainable with a very broad phase range of 1000° , which is sufficient for designing large-size reflectarrays.



(a)

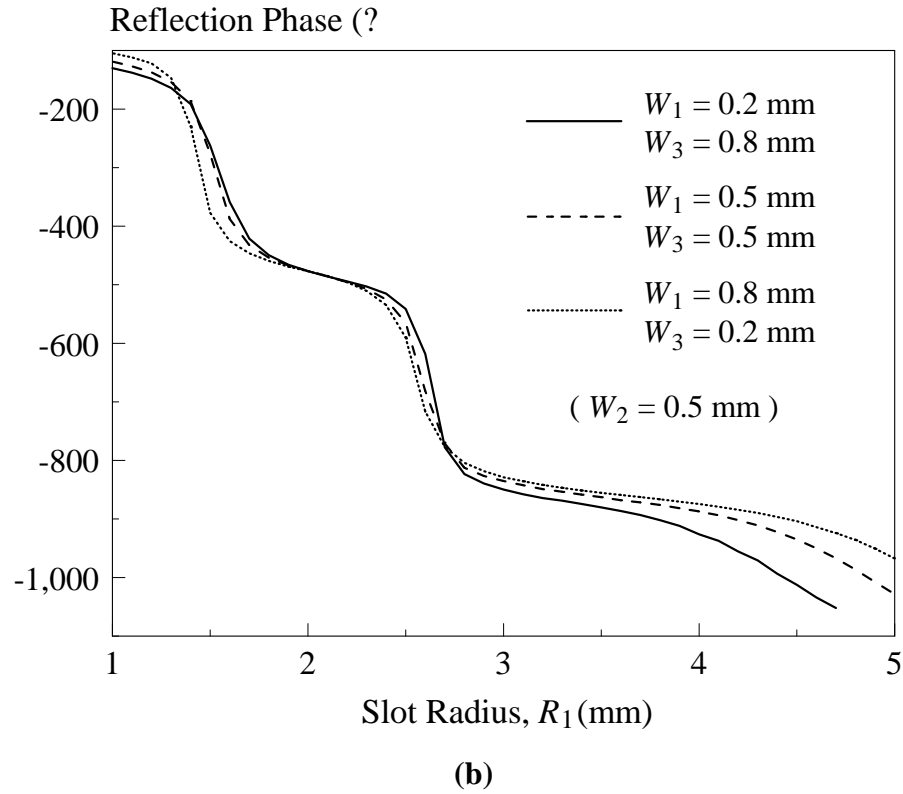
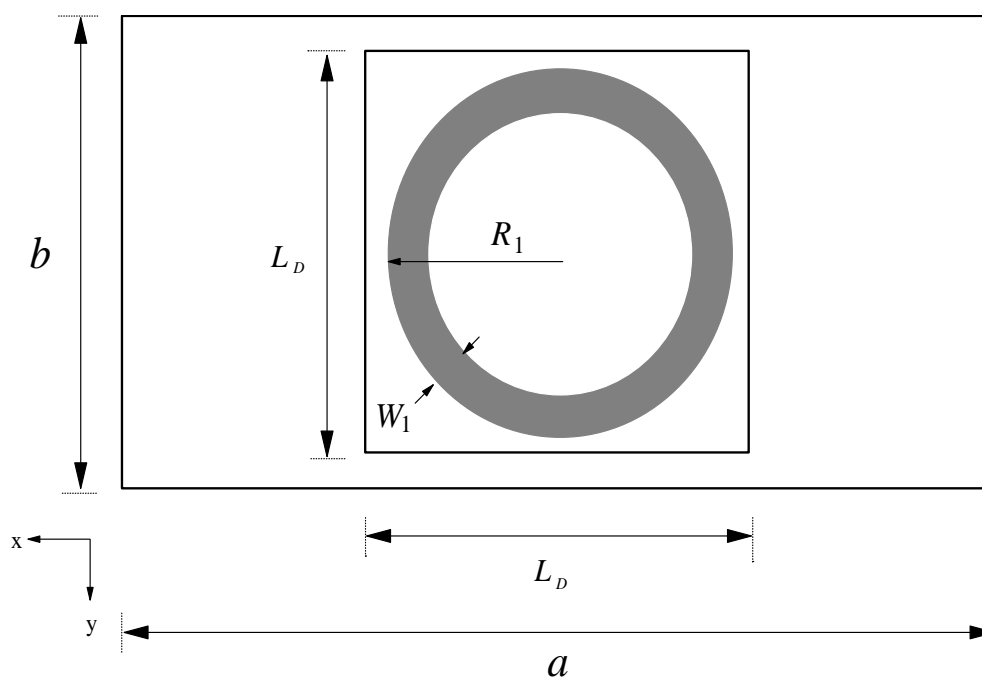


Figure 4.13: Effect of Changing the Inner and Outer Slots (W_1 and W_3) on the (a) Reflection Loss; (b) S Curve.

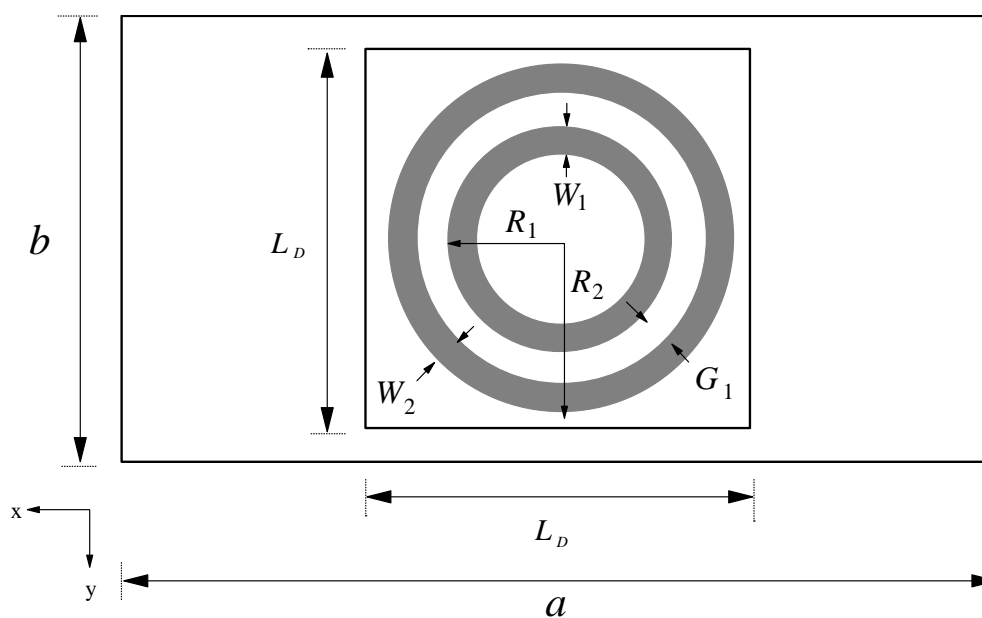
4.5.3 Multiple Slots underneath a DRA

Similar DRA reflectarray elements loaded with less slots underneath are simulated for comparison. Due to footprint limitation of the DRA, in this paper, the number of under-loading slots is limited to three. The configurations of the respective unit elements are shown in Figure 4.14. The slot width of the single slot case (Figure 4.14(a)) is $W_1 = 0.5$ mm; while the dimensions of the double slots case (Figure 4.14(b)) are given by $W_1 = W_2 = 0.5$ mm, $G_1 = 0.5$ mm. For the latter, the radius of the inner slot (R_1) is varied and the radius of the outer is defined as $R_2 = R_1 + G_1 + W_2$. In other words, R_2 changes as a function of R_1 . Other design parameters are similar to those in Figure 4.1. Again, the radii of the slots are varied simultaneously to generate phase shift in reflection. The reflection losses and S curves for the cases of single and double slots are studied in Figure 4.15. Also given are the results for the triple slots. With reference to Figure 4.15 (b), it is obvious that

only with three under-loading slots, can the slot and DRA resonances be brought together to form a broad phase range.



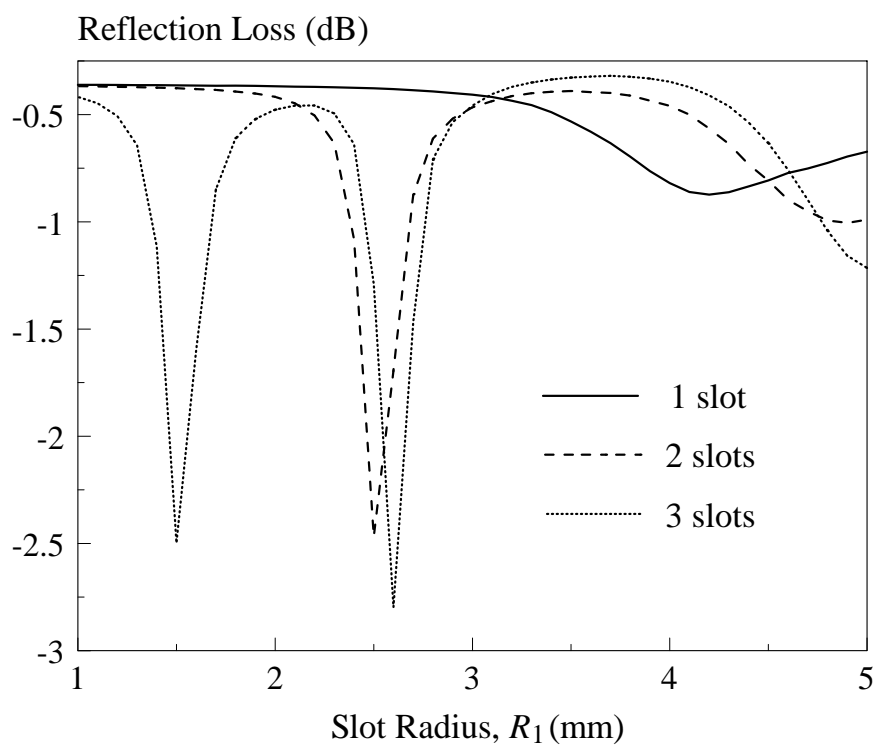
(a)



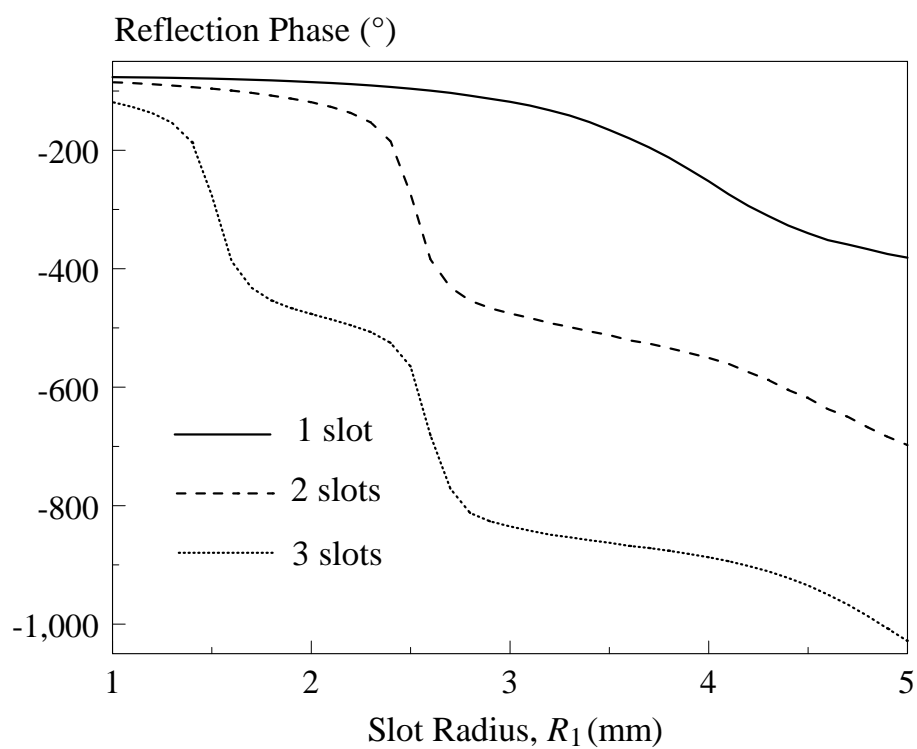
$$R_2 = R_1 + G_1 + W_2$$

(b)

Figure 4.14: (a) Square DRA Reflectarray Unit Element Loaded with (a) One Circular Slot and (b) Two Circular Slots Underneath.



(a)

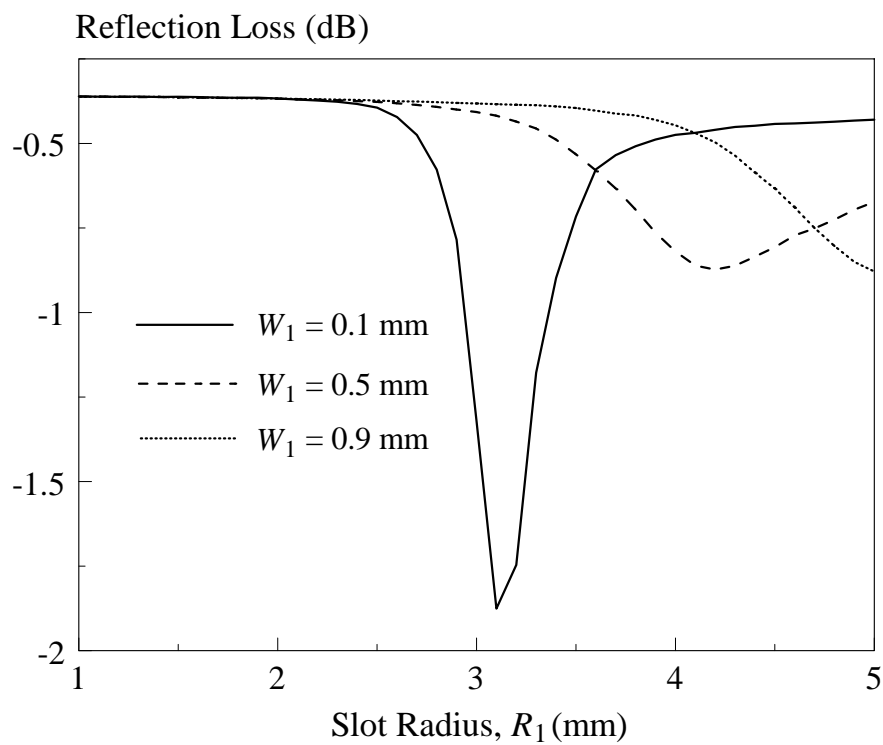


(b)

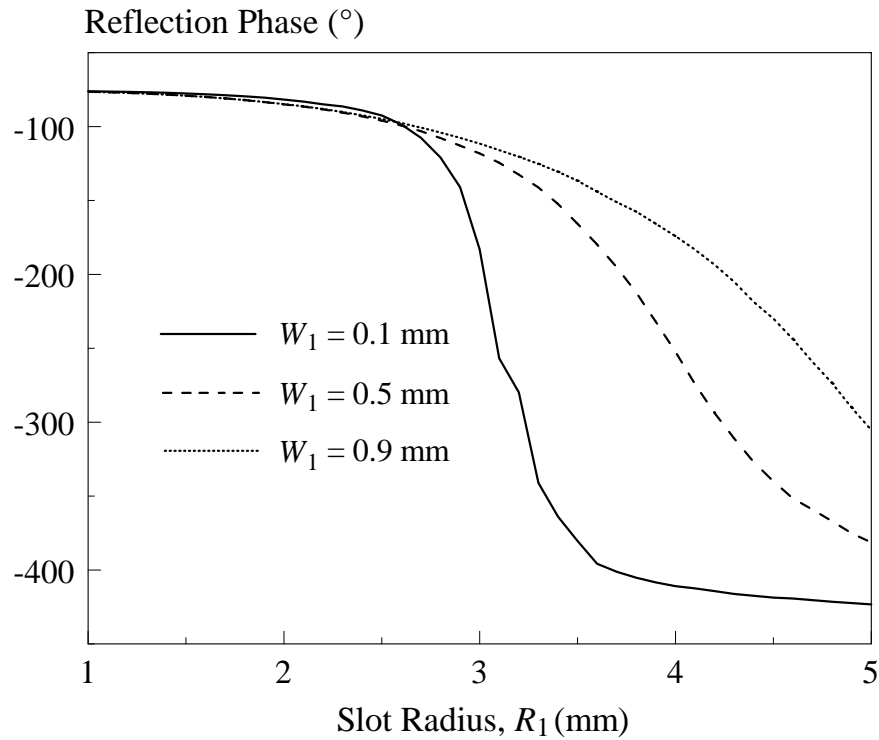
Figure 4.15: Comparison of the (a) Reflection Loss, (b) S Curve of the DRA Reflectarray Unit Elements with One, Two, and Three Under-Loading Slots.

4.5.3.1 One Slot

The effect of loading the DRA with only one slot underneath is also studied in this section. The study shows the effect of slot width on the reflection loss and reflection phase. With reference to Figure 4.16 (a), it can be observed that the reflection loss is peaking at -1.85 dB when the slot width is $W_1 = 0.1$ mm. This structure is able to provide a phase range of more than 300° , which is sufficient for designing small-sized reflectarrays. But it has steeper reflection phase slope, as shown in Figure 4.16 (b).



(a)

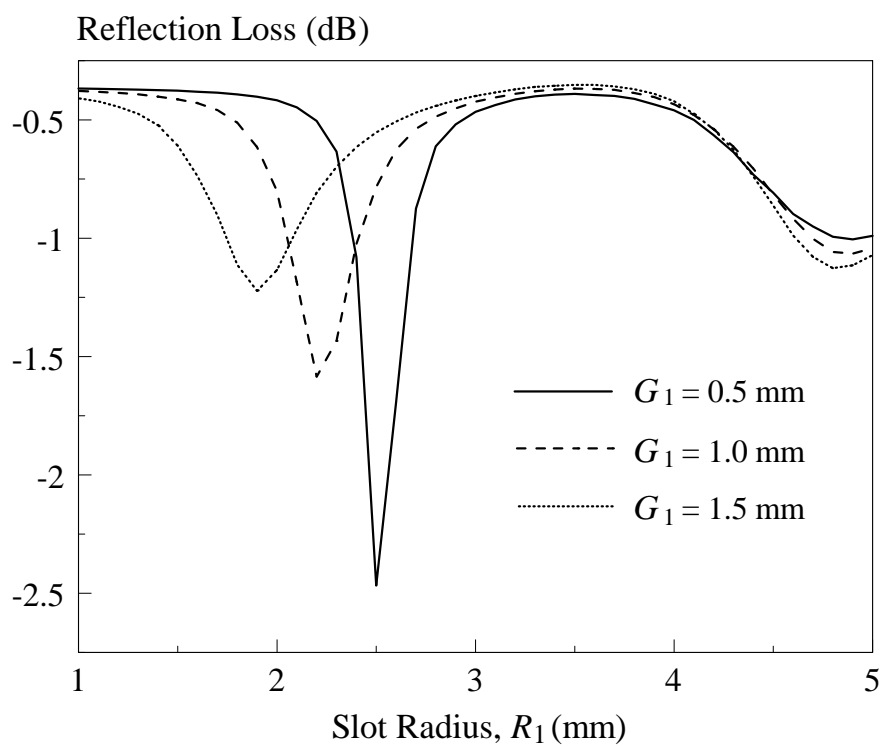


(b)

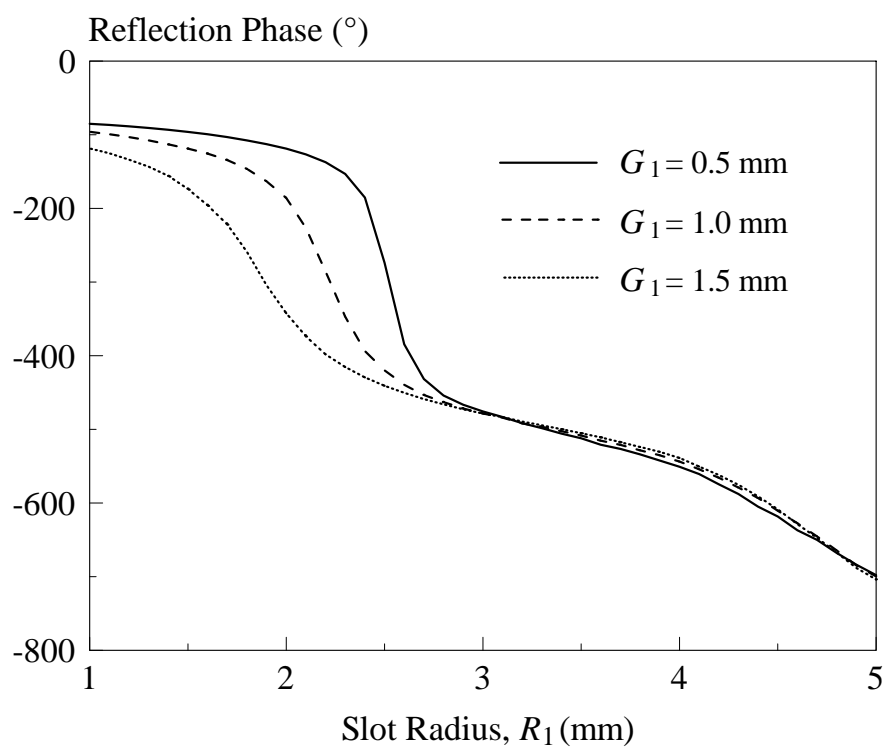
Figure 4.16: Effect of Changing Slot Width (W_1) on the (a) Reflection Loss, (b) S Curve.

4.5.3.2 Two Slots

First of all, the effect of gap separation between two circular slots is studied. With reference to Figure 4.17, changing the gap separation G_1 does not affect the reflection performance much for R_1 of more than 3 mm. Low reflection loss and slow gradient of reflection phase slope are obtained when the gap separation is increased to 1.5 mm, as depicted in Figure 4.17 (a) and (b).



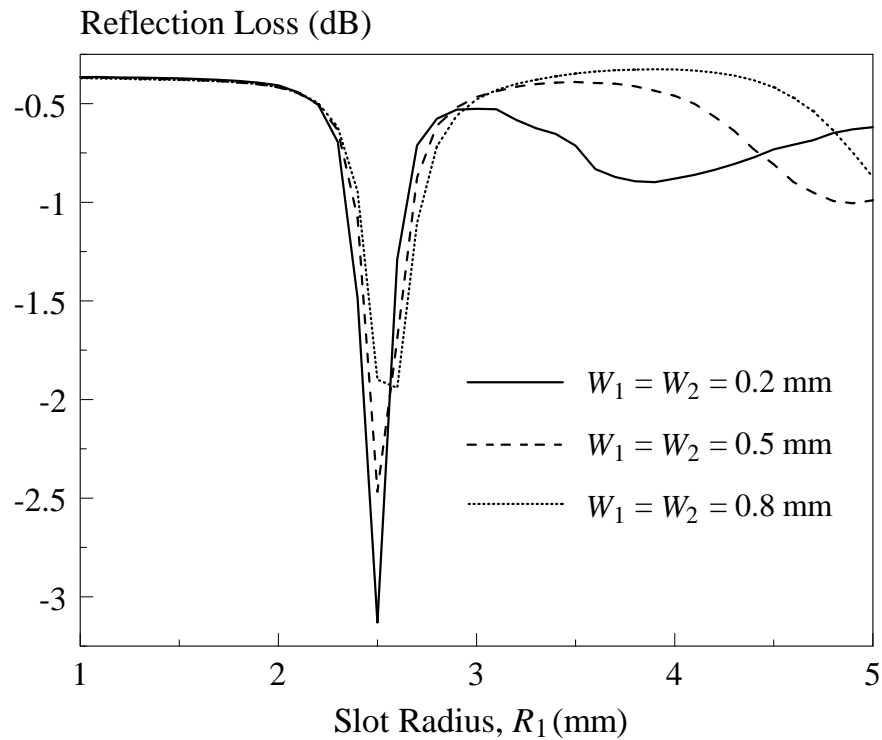
(a)



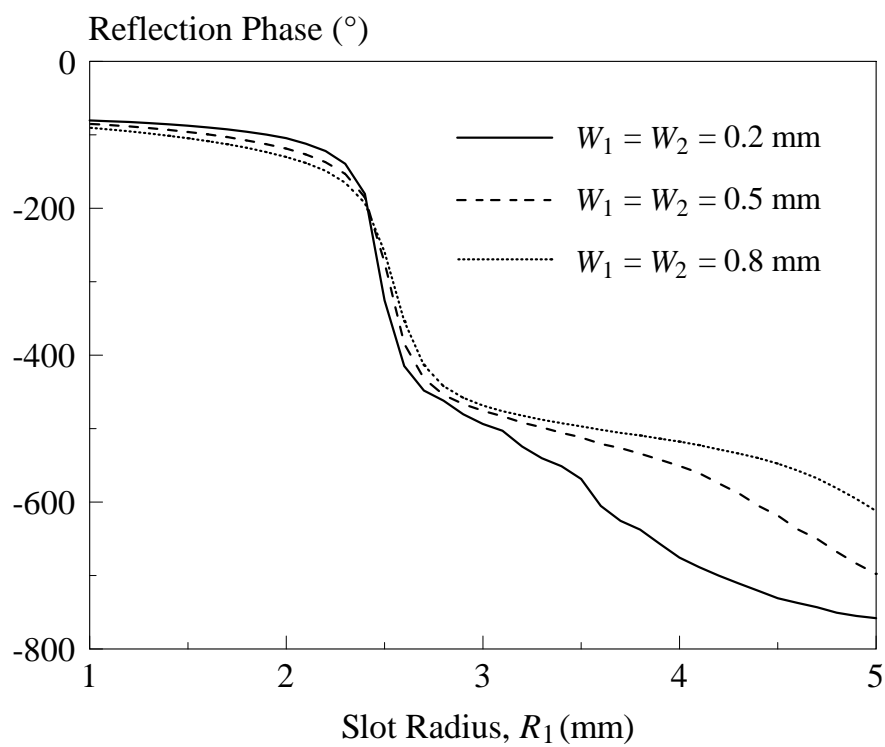
(b)

Figure 4.17: Effect of Gap Separation G_1 between Two Slots on the (a) Reflection Loss, (b) S Curve.

Next, the effect of slot widths on the reflection loss and reflection phase is studied. In the first case, with reference to Figure 4.18, the slot widths (W_1 and W_2) are varied at the same time. By changing W_1 and W_2 simultaneously, the reflection loss and reflection phase do not change much for R_1 of less than 3 mm, as can be seen in Figure 4.18 (a) and (b). However, with reference to Figure 4.18 (b), the reflection phase range can get much expanded beyond $R_1 = 3$ mm. But it cannot be stretched too much as it is restricted by the DRA footprint. In the second study, only one slot width W_2 is varied while another remains unchanged ($W_1 = 0.5$ mm). As can be seen from Figure 4.19, the unit elements resonate around frequency of 7.5 GHz. Also, it is found that varying only one slot width (W_2) does not change the reflection phase range much, as shown in Figure 4.19 (b).

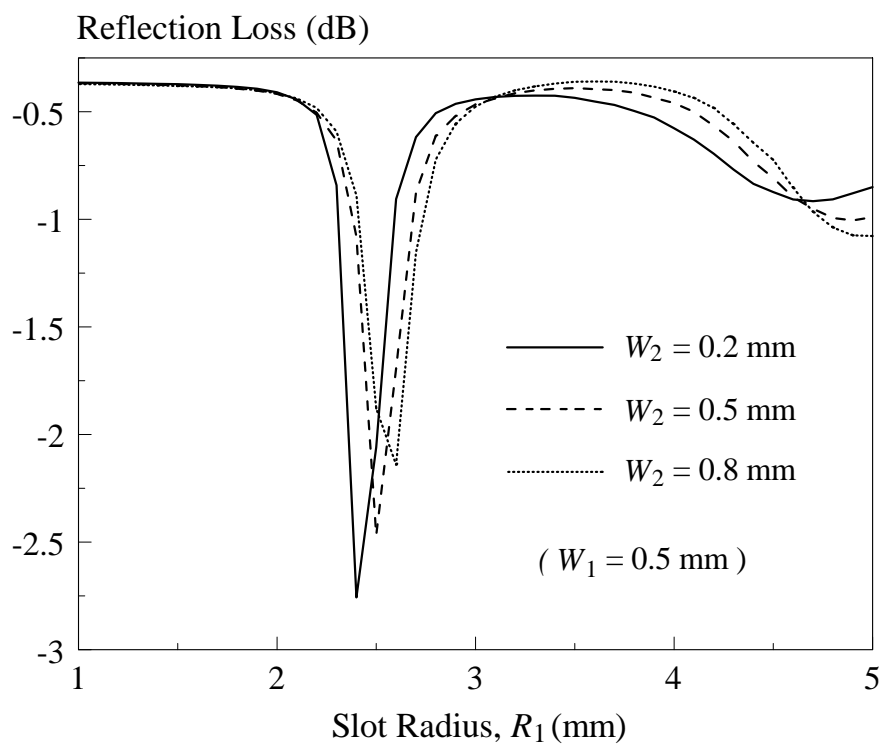


(a)

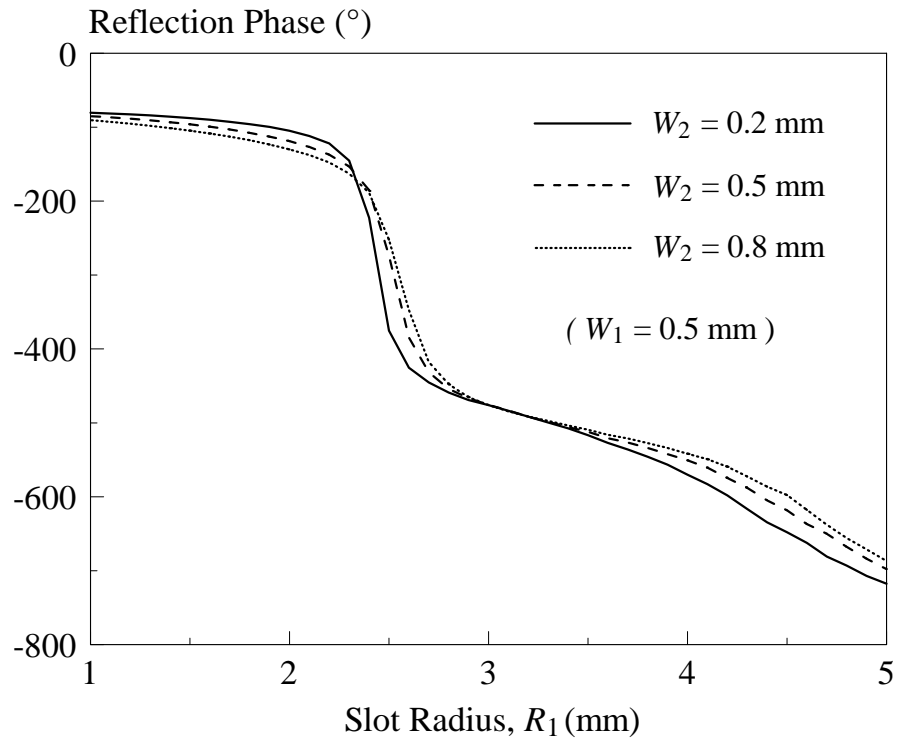


(b)

Figure 4.18: Effect of Changing Slots Widths (W_1 and W_2) of the Two Slots on the (a) Reflection Loss, (b) S Curve.



(a)

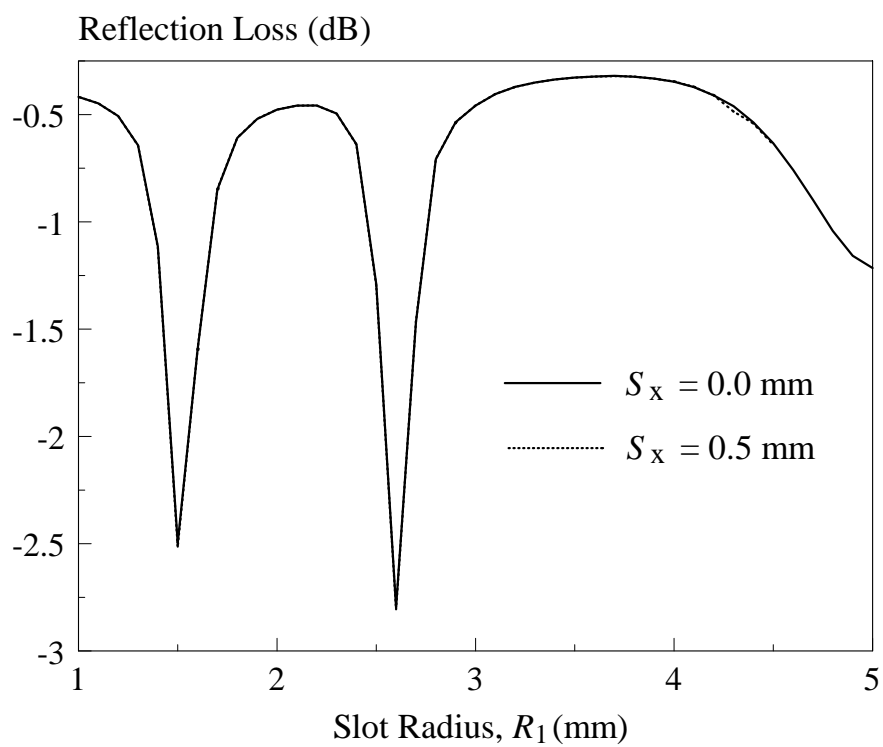


(b)

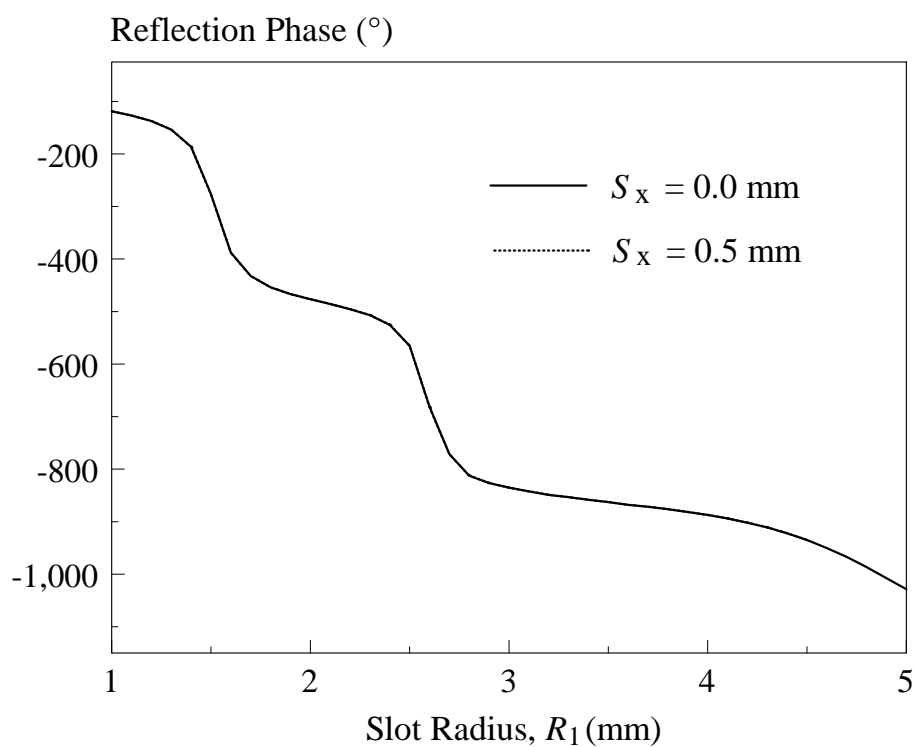
Figure 4.19: Effect of Changing Slot Width W_2 on the (a) Reflection Loss, (b) S Curve.

4.5.4 DRA Alignment

The effect of alignment between the DRA and the under-loading slots is now studied. With reference to Figure 4.20 and 4.21, it can be observed that shifting the DRA by 0.5 mm either in the x - and y -direction does not affect the reflection performance much.

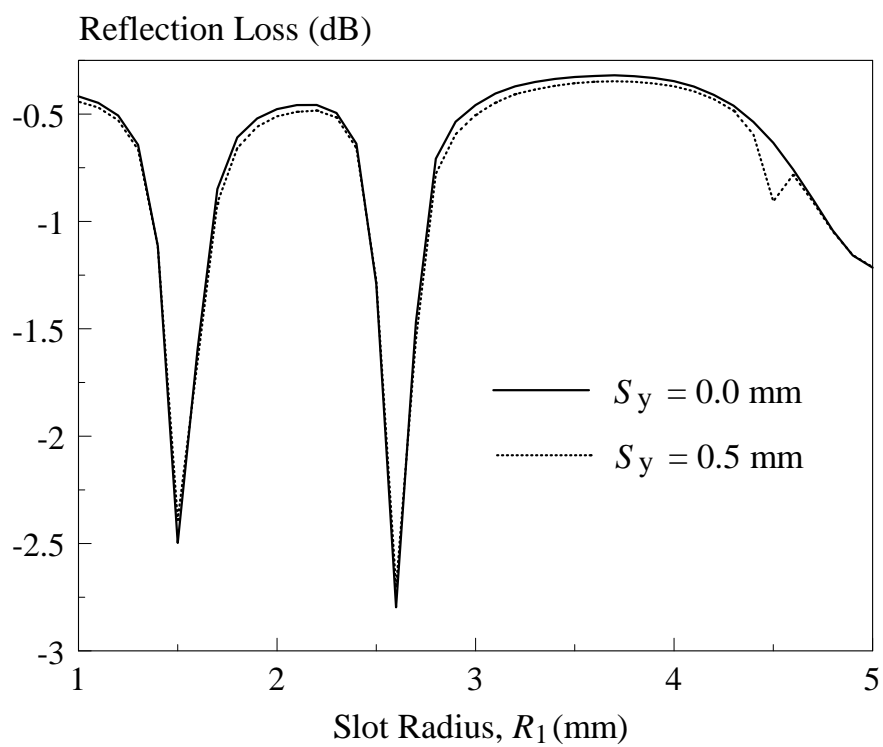


(a)

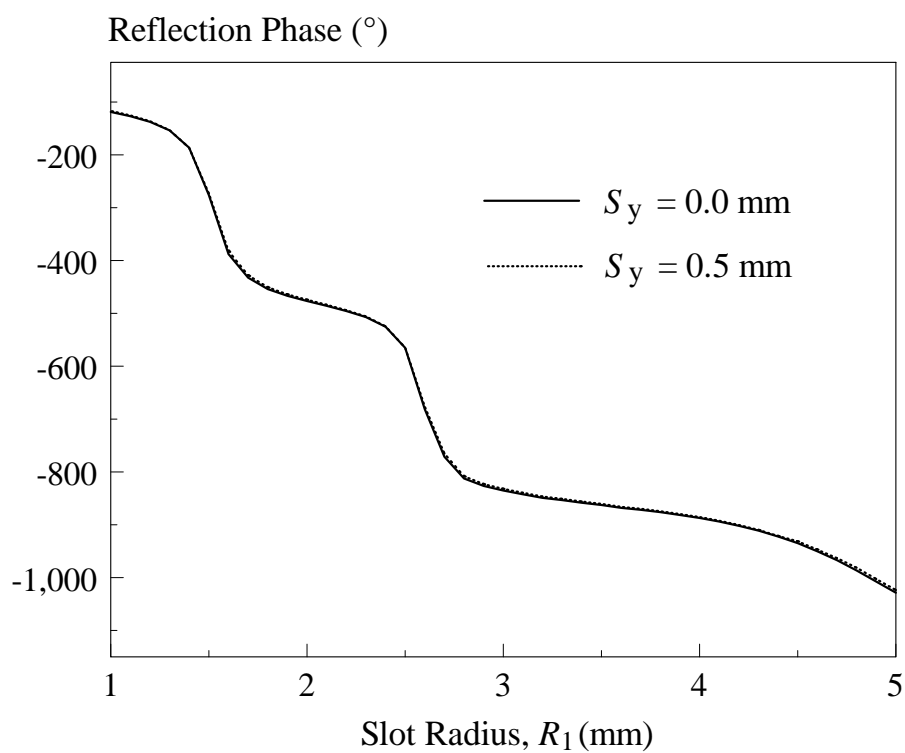


(b)

Figure 4.20: Effect of DRA Misalignment (x-direction) on the (a) Reflection Loss, (b) S Curve.



(a)



(b)

Figure 4.21: Effect of DRA Misalignment (y-direction) on the (a) Reflection Loss, (b) S Curve.

4.6 Conclusion

Multiple concentric circular slots are loaded underneath a square DRA for broadening the phase range of the S curve. It has been found that the slot resonance and the dominant resonance of the square DRA reflectarray element can be combined to achieve a broad phase range of 916° in the S curve, which is sufficient for designing many large-size reflectarrays. Also, it was found that the phase range of the DRA reflectarray unit element can be further extended by manipulating the under-loading slots. Electric fields have been analyzed for both of the slot and DRA modes, with good agreement observed between the simulated and measured results. Since the circular slots are placed beneath the DRA, this reflectarray element does not need additional footprint, making it very compact.

CHAPTER 5

CONCLUSION AND RECOMMENDATIONS

This report has discussed the design procedures of two new DRA reflectarray unit elements, with their performances explored and challenges studied. The proposed design models have been simulated. Prototypes have been fabricated to verify the simulation models. In the first design, the lengths of the under-loading parallel slots of a square DRA are varied to provide reflection phase change. In the second design, the radii of the DRA's under-loading circular slots are varied simultaneously to provide phase shifts. Broad phase ranges of 313° and 916° have been achieved in the first and second curves, respectively, with reasonably slow change in the phase gradient.

In the future, the first proposed unit element can be further used to design a small-sized reflectarray as its phase range is less than 360° . However, the second proposed unit element can be used for designing reflectarrays of any sizes since its phase range is much greater than 360° .

REFERENCES

- Abd-Elhady, A. M., Zainud-Deen, S. H., Mitkees, A. A. & Kishk, A. A., 2010. X-band linear polarized aperture-coupled DRA reflectarray. *Int. Conf. on Microwave and Millimeter Wave Technology*, pp. 1042-1044.
- Abd-Elhady, M., Zainud-Deen, S. H., Mitkees, A. A. & Kishk, A. A., 2010. Slot-loading rectangular dielectric resonator elements reflectarray. *IEEE Middle East Conf. on Antennas and Propag.*, pp. 1-3.
- Abd-Elhady, M., Zainud-Deen, S. H., Mitkees, A. A. & Kishk, A. A., 2012. Wideband rectangular dielectric resonator elements reflectarray. *Middle East Conf. Antennas and Propag.*, pp. 1-5.
- Arrebola, M., Encinar, J. A., de la Fuente, L. F. & Toso, G., 2009. Contoured-beam reflectarray for DBS application including copolar isolation requirements between missions. *3rd European Conf. on Antennas and Propag.*, pp. 844-848.
- Berry, D., Malech, R. & Kennedy, W., 1963. The reflectarray antenna. *IEEE Trans. Antennas Propag.*, 11(6), pp. 645-651.
- Bialkowski, M. E. & Sayidmarie, K. H., 2008. Investigations into phase characteristics of a single-layer reflectarray employing patch or ring elements of variable size. *IEEE Trans. Antennas Propag.*, 56(11), pp. 3366-3372.
- Boccia, L. et al., 2002. An experimental approach to active and passive reflectarray design. *32nd European Microwave Conf.*, pp. 1-4.
- Bozzi, M., Germani, S. & Perregrini, L., 2004. A figure of merit for losses in printed reflectarray elements. *IEEE Antennas and Wireless Propag. Lett.*, 3(1), pp. 257-260.
- Capozzoli, A. et al., 2009. Fast phase-only synthesis of faceted reflectarrays. *3rd European Conf. on Antennas and Propag.*, pp. 1329-1333.
- Capozzoli, A., Curcio, C., D'Elia, G. & Liseno, A., 2010. Fast phase-only synthesis of conformal reflectarrays.. *IET Microwaves, Antennas & Propagation*, 4(12), pp. 1989-2000.

- Carrasco, E., Arrebola, M., Encinar, J. A. & Barba, M., 2008. Demonstration of a shaped beam reflectarray using aperture-coupled delay lines for LMDS central station antenna. *IEEE Trans. Antennas Propag.*, 56(10), pp. 3103-3111.
- Carrasco, E., Barba, M. & Encinar, J. A., 2006. Aperture-coupled reflectarray element with wide range of phase delay. *Electronics Letters*, 42(12), pp. 667-668.
- Dzulkipli, I. et al., 2012. Mutual coupling analysis using FDTD for dielectric resonator antenna reflectarray radiation prediction. *Progress In Electromagnetics Research B*, Volume 41, pp. 121-136.
- Dzulkipli, N. I., Jamaluddin, M. H. & Yusof, M. F. M., 2012. Design of alphabet shaped slot-loaded dielectric. *IEEE Asia-Pacific Conf. on Applied Electromagnetics*, pp. 334-337.
- EMAG Technologies Inc., 2013. *Designing wideband dielectric resonator antennas using EM.cube*. [Online] Available at: <http://www.emagtech.com/content/designing-wideband-dielectric-resonator-antennas-using-emcube> [Accessed 3 4 2014].
- Encinar, J. A., 1999. Design of two-layer printed reflectarrays for bandwidth enhancement. *IEEE Antennas and Propag. Society Int. Sympos.*, Volume 2, pp. 1164-1167.
- Encinar, J. A., 2001. Design of two-layer printed reflectarrays using patches of variable size. *IEEE Trans. Antennas Propag.*, 49(10), pp. 1403-1410.
- Encinar, J. A. & Zornoza, J. A., 2004. Three-layer printed reflectarrays for contoured beam space applications. *IEEE Trans. on Antennas and Propag.*, 52(5), pp. 1138-1148.
- Han, C., Huang, J. & Chang, K., 2006. Cassegrain offset subreflector-fed X/Ka dual-band reflectarray with thin membranes. *IEEE Trans. on Antennas and Propag.*, 54(10), pp. 2838-2844.
- Hasani, H., Kamyab, M. & Mirkamali, A., 2010. Broadband reflectarray antenna incorporating disk elements with attached phase-delay lines. *IEEE Antennas and Wireless Propag. Lett.*, Volume 9, pp. 156-158.
- Huang, J., 1995. Analysis of a microstrip reflectarray antenna for microspacecraft applications. *TDA Progress Report 42-120*, pp. 153-173.
- Huang, J., 1996. Capabilities of printed reflectarray antennas. *IEEE Int. Sympos. on Phased Array Systems and Technology*, pp. 131-134.
- Huang, J. & Encinar, J. A., 2007. *Reflectarray antennas*. Hoboken, NJ: John Wiley & Sons.

- Jamaluddin, M. H. et al., 2009. A dielectric resonator antenna (DRA) reflectarray. *European Microwave Conf.*, pp. 25-28.
- Javor, R. D., Wu, X. D. & Chang, K., 1994. Beam steering of a microstrip flat reflectarray antenna. *AP-S. Digest Antennas and Propag. Society Int. Sympos.*, Volume 2, pp. 956-959.
- Karnati, K., Ebadi, S. & Gong, X., 2011. Effect of dielectric thickness on phase swing of a Ka-band microstrip reflectarray unit cell. *IEEE Int. Sympos. on Antennas and Propag.*, pp. 948-951.
- Kelkar, A., 1991. FLAPS: conformal phased reflecting surfaces. *Proceeding IEEE National Radar Conf.*, pp. 58-62.
- Keller, M. G. et al., 2000. A ka-band dielectric resonator antenna reflectarray. *30th European Microwave Conf.*, pp. 1-4.
- Li, Y., Bialkowski, M. & Abbosh, A. M., 2011. Single-layer reflectarray with circular rings and open-circuited stubs for wideband operation. *IEEE Trans. Antennas Propag.*, 60(9), pp. 4183-4189.
- Li, Y., Bialkowski, M. E., Sayidmarie, K. H. & Shuley, N. V., 2011. Single-layer microstrip reflectarray with double elliptical ring elements for bandwidth enhancement. *Microwave and Optical Technology Lett.*, 53(5), pp. 1083-1087.
- Li, Y., Bialkowski, M. E., Sayidmarie, K. H. & Shuley, N. V., 2011. Single-layer reflectarray employing circular ring with open-circuited stub as phasing element. *IEEE Int. Sympos. on Antennas and Propag.*, pp. 2168-2171.
- Long, S. A., McAllister, M. & Shen, L., 1983. The resonant cylindrical dielectric cavity antenna. *IEEE Trans. Antennas and Propag.*, 31(3), pp. 406-412.
- Makdissy, T. et al., 2012. A patch-slot combination approach for large band reflectarrays. *42nd European Microwave Conf.*, pp. 759-762.
- Malagisi, C. S., 1978. Microstrip disc element reflect array. *Electronics and Aerospace Systems Convention*, pp. 186-192.
- Mener, S. et al., 2013. Design and characterization of a CPSS-based unit-cell for circularly polarized reflectarray applications. *IEEE Trans. Antennas Propag.*, 61(4), pp. 2313-2318.
- Misran, N., Cahill, R. & Fusco, V., 2002. Reflection phase response of microstrip stacked ring elements. *Electronics Letters*, 38(8), pp. 356-357.

- Mussetta, M., Grimaccia, F. & Zich, R. E., 2012. Comparison of different optimization techniques in the design of electromagnetic devices. *IEEE Congress on Evolutionary Computation*, pp. 1-6.
- Nayeri, P., Yang, F. & Elsherbeni, A. Z., 2012. Design of single-feed reflectarrays with asymmetric multi-beams. *IEEE Antennas and Propag. Society Int. Sympos.*, pp. 1-2.
- Neshati, M. H. & Wu, Z., 2000. Theoretical and experimental investigation of a probe-fed rectangular DR antenna. *5th Int. Sympos. on Antennas, Propag. and EM theory*, pp. 265-268.
- Niaz, M. W., Ahmed, Z. & Ihsan, M. B., 2010. Performance comparison of different aperture shapes for microstrip reflectarray. *German Microwave Conf.*, pp. 250-253.
- Pan, Y., Zhang, Y. & Karimkashi, S., 2012. Broadband low-cost reflectarray for multi-mission radar applications. *IEEE Radar Conf.*, pp. 0613-0617.
- Petosa, A., 2007. Coupling to DRAs. In: *Dielectric resonator antenna handbook*. Norwood: Artech House, Inc., pp. 49-81.
- Petosa, A. & Ittipiboon, A., 2010. Dielectric resonator antennas: a historical review and the current state of the art. *IEEE Antennas and Propag. Mag.*, 52(5), pp. 91-116.
- Phelan, H. R., 1977. Spiralphase reflectarray for multitarget radar. *Microwave Journal*, Volume 20, pp. 67-73.
- Pozar, D. M. & Metzler, T. A., 1993. Analysis of a reflectarray antenna using microstrip patches of variable size. *Electronics Letters*, 29(8), pp. 657-658.
- Pozar, D. M., Targonski, S. D. & Syrigos, H. D., 1997. Design of millimeter wave microstrip reflectarrays. *IEEE Trans. Antennas Propag.*, 45(2), pp. 287-296.
- Rajagopalan, H. & Rahmat-Samii, Y., 2010. On the reflection characteristics of a reflectarray element with low-loss and high-loss substrates. *IEEE Antennas Propag. Mag.*, 52(4), pp. 73-89.
- Robinson, A. W., Bialkowski, M. E. & Song, H. J., 1999. An X-band passive reflectarray using dual-feed aperture-coupled patch antennas. *Aisa Pacific Microwave Conf.*, Volume 3, pp. 906-909.
- Venneri, F., Costanzo, S. & Massa, G. D., 2013. Design and validation of a reconfigurable single varactor-tuned reflectarray. *IEEE Trans. Antennas Propag.*, 61(2), pp. 635-645.

- Zainud-Deen, S. H., Abd-Elhady, A. M., Mitkees, A. A. & Kishk, A. A., 2010. Dielectric resonator reflectarray with two DRA sizes and varying slot loading. *IEEE Antennas and Propag. Society Int. Sympos.*, pp. 1-4.
- Zainud-Deen, S. H. et al., 2011. Wideband perforated rectangular dielectric resonator antenna reflectarray. *IEEE Int. Sympos. on Antennas and Propag.*, pp. 113-116.
- Zhang, W.-X., Fu, D.-L. & Wang, A.-N., 2007. A compound printed air-fed array antenna. *Int. Conf. on Electromagnetics in Advanced Applications*, pp. 1054-1057.
- Zhao, M. -Y. et al., 2013. Design of new single-layer multiple-resonance broadband circularly polarized reflectarrays. *IEEE Antennas and Wireless Propag. Letters*, Volume 12, pp. 356-359.
- Zhou, M. et al., 2013. Direct optimization of printed reflectarrays for contoured beam satellite antenna applications. *IEEE Trans. Antennas Propag.*, 61(4), pp. 1995-2004.